

1 **A comparison of the Atlantic and Pacific Bjerkn**
2 **es feedbacks: Seasonality, Symmetry, and Stationarity**

3 **T. Dippe^{1*}, J. F. Lübbecke^{1,2}, R. J. Greatbatch^{1,2}**

4 ¹GEOMAR Helmholtz Centre for Ocean Research Kiel, Germany

5 ²Faculty of Mathematics and Natural Sciences, Christian Albrechts University, Kiel, Germany

6 **Key Points:**

- 7 • The elements of the Atlantic Bjerkn
- 8 es feedback display asymmetries.
- 9 • These asymmetries are less consistent in the Atlantic, compared to their Pacific
- 10 counterparts.
- The Atlantic Bjerkn
- es feedback varies substantially on decadal time scales.

This article has been accepted for publication and undergone full peer review but has not been through the copyediting, typesetting, pagination and proofreading process which may lead to differences between this version and the Version of Record. Please cite this article as doi: 10.1029/2018JC014700

Abstract

The Bjerknes feedback is the dominant positive feedback in the equatorial ocean basins. To examine the seasonality, symmetry, and stationarity of the Pacific and Atlantic Bjerknes feedbacks we decompose them into three feedback elements that relate thermocline depth, sea surface temperature (SST), and western basin wind stress variability to each other. We partition feedback elements into composites associated with positive or negative anomalies. Using robust regression, we diagnose the strength of each composite.

For the recent period 1993-2012, composites of the Pacific Bjerknes feedback elements agree well with previous work. Positive composites are generally stronger than negative composites, and all feedback elements are weakest in late boreal spring. In the Atlantic, differences between positive and negative composites are less consistent across feedback elements. Specifically, wind variability seems to play a less important role in shaping atmosphere-ocean coupling in the Atlantic when compared to the Pacific. However, a clear seasonality emerges: Feedback elements are generally strong in boreal summer and, for the negative composites, again in boreal winter. The Atlantic Bjerknes feedback is dominated by subsurface-surface coupling.

Applying our analysis to overlapping 25-year periods for 1958-2009 shows that the strengths of feedback elements in both ocean basins vary on decadal time scales. While the overall asymmetry of the Pacific Bjerknes feedback is robust, the strength and symmetry of Atlantic feedback elements vary considerably between decades. Our results indicate that the Atlantic Bjerknes feedback is non-stationary on decadal time scales.

1 Introduction

The Bjerknes feedback is the dominant coupled, positive feedback in the equatorial oceans (Bjerknes, 1966, 1969). It plays a crucial role in shaping Atlantic and Pacific equatorial variability, tying three key properties of an equatorial ocean basin into a closed feedback loop. These properties are the thermocline depth along the equator, which can be approximated by sea surface height (SSH) in the central and eastern ocean basin (Cane, 1984; Rebert et al., 1985); eastern basin sea surface temperature (SST); and western basin zonal wind stress (USTR). The closed feedback loop operates as a positive feedback for both positive and negative anomalies in either SSH, SST, or USTR and can be decomposed into three feedback elements that act in concert:

- (i) SSH→SST: “*Subsurface-surface coupling*”. The thermocline depth in the eastern ocean basin is related to net upwelling of cold water into the surface mixed layer, and mixing at the base of the mixed layer (Hummels et al., 2013). Variations of thermocline depth are related to variations in the local warm water volume that in turn affect how effectively upwelling alters the mixed layer temperature.
- (ii) SST→USTR: “*SST-wind coupling*”. Eastern basin SST anomalies produce a local, Gill-type atmospheric response (Gill, 1980) that alters the sea level pressure gradient along the equator and affects surface winds in the western ocean basin.
- (iii) USTR →SSH: “*Wind-thermocline coupling*”. Zonal wind anomalies in the western ocean basin change the local balance between zonal wind stress and the subsurface pressure gradient in the ocean. The thermocline adapts to the varying subsurface pressure gradient transmits the information eastward along the equator via an equatorial Kelvin wave. In the eastern ocean basin, thermocline variability couples to SST variability and closes the Bjerknes feedback loop.

Since Bjerknes (1966) first described the closed feedback loop outlined above, different studies have referred to different mechanisms as “the Bjerknes feedback”, sometimes focusing on the atmospheric or ocean parts of the coupled feedback only. Here, when we

59 discuss “the” Bjerknes feedback, we refer to the coupled feedback that links oceanic and
60 atmospheric variability.

61 In the equatorial Atlantic and Pacific Oceans, the Bjerknes feedback supports the
62 growth of coupled air-sea anomalies associated with the Atlantic and Pacific Niños (Bjerknes,
63 1969; Keenlyside & Latif, 2007; Burls et al., 2012; Lübbecke & McPhaden, 2013; Dep-
64 penmeier et al., 2016; Dippe et al., 2018). While the phrase “Pacific Niño” in a strict
65 sense refers to the SST manifestation of a positive El Niño-Southern Oscillation (ENSO)
66 event, we use the name to refer to the entire coupled process. Likewise, when we talk
67 about the “Atlantic Niño”, we mean the complete coupled atmosphere-ocean process,
68 including negative events that are generally known as Niñas.

69 In their respective basins, the Niños are the dominant mode of interannual SST vari-
70 ability. While their corresponding names and similar patterns suggest that they are es-
71 sentially manifestations of the same process, significant differences exist (Xie et al., 1999;
72 Keenlyside & Latif, 2007; Burls et al., 2011; Lübbecke & McPhaden, 2013; Richter et
73 al., 2013). The canonical Pacific Niño generally peaks in boreal winter and lasts for sev-
74 eral months, while the Atlantic Niño is tightly phase-locked to boreal summer and rarely
75 outlasts a season, achieving roughly half of the Pacific SST anomaly amplitude. The phase-
76 locking of the Niños is accompanied by a strong seasonality of their supporting Bjerk-
77 nes feedbacks. The Pacific Bjerknes feedback operates for most of the year, while the At-
78 lantic Bjerknes feedback is active for a few months only twice a year, in boreal summer
79 and again, briefly, at the beginning of boreal winter (Burls et al., 2011; Dippe et al., 2018).

80 Another interesting feature of the Atlantic is that it hosts a secondary, Niño-like
81 phenomenon in boreal winter. Okumura and Xie (2006) found that the “winter Niño”
82 – their “Niño II” – is the product of a secondary, seasonal weakening of the trade winds
83 in the Gulf of Guinea, which is able to briefly organize coupled atmosphere-ocean vari-
84 ability into the Bjerknes feedback.

85 Characteristics of the Atlantic and Pacific Niños vary on decadal and longer time
86 scales. Losada and Rodríguez-Fonseca (2016) and Martín-Rey, Polo, Rodríguez-Fonseca,
87 Losada, and Lazar (2017) report that the Atlantic Multidecadal Oscillation (AMO) –
88 a low-frequency phenomenon that is mainly characterized by variations of basin-wide SST
89 in the North Atlantic (Schlesinger & Ramankutty, 1994; Delworth & Mann, 2000; Knight
90 et al., 2006) – modulates both the spatial configuration of the Atlantic Niño SST pat-
91 tern and the atmospheric response to these patterns. Martín-Rey et al. (2017) argue that
92 eastern equatorial Atlantic SST variability is enhanced by more than 150% in boreal sum-
93 mer during negative AMO phases. Similarly, Cobb et al. (2013) and Li et al. (2013) demon-
94 strate for centennial and millennial time scales that the spatiotemporal characteristics
95 of the Pacific Niño are subject to low-frequency variations. For the recent decades, stud-
96 ies such as Lübbecke, Burls, Reason, and McPhaden (2014) show that low-frequency vari-
97 ations in the Pacific background state modulate the strength of the Pacific Bjerknes feed-
98 back and hence the characteristics of the Pacific Niño.

99 The spatiotemporal characteristics of warm and cold Pacific Niño events are sub-
100 ject to a number of asymmetries (Takahashi et al., 2011; Dommenges et al., 2013; Capo-
101 tondi et al., 2015; Chen et al., 2015; Takahashi & Dewitte, 2016). Warm events are gen-
102 erally stronger in terms of their SST amplitude than cold events, while cold events last
103 longer and evolve in a different spatial manner. Another aspect of the complex nature
104 of the Pacific Niño is highlighted by the existence of different manifestations of Pacific
105 Niño events that appear to have distinct spatiotemporal signatures (Yeh et al., 2009; Taka-
106 hashi et al., 2011; Capotondi et al., 2015; Takahashi & Dewitte, 2016). Yeh et al. (2009)
107 document that the last decades saw an increase in the frequency of the central Pacific
108 Niño. In contrast to the canonical eastern Pacific Niño with its clear signature in the east-
109 ern Pacific and seesaw-response in the anomalous Walker circulation, the pattern of the
110 central Pacific Niño is constrained to the region between $160^{\circ}E$ and $120^{\circ}W$ and splits

111 the Walker circulation into two cells (Ashok & Yamagata, 2009). A generalization of these
112 ENSO “flavours” has recently been proposed by Timmermann et al. (2018), who pro-
113 vide an overview on what they call ENSO complexity.

114 Some of the above asymmetries in the Pacific have been linked to asymmetries in
115 the strength of the Pacific Bjerknes feedback elements. Dommenget et al. (2013) and DiNezio
116 and Deser (2014) show that the different lengths of warm and cold events are related to
117 non-linearities in the SSH-SST and SST-USTR feedback elements. In a different approach,
118 Hu et al. (2017) shows that the “recharge/discharge” processes associated with wind-
119 thermocline coupling operate differently for warm and cold events, favoring long cold events
120 and rather short, intense warm events. Levine and McPhaden (2016) show that state-
121 dependent noise forcing contributes to the SST amplitude asymmetry of the Pacific Niño.
122 State-dependent noise provides an additional positive feedback between warm Pacific Niño
123 events and zonal wind variability. The evolving warm event amplifies its own wind forc-
124 ing by creating a state that promotes the occurrence of subsequent strong westerly wind
125 bursts in the western and central ocean basin. This mechanism enhances wind-thermocline
126 coupling.

127 In contrast to the prominent Pacific SST amplitude asymmetry, the Atlantic Niño
128 is rather symmetric. Lübbecke and McPhaden (2017) show that warm and cold Atlantic
129 Niño events are effectively mirror images of each other. Additionally, they diagnose the
130 strength of the Bjerknes feedback elements for both positive and negative summer events
131 and conclude that, unlike the Pacific Bjerknes feedback, the Atlantic summer Bjerknes
132 feedback is largely symmetric.

133 Here, we revisit the work of Lübbecke and McPhaden (2017) by taking into account
134 zonal, seasonal, and decadal variations of the Bjerknes feedback strengths associated with
135 positive and negative events in the equatorial Atlantic. Specifically, we seek to answer
136 the following question: For the summer and winter Niños in the equatorial Atlantic, does
137 the Bjerknes feedback operate symmetrically for cold and warm events? Are these find-
138 ings stationary, or do they depend on the analysis period?

139 The remainder of this study is structured as follows. Section 2 explains how we esti-
140 mate the Bjerknes feedback and on which datasets we base our analysis. Section 3 dis-
141 cusses the results of our analysis. In Section 4, we discuss our findings in comparison to
142 Lübbecke and McPhaden (2017) and attempt to assess the stationarity of our results.
143 A discussion is provided in the last section.

144 2 Data and Methods

145 2.1 Data

146 Our analysis is based on two groups of datasets that each contain monthly mean
147 SSH, SST, and USTR in the equatorial Atlantic and Pacific ocean basins.

- 148 1. “*OBS*”, 1993-2012, direct satellite observations, reconstructions, and reanalysis.
149 We use SSH provided by AVISO (<https://www.aviso.altimetry.fr/en/home.html>);
150 SST from NOAA’s Extended Reconstructed Sea Surface Temperature (Smith &
151 Reynolds, 2003, ERSST), version 5 (Huang et al., 2017); and USTR from the ERA-
152 Interim Reanalysis (Dee et al., 2011). While ERA-Interim is not an observational
153 dataset, we call this group “*OBS*” for the sake of readability.
- 154 2. “*ORAS4*”, 1958-2009, ECMWF’s Ocean Reanalysis System Version 4 (Balmaseda
155 et al., 2012), which provides dynamically consistent SSH, SST, and USTR. SSH
156 and three-dimensional ocean potential temperature data were downloaded from
157 the University of Hamburg’s Integrated Climate Data Center (<http://icdc.cen.uni-hamburg.de/projek->
158 [te/easy-init/easy-init-ocean.html](http://icdc.cen.uni-hamburg.de/projekte/easy-init/easy-init-ocean.html)). We use SSH as provided by the reanal-
159 ysis; the first level of the ocean potential temperature as SST; and the same wind

160 stress dataset as in Lübbecke and McPhaden (2017). This corresponds to the wind
161 stress forcing of ORAS4, using ERA-40 (Uppala et al., 2006) data from January
162 1958 to December 1988, and ERA-Interim data afterwards. Note that reanalysis
163 products potentially suffer from model-induced biases, and that the accuracy of
164 results is highly sensitive to the quality of the assimilated data. Uncertainties are
165 generally larger prior to the advent of satellite observations in the late 1970s. Be-
166 cause of this, our discussion of ORAS4-based results in Section 4 will focus on gen-
167 eral issues rather than on exact numerical values.

168 As pointed out in the Introduction, SSH is a reliable proxy for thermocline depth
169 in the central and eastern equatorial ocean basins only (Cane, 1984). Hence, results in-
170 volving SSH should be treated cautiously in the western warm pool regions.

171 Anomalies in this study are calculated as follows: We first remove the linear trend
172 from the entire time series, then subtract the seasonal cycle to obtain monthly anoma-
173 lies. For each analysis, we calculate the anomalies with respect to the chosen analysis
174 periods.

175 For the overlap period 1993-2009, we compare the time series of anomalies and the
176 seasonal distribution of standard deviations between the two dataset groups for each vari-
177 able (Fig. 1). To facilitate comparison, we average our data into indices of the Atl3 and
178 Nino3.4 regions ($3^{\circ}S$ to $3^{\circ}N$, $20^{\circ}W$ to $0^{\circ}E$, and $5^{\circ}S$ to $5^{\circ}N$, 170° to $120^{\circ}W$, respec-
179 tively) in the Atlantic and Pacific for both SSH and SST; and into the WAtl and Nino4
180 regions ($3^{\circ}S$ to $3^{\circ}N$, 40° to $20^{\circ}W$, and $5^{\circ}S$ to $5^{\circ}N$, $160^{\circ}E$ to $150^{\circ}W$) for USTR. The
181 datasets agree well with each other, and anomaly correlation values between pairs of time
182 series of the same variable all exceed values of 0.9. Additionally, Fig. 1 highlights dif-
183 ferences between the Atlantic and Pacific Niños (see Introduction). It is obvious that Pa-
184 cific Niño events have a distinct signature in the anomaly time series of SSH, SST, and
185 USTR, being characterized by intermittent, strong events that are clearly phase-locked
186 to boreal winter (Fig. 1a,e,i). In contrast, variances in the Atlantic are much smaller and
187 events occur more regularly, producing anomaly time series that resemble white noise
188 (Fig. 1b,f,j). Panels 1k,l indicate that the ERA-Interim and ORAS4 USTR data are not
189 exactly equal, although they are both ERA-products. This could be due to the blend-
190 ing in ORAS4, and to a lesser degree to the different horizontal resolutions of the two
191 datasets, with ORAS4 USTR being higher resolved than the ERA-Interim data used in
192 this study.

93 2.2 Estimating the strength of the Bjerknes feedback elements

195 We use robust regression to diagnose the strength of individual Bjerknes feedback
196 elements (Holland & Welsch, 1977; Street et al., 1988; Huber & Ronchetti, 2009). In sta-
197 tistical analysis, developing a model of a given dataset requires assumptions about the
198 processes that generated the data. Ordinary least squares-based linear regression (OLS)
199 can be unreliable when these assumptions are violated, especially in the presence of out-
200 liers, since OLS minimizes the squared distances between the original data and the guess
201 of the prediction. Robust regression techniques – a collection of methods that seek to
202 lessen the sensitivity of the regression coefficients to outliers – generally change the weight
203 that is attributed to each residual when considering its impact on the final regression
204 coefficients. A common approach is to assign a relatively strong weight to small resid-
205 uals, and decrease the weight of large residuals that are likely associated with outliers.
206 While robust regression has been designed with outliers in mind, Zheng, Fang, Yu, and
207 Zhu (2014) demonstrated that it is a valid way to perform regression analysis based on
208 small datasets in climate science. We adopt this approach here, using Matlab’s imple-
209 mentation of robust regression (`robustfit`, current documentation provided by <https://de.mathworks.com/help>).
210 For our analysis, we use the default `robustfit` of Matlab’s 2018-distribution, which it-
eratively re-weights least squares with a bisquare weighting function.

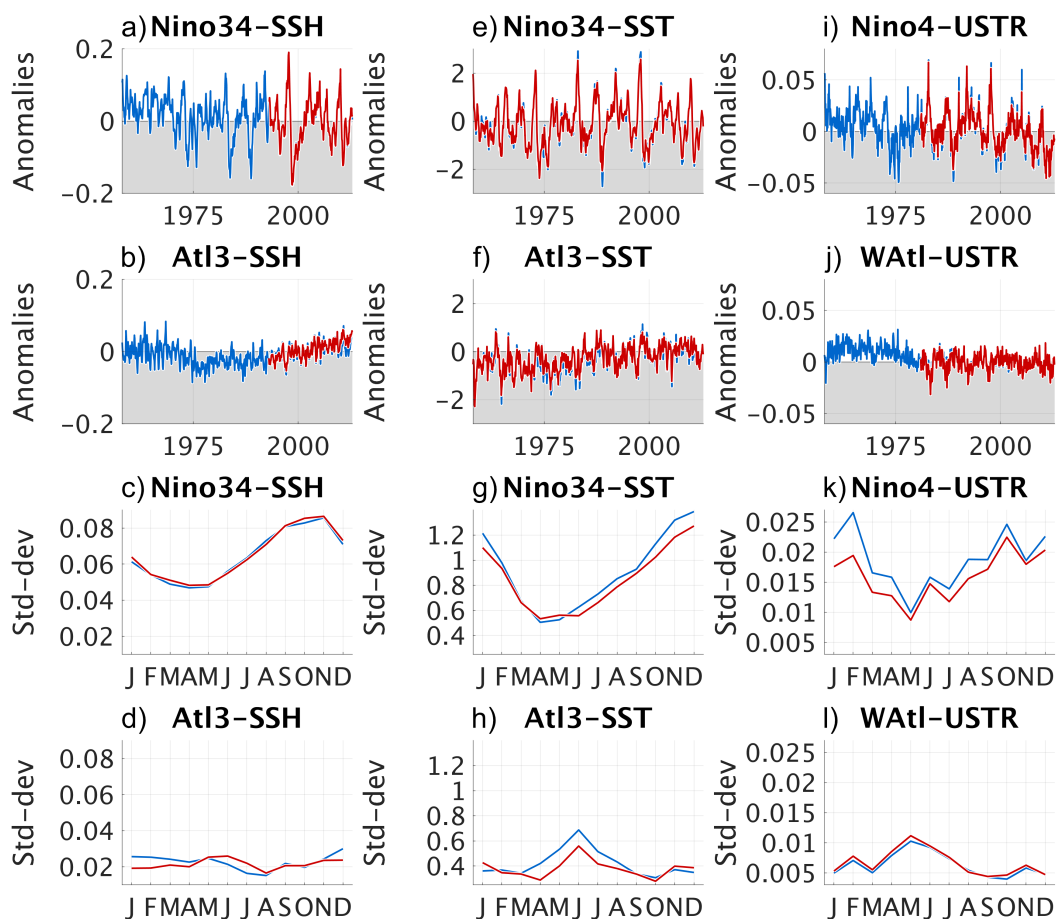


Figure 1: Key features of employed datasets. Time series of anomalies with respect to the linear trend and the seasonal cycle (upper two rows, panels a-b, e-f, i-j), and monthly stratified standard deviations (lower two rows, c-d, g-h, k-l, months from January to December indicated by their first letter on the x-axis). Both quantities have been diagnosed with respect to the overlap period of the two dataset groups, 1993-2009. Each panel shows the same quantity for the OBS and ORAS4 dataset groups as red and blue lines, respectively, and all quantities are shown for SSH, SST, and USTR in the left-hand (a-d), middle (e-h), and right-hand row (i-l). The OBS group contains AVISO-SSH, ERSST-SST, and ERA-Interim zonal wind stress (USTR). Data has been averaged into the Atl3 and Nino3.4 regions in the Atlantic and Pacific for both SSH and SST; and into the WAtl and Nino4 regions for USTR.

To diagnose the strength of the Bjerknes feedback elements in our zonal analysis, we average equatorial SSH and SST into 4° longitude \times 4° latitude boxes that slide along the equator. Zonal wind stress (USTR) is fixed to WAtl in the Atlantic, and Nino4 in the Pacific, since it is the western basin wind stress that dominantly contributes to the closed Bjerknes feedback, and not the local wind stress.

As in the case of OLS, robust regression, too, assumes a linear relationship between the two variables that are related to each other. In the tropical Atlantic, Lübbecke and McPhaden (2017)'s recent study shows a fairly linear relationship for all elements of the Bjerknes feedback (see their Fig. 3). In the equatorial Pacific, on the other hand, a number of studies have shown that non-linear processes affect the variability associated with

221 the Pacific Niño (Dommenget et al., 2013; Takahashi & Dewitte, 2016; Timmermann et
222 al., 2018). These processes, however, usually serve to explain the strongest events or the
223 overall asymmetry between warm and cold events (see Introduction). Here, we recog-
224 nize the overall asymmetries and are interested in a canonical analysis of the Bjerknes
225 feedback associated with the Pacific Niño. Because of this, and for the sake of direct com-
226 parability between the Atlantic and Pacific basins, we have decided to apply the same
227 (linear) analysis to both ocean basins.

228 2.3 Including lagged feedback elements into the analysis

229 Unless stated otherwise, we take into account that any of the Bjerknes feedback
230 elements could be lagged when we calculate composite strengths in this study (see Sec-
231 tion 2.4 for details on the feedback element composites). To identify lags, we use robust
232 regression to conduct a cross-regression analysis prior to diagnosing the composite strengths
233 for each analysis period. During the cross-regression analysis, we fix the forcing variable
234 of the feedback element – the variable that “drives” the feedback element, i.e. SSH, SST,
235 and USTR for the SSH-SST, SST-USTR, and USTR-SSH feedback elements – to our
236 analysis month and shift the month at which the response variable is measured for up
237 to ± 8 months. Negative lags indicate that the relationship is strongest when the response
238 variable leads the forcing variable. In this case, the causality of the three relationships
239 forming the Bjerknes feedback is severed. For this reason, we will discard results asso-
240 ciated with negative lags for the remainder of the study.

241 Figure 2 shows the lags that our cross-regression analysis identified, for the OBS
242 dataset group and the period 1993-2012. To produce the results shown in Section 3, we
243 assume that the lags are independent of the subset of data that was used to diagnose
244 them (see Section 2.4). In Section A.1 of the Appendix, we discuss the validity of this
245 assumption and find that it generally holds. However, this assumption can *locally* de-
246 grade the strength of the feedback element, demonstrating again how diverse the mech-
247 anisms are that produce the variability of the Atlantic and Pacific Niños, and that it may
248 not be justified to make equivalent assumptions for warm and cold events.

249 Figure 2 shows that in the Pacific, all feedback elements are generally character-
250 ized by positive lags that start to occur in May and decrease until boreal winter, indi-
251 cating that the closed feedback loop becomes more instantaneous in the latter half of the
252 year (Fig. 2a-c). Zonal variations are small, and lags tend to occur uniformly across large
253 parts of the Pacific.

254 In the Atlantic, lags associated with subsurface-surface coupling are generally posi-
255 tive (Fig. 2d), indicating that SSH leads SST variability by three months at most. Dur-
256 ing June and July, and again in boreal winter, lags vanish and subsurface-surface cou-
257 pling becomes instantaneously. The SST-USTR and USTR-SSH feedback elements, on
258 the other hand, are characterized by lags ≥ 0 only during spring and early summer, and
259 again during boreal winter. In agreement with previous studies on the seasonality of the
260 Atlantic Bjerknes feedback by Keenlyside and Latif (2007) and Burls et al. (2011), this
261 indicates that the Bjerknes feedback can only establish a closed feedback loop during early
262 summer and winter. Another feature of Fig. 2d-f is that the lags of the feedback elements
263 are not distributed evenly across the zonal extent of the basin. Rather, positive lags oc-
264 cur predominantly in or close to the Atl3 region, showing that not only is the Atlantic
265 Bjerknes feedback constrained to two short periods, but also to a narrow spatial domain.

266 We include lags into our robust regression analysis by shifting the time series of
267 the response variable according to the identified lag.

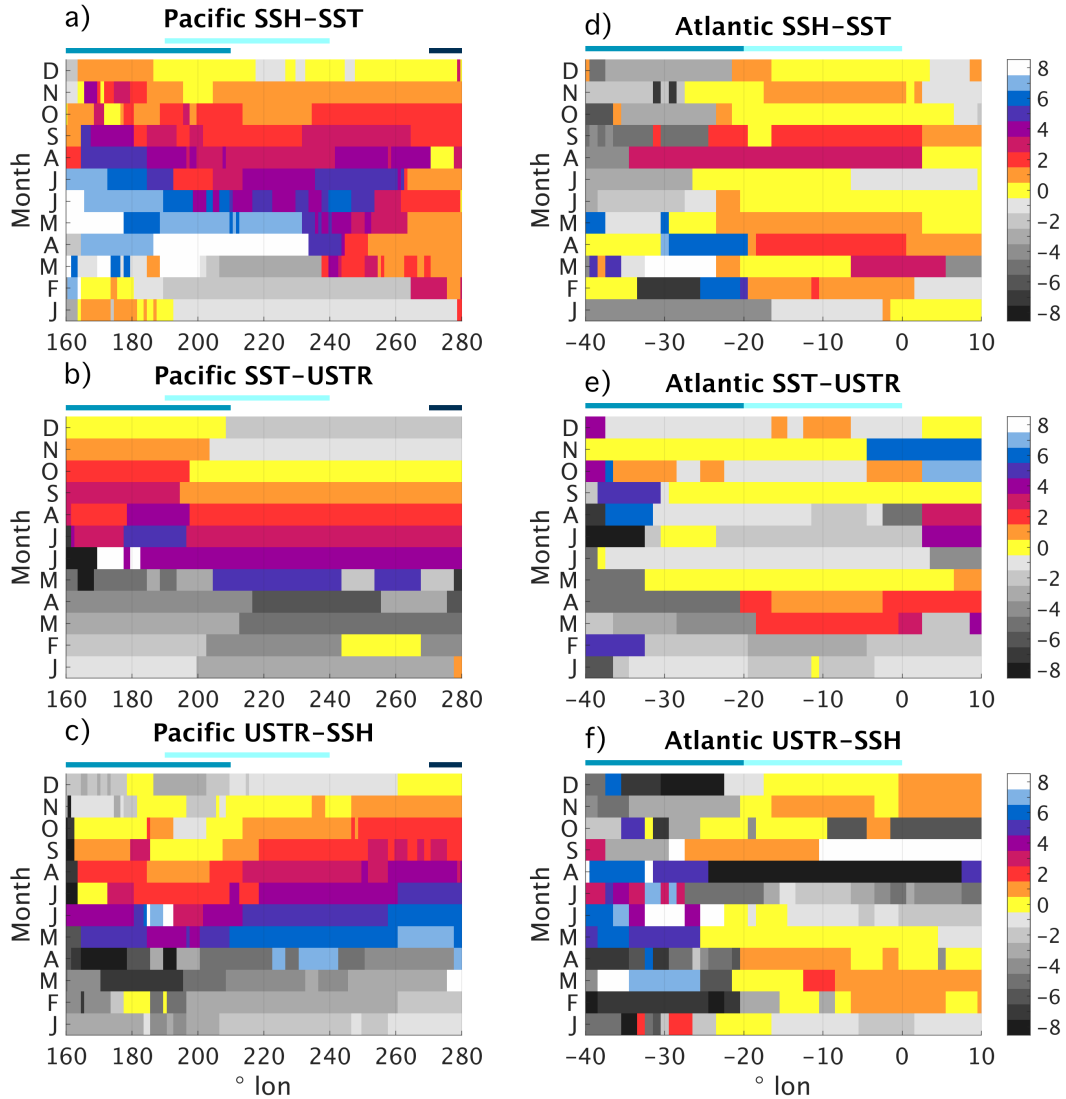


Figure 2: Lag in months at which the relationship for each of the three Bjerknes feedback elements is strongest. Data is shown along the equator (x -axis) and stratified into calendar months (y -axis) for both the Pacific (left column, panels a-c), and the Atlantic (right column, d-f). The sign of the lag is with respect to the forcing variable of the feedback element, i.e. SSH, SST, and USTR for the SSH-SST, SST-WSTR, and USTR-SSH feedback elements, respectively. A positive lag indicates that the forcing variable leads the response variable. Positive lags are shown in colour, with a lag of zero months indicated by yellow. Negative lags are shown in grey shading. The top, middle, and bottom rows show results for subsurface-surface coupling (a,d), SST-wind coupling (b,e), and wind-thermocline coupling (c,f). For each longitude, data has been averaged into 4° longitude $\times 4^\circ$ latitude bins prior to calculation. This binning has been done for each analysis, unless stated otherwise. Coloured bars below the titles indicate the zonal extent of the Nino₄, Nino_{3.4}, and Nino_{1.2} (WAtl and Atl3) regions in the Pacific (Atlantic) in blue, light blue, and dark blue (blue and light blue)

2.4 Assessing the symmetry of the Bjerknes feedback: Compositing feedback elements

To assess the symmetry of a Bjerknes feedback element, we partition it into positive and negative composites. Note that we do *not* separate our feedback elements into

272
273

consistent warm/cold composites according to SST conditions, but rather assign individual composites to each feedback element, based on its forcing variable.

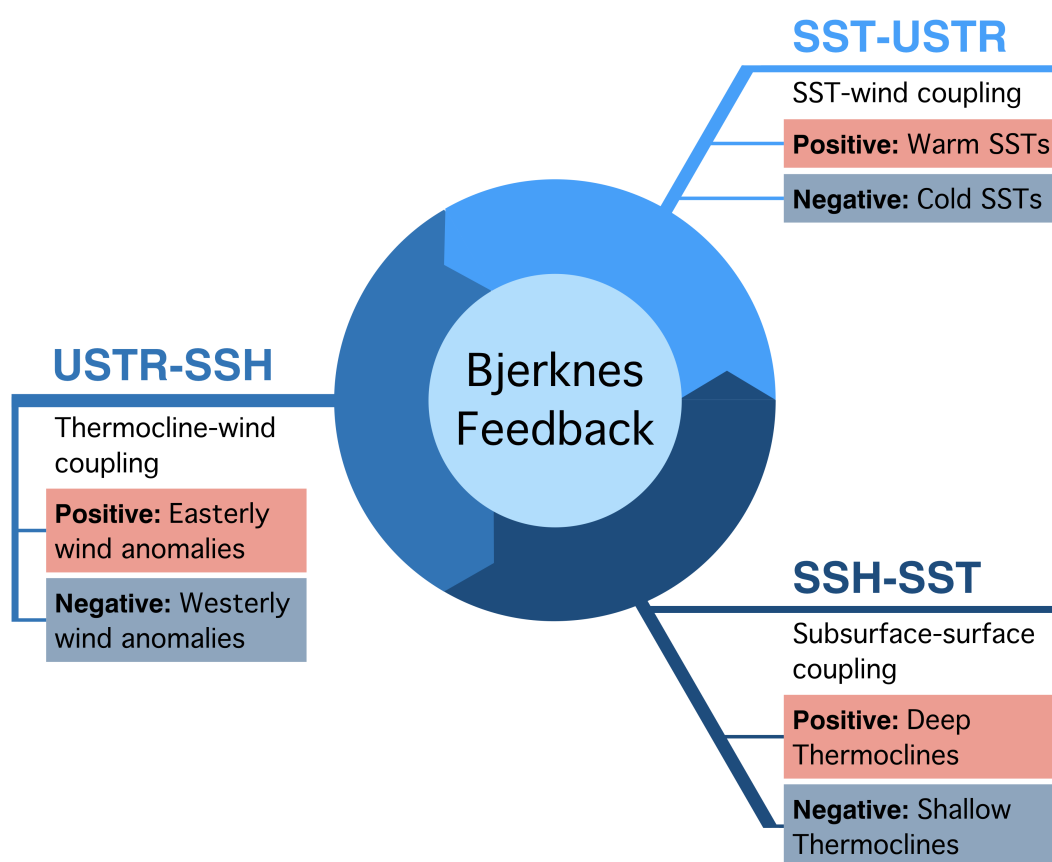


Figure 3: Schematic of the feedback decomposition approach. The closed Bjerknes feedback loop is decomposed into three interacting feedback elements (partitioned ring around the central circle). These feedback elements are the subsurface-surface coupling (SSH-SST, dark blue, bottom right), SST-wind coupling (SST-USTR, light blue, top right), and wind-thermocline coupling (USTR-SSH, blue, left). Each feedback element is additionally partitioned into two composites (red and blue boxes below each feedback element). Composites are based on the sign of the anomalies of the forcing variable, i.e. SSH, SST, and USTR for the SSH-SST, SST-USTR, and USTR-SSH feedback elements, respectively. The text in the composite boxes explains how each composite can be interpreted with respect to its “parent” feedback element (see Section 2.4).

274
275
276
277
278
279
280
281
282

Figure 3 illustrates this two-step decomposition of the Bjerknes feedback loop – into feedback *elements* first, then into *composites* of the feedback elements – and lists how negative and positive composites of each feedback element can be interpreted in terms of the forcing variable. Because of the partitioning of our base data pool into positive and negative composites prior to our regression analysis, the effective sample sizes for our robust regression are on the order of 10 for the period 1993-2012 (Section 3), and 12 for the 25-year periods considered in Section 4. This is a very small sample size. Even though we employ robust regression, we will refrain from attributing too much value to individual numbers, and will rather focus on general patterns.

2.5 Bootstrapping significances

Significance in our study indicates that a given composite of a feedback element (or their difference) is significantly different from the expected strength (difference) of that feedback element when it is diagnosed from a random sub-sample of the data. We estimate this significance using a simple bootstrapping approach outlined below.

For a (strength) composite of a Bjerknes feedback element, we generate a distribution of the expected feedback element strength by re-diagnosing the robust regression coefficients for random sub-samples of the full data pool. Sub-samples ignore composites, but have the same sample size as the composites they test and obey the same lags (see Fig. 2). By iterating through a large number of sub-samples, we bootstrap a distribution of pseudo-composite strengths, whose expected value corresponds to the relationship strength of the feedback element when the data is not partitioned into composites. Next, we use the bootstrapped distribution to perform a simple significance test. If the composite strength is outside the 90%-area of the bootstrapped distribution for a significance level of $\alpha = 0.1$ and the case of a one-sided test, we reject the null hypothesis that the composite strength is equal to the relationship strength based on the full dataset. The composite strength is significant.

For the difference between the positive and negative composites, we repeat the above method, but use the difference between the calculated composite strengths as the target of the test, instead of the absolute composite strength. For this, we again determine the size of our sub-sample, randomly draw a new sample of the same size, and use the remaining data in the pool as the pseudo-counter composite. In both cases, we perform 1,000 bootstraps and use a significance level of 0.1.

3 Symmetry of the Atlantic and Pacific Bjerknes feedbacks 1993-2012

3.1 Bjerknes feedback element strengths

To validate our method of partitioning the strength of the Bjerknes feedback elements into positive and negative composites, we discuss our results based on the OBS dataset group for the Pacific (Figs. 4, differences shown in Fig. 5a-c). We use the lags shown in Fig. 2.

In agreement with the equatorial Pacific “spring barrier”, both the composites of the SST-WSTR and WSTR-SSH feedback elements decline during late boreal winter and spring in the Pacific (Fig. 4b-c,e-f). The spring barrier is a concept that originates from seasonal predictability studies and refers to the drop in predictability of the Pacific Niño during boreal spring (Torrence & Webster, 1998; Duan & Wei, 2013). Wengel, Latif, Park, Harlaß, and Bayr (2018) showed that the spring barrier is associated with a weakening of the atmosphere-ocean coupling in the tropical Pacific, which temporarily decreases the strength of the Bjerknes feedback estimated by Jin, Kim, and Bejarano (2006)’s Bjerknes stability index (see Section 5). Our results confirm this.

In the Niño3.4 region and the eastern ocean basin, negative composites are significantly different from the expected relationship strength more frequently than positive composites. This is shown by the distribution of significance, indicated by overlaid black crosses in Fig. 4. The dominance of positive events over negative events is in agreement with previous studies on Pacific Niño asymmetries. In particular, while cold events are rather modest in magnitude, virtually all extreme events are warm and hence strongly shape the overall characteristics of the Pacific Niño (note, however, that really only one “extreme event” occurred in the short period 1993-2012). Consequently, the positive composites of the feedback element strengths are in better agreement with the expected overall relationship strengths than the negative composites.

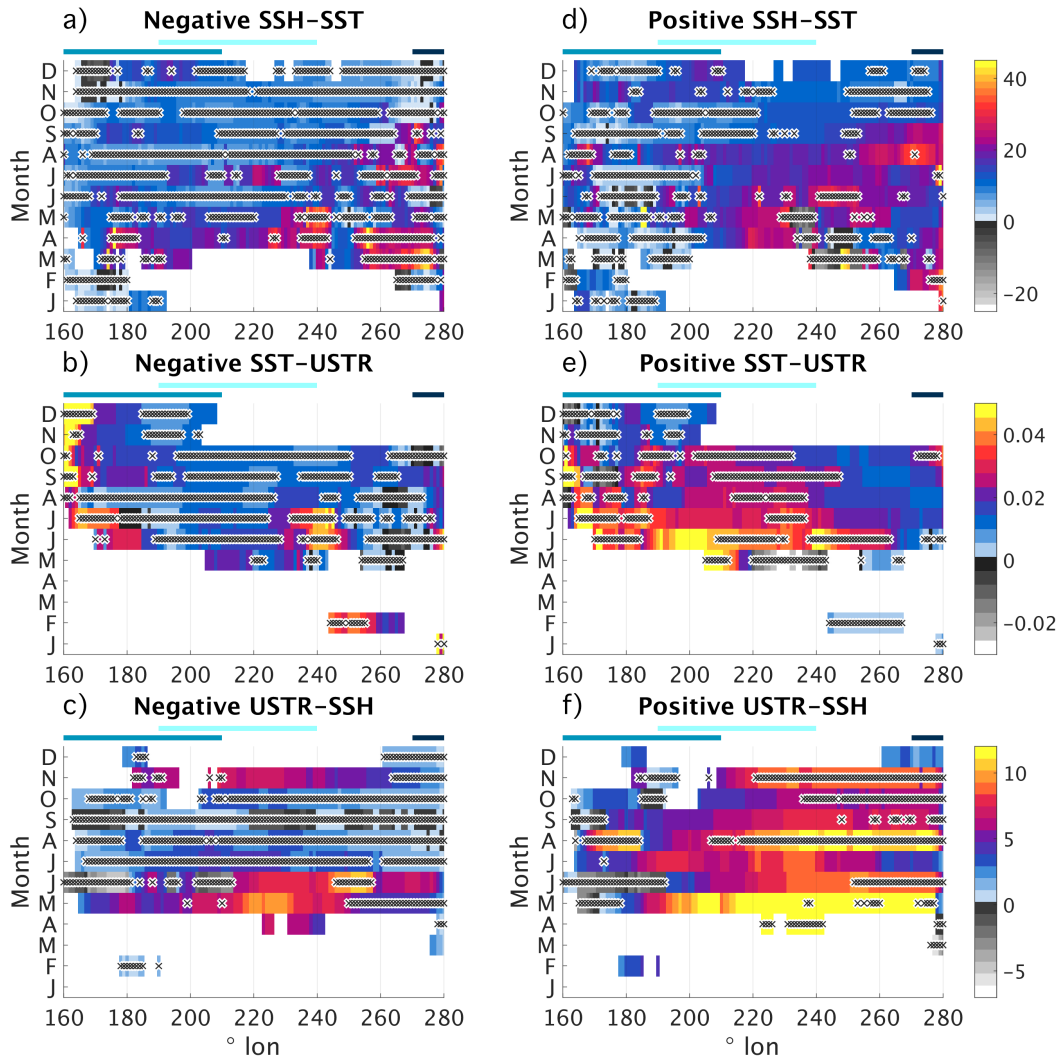


Figure 4: Composites of the OBS-based feedback elements in the Pacific, for the recent period 1993-2012 along the equator (x -axis) and stratified into calendar month (y -axis) with respect to the forcing variable. The top, middle, and bottom row show results for the SSH-SST (panels a,d), SST-USTR (b,e), and USTR-SSH feedback elements (c,f), with forcing variables SSH, SST, and USTR, respectively. To estimate the sensitivity of the two involved variables for the case of either positive or negative anomalies of the forcing variable, cf. Section 2.4, we use the slope parameter provided by robust regression. Colour shading indicates positive values, with small values shown in blue, and the highest values shown in reds and yellows. Negative values, indicating that a feedback element disrupts the closed Bjerknes feedback, are shown in grey shading, with the lightest greys indicating the largest negative values. White indicates that, at the given longitude and month, the lag diagnosed in Fig. 2 is negative and hence is not in agreement with the framework of the Bjerknes feedback. Sensitivities are given in units of K/m , $N/(m^2K)$, and m^3/N for the three feedback elements, respectively. The left and right columns show the sensitivities for the negative (a-c) and positive composites (d-f). Significance is indicated by black crosses with a white outline (see text for details). Coloured bars below the title indicate the zonal extent of the Nino₄, Nino_{3.4}, and Nino_{1.2} regions in blue, light blue, and dark blue, respectively.

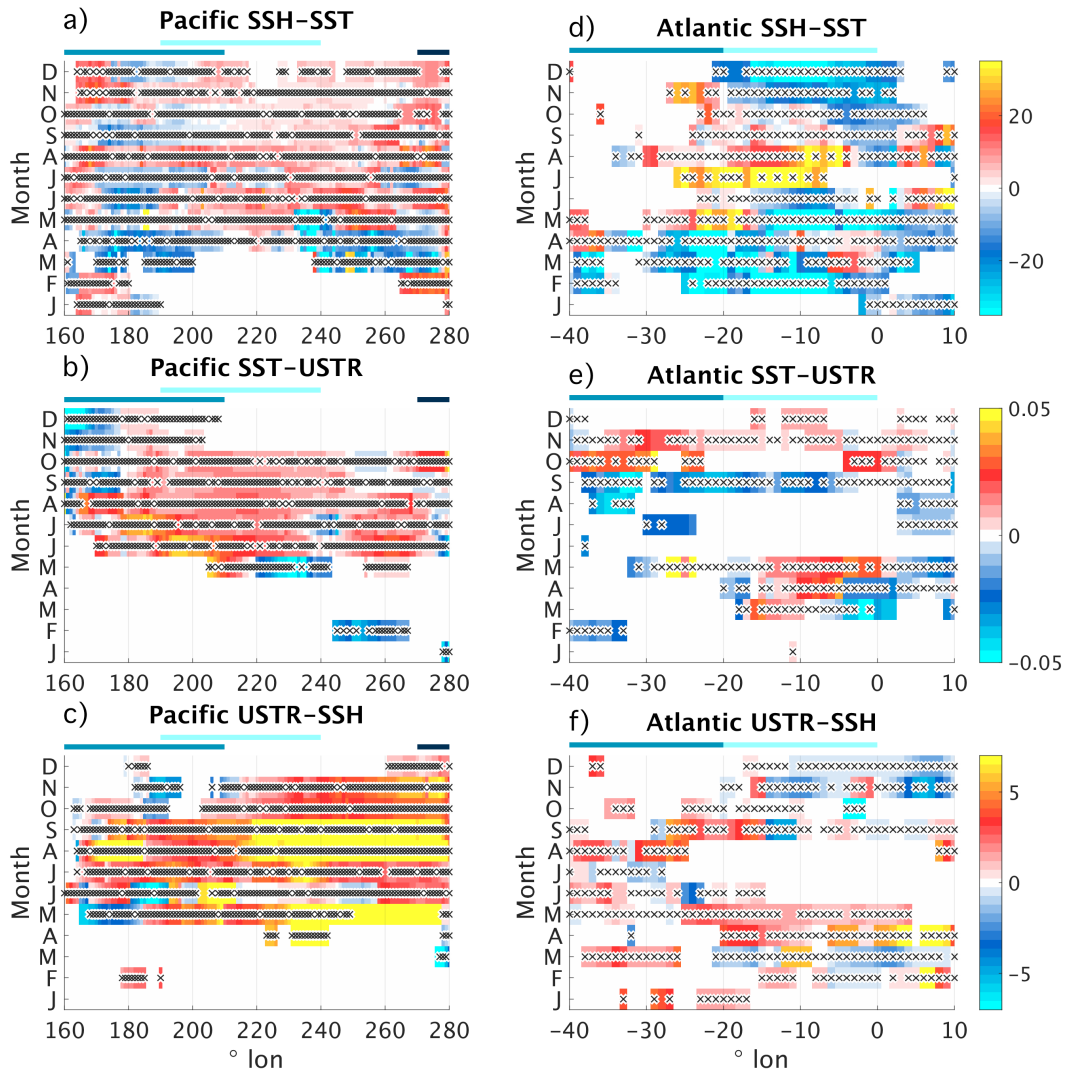


Figure 5: Similar to Fig. 4, but showing the difference between positive and negative composites of the feedback elements in the Pacific (left column, panels a-c) and the Atlantic (right column, d-f), for the SSH-SST (a,d), SST-USTR (b,e), and USTR-SSH (c,f) feedback elements. Blue (red-yellow) shading indicates that the negative composite is larger (smaller) than the positive composite. Coloured bars below the titles indicate the zonal extent of the Niño₄, Niño_{3.4}, and Niño_{1.2} (WAtl and Atl3) regions in the Atlantic (Pacific) in blue, light blue, and dark blue (blue and light blue).

331 Pacific subsurface-surface coupling (Figs. 4a,d) is positive for almost the entire year
 332 and across most of the Pacific basin. East of 150°W (210°E), the positive composite is
 333 generally stronger than the negative composite (Fig. 5a), in particular in the far east-
 334 ern basin during late boreal summer, coinciding with the main onset phase of warm Pa-
 335 cific Niño events.

336 Pacific SST-wind coupling, too, is generally stronger for the positive composite (Figs.
 337 4b,e, and 5b). Physically, this could be due to a threshold dependence of equatorial deep
 338 convection. While warm SST anomalies promote overlying convection effectively, cold
 339 SSTs do not necessarily suppress convection to the same degree (Levine & Jin, 2017).

340 Consequently, wind variability is more sensitive to warm SST anomalies than to cold SST
341 anomalies.

342 An interesting feature of the positive composite of the Pacific SST-USTR feedback
343 element is that it is strongest in the central Pacific (Fig. 4e) – it seems to operate more
344 locally in our analysis framework than expected (this, however, could be a consequence
345 of USTR being fixed to the western ocean basin). The strength of the positive feedback
346 element peaks just after the collapse of the spring barrier in early boreal summer, when
347 a clear asymmetry between the negative and positive composites emerges. This asym-
348 metry persists into boreal winter and is strongest in the Niño3.4 region (Fig. 5b). SST-
349 wind coupling stops contributing to a closed Bjerknes feedback in November for both
350 composites (Fig. 4b,e, and lags shown in Fig. 2b).

351 Last, Figs. 4c,f, and 5c indicate that Pacific wind-thermocline coupling is highly
352 asymmetric for the second half of the year, especially in the eastern portion of the basin.
353 Again, the feedback element is strongest after the collapse of the spring barrier. The zonal
354 distribution of the feedback strength composites indicates that the Niño4 wind stress in-
355 deed is strongly related to thermocline variability in the central and eastern ocean basin,
356 in good agreement with the Bjerknes feedback framework.

357 Overall, the elements of the Pacific Bjerknes feedback display a clear asymmetry.
358 Positive composites are generally stronger than negative composites, especially so in the
359 eastern ocean basin when SSH is involved. Simultaneously, negative composites are more
360 frequently significantly different from the overall expected relationship strength, indi-
361 cating that the characteristics of the Pacific Bjerknes feedback elements are largely shaped
362 by the positive composites. These findings are in excellent agreement with previous stud-
363 ies on Pacific Niño asymmetries and demonstrate that our lagged, robust regression-based
364 feedback analysis is well suited to investigate feedback asymmetries in an equatorial ocean
365 basin.

366 A peculiar finding is that our lagged feedback strengths appear to be phase-locked
367 to early boreal summer rather than winter. While the feedback elements do persist into
368 boreal winter, they are strongest in summer. This suggests that the weak spring cou-
369 pling very rapidly turns into effective coupling that organizes incipient anomalies in the
370 atmosphere and the ocean into the Bjerknes feedback. During the peak phase of the Pa-
371 cific Niño these feedback elements are still active, but they are weaker than during the
372 initial growth phase in boreal summer. On the one hand, these findings seem to be at
373 odds with a number of previous studies, including Zhu, Kumar, and Huang (2015)'s dis-
374 cussion of the seasonality of Pacific subsurface-surface coupling (their “thermocline feed-
375 back”). They report that instantaneous subsurface-surface coupling is weakest in March,
376 and then gradually increases until it peaks in October and November. However, their
377 study does neither explicitly consider lags, nor does it distinguish between “deep” and
378 “shallow” thermocline depths as we do here. On the other hand, recent work by Wengel
379 et al. (2018), supported by early work by Zebiak and Cane (1987), suggests that atmosphere-
380 ocean coupling in the tropical Pacific indeed is strongest in late boreal spring and early
381 summer, in agreement with our findings. The discrepancies between these studies and
382 our findings will have to be resolved by future research.

383 Next, we present our results for the Atlantic Bjerknes feedback (Figs. 5d-f, 6). In agree-
384 ment with Lübbecke and McPhaden (2017), the range of the feedback element strengths
385 is generally comparable to the Pacific, except for the weak Atlantic wind-thermocline
386 coupling (Figs. 6c,g). In addition to the weak sensitivity between USTR and subsurface
387 variability, the following factors are commonly discussed to explain the muted amplitude
388 of the Atlantic Niño. First, the zonal extent of the Atlantic is much smaller than in the
389 Pacific, which could constrain the fully coupled feedback. Second, the Bjerknes feedback
390 operates on shorter time scales in the Atlantic, effectively coupling the atmosphere and

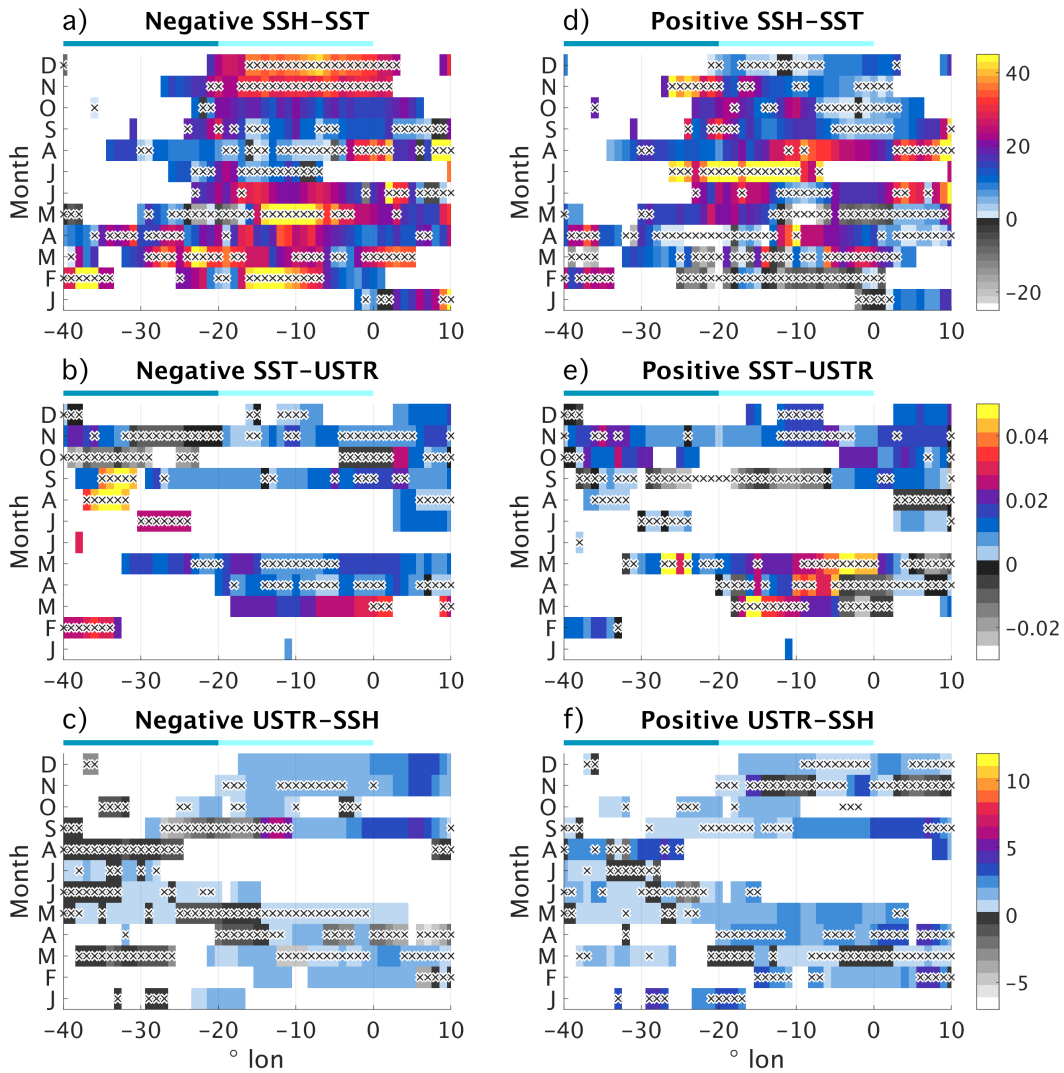


Figure 6: Same as Fig. 4, but for the Atlantic. Coloured bars below the title indicate the zonal extent of the WAtl and Atl3 regions in dark and light blue, respectively.

91 the ocean for only two-to-three months in a row at best, and hence diminishing the am-
 92 plitude that anomalies can grow to. This is consistent with our analysis.

393 Atlantic subsurface-surface coupling appears to be the dominant element of the At-
 394 lantic Bjerknes feedback (Fig. 6). Clear asymmetries emerge throughout boreal summer
 395 and early winter (Fig. 5d). In boreal summer, during the peak season of the summer Niño,
 396 the negative composite is stronger until July; for the remainder of boreal summer and
 397 early fall, the positive composite contributes more effectively to the overall feedback ele-
 398 ment. This suggests that subsurface-surface coupling sets in earlier for cold Atlantic Niño
 399 events. (While it is tempting to argue that the SSH-SST feedback element should nat-
 400 urally be stronger for shallow thermoclines due to the enhanced sensitivity of SST to small
 401 changes in thermocline depth, this reasoning clearly breaks down in the equatorial Pa-
 402 cific, where subsurface-surface coupling is strongest for deeper-than-normal thermoclines,
 403 cf. Fig. 5d. A possible explanation for this is that shallow thermoclines have to outcrop
 404 at some point, capping the maximum strength of the negative SSH-SST feedback ele-

ment, while the thermocline can deepen more or less without constraints for the positive SSH-SST composite.) In boreal winter, the negative composite re-emerges, while the positive composite is practically absent. The overall seasonality of Atlantic subsurface-surface coupling is in good agreement with our understanding of the Atlantic Niño. An interesting side note is that the Atlantic SSH-SST feedback element appears to be stronger than its Pacific counterpart when it peaks (cf. Figs. 4a,d and 6a,d).

Atlantic SST-wind coupling, on the other hand, appears to be weaker than its Pacific counterpart (cf. Figs. 4b,e and 6b,e). Nevertheless, consistent asymmetries arise between positive and negative composites. In agreement with the enhanced sensitivity of wind variability to warm SST anomalies discussed for the Pacific SST-WSTR feedback element, the positive composite is generally stronger than the negative composite. However, the lags that we used to diagnose the Atlantic SST-WSTR feedback element are negative from June to September (Fig. 2f) and SST-wind coupling hence only really contributes to a closed Bjerknes feedback loop in May. This limited contribution of the SST-WSTR feedback element indicates that equatorial wind variability is less sensitive to ocean variability in the Atlantic than in the Pacific.

Last, Atlantic wind-thermocline coupling is clearly weaker than its Pacific counterpart (Figs. 6c,f). In the case of the negative composite, it changes from being weakly positive to negative in August, indicating that it blocks anomaly growth and hence effectively contributes to the breakdown of the Atlantic Bjerknes feedback. This agrees with Dippe et al. (2018), who show that the closed Atlantic Bjerknes feedback collapses in August. Differences between the negative and positive composites are generally small, with the positive composite prevailing slightly. (The substantial difference in August is of no practical concern, since even the apparently overwhelming positive composite is only weakly positive in absolute terms, cf. Fig. 6f.) Similar to the SST-wind coupling discussed above, wind-thermocline coupling, too, can only contribute to a closed Bjerknes feedback in early boreal spring and winter, when the lag relationships are positive.

Overall, we identified asymmetries for all Atlantic Bjerknes feedback elements. These asymmetries occur mainly in boreal summer and are most pronounced for the SSH-SST feedback element associated with subsurface-surface coupling. The two feedback elements that involve wind variability produce a less straight-forward picture. They are weaker than their Pacific counterparts and constrain the Atlantic Bjerknes feedback to boreal summer and winter. This rather disruptive wind variability and decreased wind sensitivity to SST is in agreement with previous studies on the Atlantic Niño. A physical explanation of this difference between the Pacific and Atlantic Niños could be linked to the small zonal extent of the Atlantic, which substantially decreases the “fetch” of the wind stress variability in comparison to the Pacific. Additionally, enhanced interference, for example from mid-latitudes or the tropical Pacific, could explain why wind plays a somewhat different role for the Atlantic.

3.2 The total Bjerknes feedback

In Section 3.1, we have demonstrated that both the Atlantic and Pacific Bjerknes feedback elements can be asymmetrical. Here, we attempt to combine our findings for the individual feedback elements, and assess how symmetric the overall effect of the closed Bjerknes feedback loop is for warm and cold conditions in the central equatorial ocean basin. We call this integrative measure the total Bjerknes feedback.

We diagnose the total Bjerknes feedback by adding the strengths of the instantaneous feedback elements of the positive and negative composites. Instantaneous feedback elements are calculated in the same manner as lagged feedback elements, but use a constant lag of zero months, i.e. the two time series contributing to each strength estimate have been sampled at the same calendar month. We use instantaneous feedback elements to avoid running into timing discrepancies.

Our approach of adding up the strength composites of the individual Bjerknes feedback elements is much simpler than the existing framework of Jin et al. (2006)'s Bjerknes stability (BJ) index. The BJ index assesses the overall stability of the coupled equatorial system, and hence its ability to support self-sustained growth of SST anomalies. The BJ index implicitly considers both processes that damp and promote anomaly growth. Damping processes are associated with mean upwelling and thermal damping; amplifying processes are the positive thermocline, zonal advection, and Ekman feedbacks. Our analysis, on the other hand, is confined to the framework of the positive, anomaly-growth-promoting Bjerknes feedback.

In contrast to the Bjerknes feedback elements shown in Figs. 4 and 6, the total Bjerknes feedback corresponds to warm and cold SSTs in the equatorial ocean basin. See Section A.2 of the Appendix for the total Bjerknes feedback associated with westerly/easterly wind anomalies or with deep/shallow thermoclines, or for the case using the “native” composites of each feedback element.

For the previous analysis, our estimate of the composite strengths was the regression parameter that we obtained from robust regression. This method produced strength estimates that preserved a meaningful physical unit. Now, we normalize our feedback strengths to constrain them to values between -1 and $+1$, without units. For the normalization in both the Atlantic and the Pacific basins, we use the values $60K/m$, $0.075N/(m^2K)$, and $11m^3/N$ for the SSH-SST, SST-USTR, and USTR-SSH feedback elements, respectively. Strength estimates whose magnitude exceeds these “cut-off values” are set to ± 1 , depending on their sign. The cut-off values were chosen such that, based on all diagnosed strengths of the same composite in both basins, the magnitude of 95% of all values are smaller or equal to the cut-off value. Last, we add up all normalized feedback strengths contributing to the same composite, and obtain composites of the total Bjerknes feedback with respect to cold and warm SSTs.

Figure 7 shows the total feedback according to our simple measure. Instances where the feedback loop is “broken” by a single feedback element contributing negative values and hence inhibiting anomaly growth are shown in white.

In agreement with previous studies, the total (instantaneous, SST-based) Pacific Bjerknes feedback is dominated by contributions from its positive composite, i.e. it is stronger for warm SSTs (Figs. 7a-c). The feedback forms a closed loop for practically the entire year, indicating that feedback-driven anomaly growth can be active for much of the year. A clear, common seasonality for both the cold and warm composites does not exist. The cold composite is weakest in boreal summer, while the warm composite is diminished at the beginning of the calendar year, indicating that the spring barrier affects positive and negative composites in a slightly different fashion. An interesting detail in the distribution of the composite totals is that the Bjerknes feedback is not closed in the negative composite in the far-eastern basin, not even during the peak time of the Pacific Niño in boreal winter. This is in agreement with studies on different regimes of the Pacific Niño arguing that negative Pacific Niño events (La Niñas) tend to develop in the central basin and hardly ever manifest in the far eastern basin in their extreme form (Takahashi et al., 2011; Dommenges et al., 2013; Capotondi et al., 2015; Takahashi & Dewitte, 2016).

In contrast to the Pacific, the total Atlantic Bjerknes feedback displays a pronounced seasonality (Figs. 7d-f). Both the warm and cold composites are generally strong in summer and early boreal winter, but almost vanish in-between. However, Fig. 7d,e shows that the timing and magnitude of these seasonal peaks is different for the warm and cold composites – asymmetries emerge in the total Atlantic Bjerknes feedback.

During boreal summer, the cold composite is strongest in May and June, while the warm composite lasts a month longer. This agrees with Burls et al. (2012), who argued

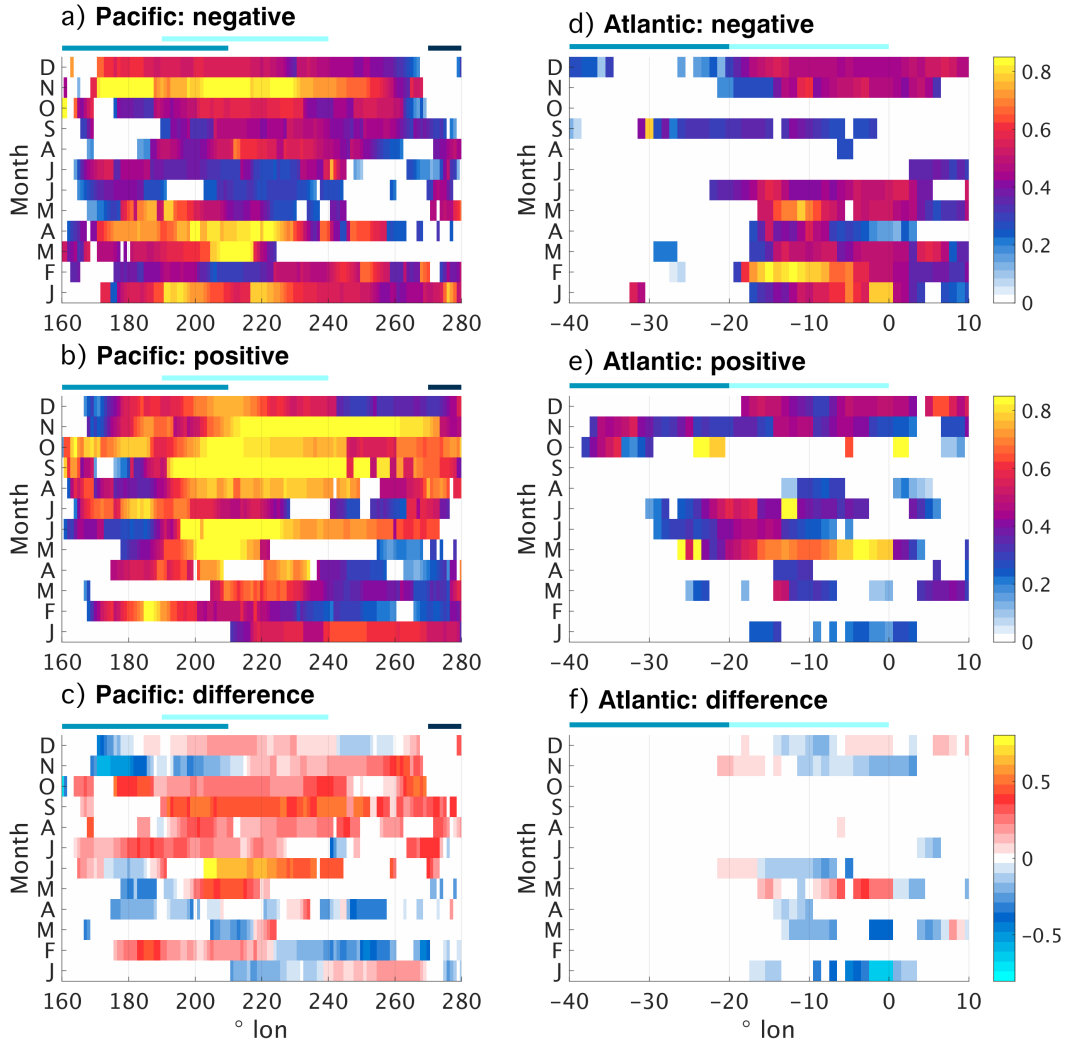


Figure 7: SST-based estimate of the total Bjerknes feedback during 1993-2012 in the Pacific (panels a-c) and Atlantic (d-f), along the equator (x-axis) and stratified into calendar months (y-axis), diagnosed for the OBS dataset group. The top, middle, and bottom rows show the total of all negative composites (a,d), the total of all positive composites (b,e), and the difference between the positive and negative composites of the total Bjerknes feedback (c,f). Feedback strengths of the individual Bjerknes feedback elements have been normalized with $60K/m$, $0.075N/(m^2K)$, and $11m^3/N$ for the SSH-SST, SST-USTR, and USTR-SSH feedback elements, respectively. All feedback elements have been diagnosed without considering lag, and for each composite, they all use the same subsample of the data. These composites were diagnosed from the sign of the SST anomaly. Hence, the positive and negative composites of the total feedback assess the strength of the Bjerknes feedback when SSTs are warm or cold, respectively. The composites of the total feedback are the sum of all normalized composites. See text for additional details on how the total Bjerknes feedback was computed. White indicates that at least one of the feedback elements was negative, i.e. that the Bjerknes feedback loop was not closed. For the difference plots (c,f), white indicates that at least one feedback element was negative in either of the positive or negative composites.

507 that cold summer Niño events are associated with an early onset of the cold tongue, while
508 cold tongue development is delayed during warm events. In boreal winter, cold SST anomalies
509 feed coupled anomaly growth in late winter, with warm SST anomalies lending little
510 support to anomaly growth. These results suggest that the Bjerknes feedback supporting
511 the Atlantic summer Niño relies on contributions from both cold and warm conditions.
512 The winter Niño and possible coupled variability during the first months of the
513 year, on the other hand, is mainly associated with negative SST anomalies, at least within
514 the framework of the Bjerknes feedback.

15 4 Stationarity of the Bjerknes feedback

516 The results of the previous section for the Atlantic appear to be at odds with the
517 results of Lübbecke and McPhaden (2017). One core result of their study is that the SST
518 anomalies associated with warm and cold Atlantic Niño events are effectively mirror images
519 of each other, and that the associated, seasonal Bjerknes feedbacks appear to be
520 symmetric as well. While Lübbecke and McPhaden (2017) find a weak disparity for the
521 positive and negative composites of the strength of subsurface-surface coupling, this asym-
522 metry is not comparable to the pronounced asymmetries associated with the Pacific Niño.
523 Lübbecke and McPhaden (2017) base their analysis on the approximately 50-year period
524 1958-2009, and diagnose feedback strengths using data of at least two months, allow-
525 ing for lags of one month between the involved time series.

526 Our data situation is different. The OBS dataset group spans the 20-year period
527 1993-2012, and we have chosen to resolve our results as highly as possible, taking into
528 account month-to-month variations and a possible dependence on longitude as well.

529 To facilitate a direct comparison and assess the robustness of our results, we calcu-
530 late the index-based monthly composite strengths of all feedback elements for the over-
531 lap period of the OBS and ORAS4 dataset groups 1993-2009 (Fig. 8). The feedbacks
532 are calculated in the same manner as above, but use indices that are averaged over the
533 Atl3/WAtl and Nino3.4/Nino4 regions in the Atlantic and Pacific for SSH and SST/USTR,
534 respectively. Lags are re-diagnosed for the period 1993-2009, and incorporated in the same
535 manner as in Section 3.

536 Agreement between the two dataset groups is excellent in the Pacific (Fig. 8d-f).
537 Timing is mostly congruent, apart from the very sharp drop in the positive composite
538 of the SST-USTR feedback element that occurs in May in the OBS, and in April in the
539 ORAS4 dataset group, consistent with the spring barrier. Additional smaller discrep-
540 ancies are apparent for wind-thermocline coupling, while preserving the overall seasonal
541 structure of the two composites.

542 In the Atlantic, discrepancies are apparent mainly for the SSH-SST and SST-USTR
543 feedback elements. Timing in these cases can be very different. For example, the neg-
544 ative composite of the SSH-SST feedback element peaks in June in ORAS4, but in May
545 in OBS. ORAS4 produces a stronger positive SSH-SST feedback element composite, how-
546 ever largely preserving significances. On the other hand, the dominant features identi-
547 fied in Section 3.1 are evident in both datasets: strong negative composites in early sum-
548 mer, strong positive composites in late summer, weak positive composites during win-
549 ter. In a similar fashion, small discrepancies are apparent for SST-wind coupling, while
550 the general distribution of feedback strengths and asymmetries is present in both dataset
551 groups. In particular, the negative composite is weakest in summer and strongest in late
552 winter, while the positive composite peaks in May.

553 Overall, the OBS and ORAS4 dataset groups agree well in the Pacific, and sup-
554 port the main features identified in our analysis for the Atlantic, while differing in the
555 details there. It follows that the apparent discrepancies between our work and Lübbecke
556 and McPhaden (2017)'s study must be partially attributed to the different analysis pe-

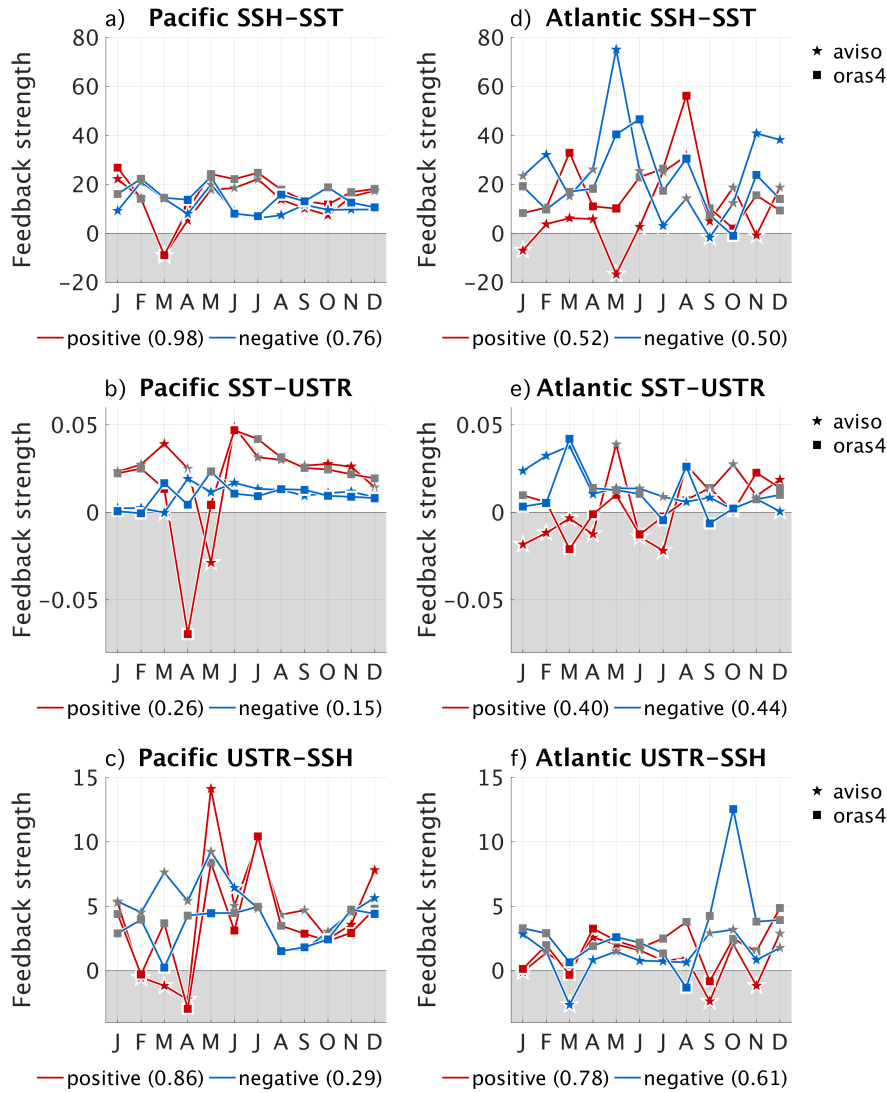


Figure 8: Comparison of feedback element composites in the OBS and ORAS4 dataset groups in the Pacific (left column, panels a-c) and Atlantic (right column, d-f) for the overlap period 1993-2009. The top, middle, and bottom row shows results for the SSH-SST, SST-USTR, and USTR-SSH feedback elements, respectively. Composites of the feedback elements have been diagnosed with respect to *Atl3/WAtl* in the Atlantic, and *Nino3.4/Nino4* in the Pacific, for SSH and SST/USTR, respectively. Line colour indicates the positive and negative composites in red and blue, respectively. Star-shaped and square line markers indicate the OBS and ORAS4 dataset groups. Coloured (grey) line markers show that the respective composite is (not) significant (see text for details). For the two sets of twelve values each associated with the two dataset groups shown here, the resulting anomaly correlation coefficients are given in parentheses below each panel. Note, however, that correlations for small sample sizes can be unreliable. As in Fig. 4, white shading indicates that the associated lags (not shown) were negative.

riods. In agreement with Martín-Rey et al. (2017)'s proposed non-stationarity of the Atlantic Niño itself, the Atlantic Bjerknes feedback appears to vary on decadal time scales.

To illustrate this further, we apply a “running” analysis that highlights low-frequency variations in the composite strengths of the Bjerknes feedback elements and their symmetry. For this analysis, we again use ORAS4 index data confined to the Atl3/WAtl and Nino3.4/Nino4 regions employed above. For consecutive, overlapping periods of 25 years, we re-diagnose our lags and repeat our robust regression analysis, producing composites of running index-based feedback elements. Anomalies are calculated separately with respect to each period of the running analysis. This means that for each 25-year-long sub-period the data is detrended independently, and anomalies are diagnosed relative to the local seasonal cycle of each sub-period. Because both the equatorial Pacific and Atlantic basins are subject to decadal variability, this method could potentially distort our results when a common reference frame for the anomalies is required. However, repeating our analysis without detrending the data yielded practically the same results in the Pacific, and minor deviations in the Atlantic (not shown). Because of this and consistency, we calculate the composite strengths of our feedback elements in the same manner as above, including a “running” detrending.

Figures 9 to 11 show the results of our running analysis. The Pacific Bjerknes feedback elements exhibit low-frequency variations (Fig. 9). All feedback elements, and generally both the positive and negative composites, show a basic change that occurs around the early 1970s and is characterized by (i) a weakening subsurface-surface coupling; (ii) SST-wind coupling that appears to decrease for the negative composite, but shows no clear change for the positive composite; and (iii) strengthening wind-thermocline coupling that is more apparent in the negative composite than in the positive composite. These changes are in rough agreement with the “Pacific climate shift” that took place in 1976/77 (Graham, 1994; Trenberth & Hurrell, 1994; Ding et al., 2013). A secondary climate shift in the Pacific occurred in 1998/99, exchanging intense, eastern warm events for a more moderate regime characterized by warm events that occur closer to the center of the basin and are reduced in amplitude (Lübbecke et al., 2014; Hu et al., 2012). Both climate shifts have been related to the low-frequency variability of the Pacific Decadal Oscillation (Minobe, 1997, 2000; Mantua & Hare, 2002, PDO). The 1998/99 shift, however, is not resolved in our analysis, since our datasets span only twelve years of the post-shift era, which constitutes half a period of our running analysis.

As for the OBS-based subsurface-surface coupling discussed in Section 3.1, our results for the SSH-SST feedback element are not consistent with Zhu et al. (2015). Seasonalities of the two results disagree (with our SSH-SST feedback elements being strongest in April-June, while Zhu et al. (2015)’s thermocline feedback consistently peaks in September-December). Periods of enhanced subsurface-surface coupling, too, do not agree. In particular, our results indicate that the SSH-SST feedback element was strongest in the period spanning the 1960s to 1990s, for both the positive and the negative composites. Zhu et al. (2015) find fairly consistent thermocline feedbacks in winter, while relationships in boreal spring were very weak in the 1960s-1980s, and again in the mid-1990s to early 2000s. We suspect that methodological differences will most likely explain the apparent discrepancies in seasonality and timing of exceptionally weak or strong relationships: Zhu et al. (2015) used correlations as a measure for the sensitivity between thermocline depth – theirs diagnosed from the depth of the 20°C-isotherm, ours gleaned from SSH – their running analysis periods had lengths of eleven years in contrast to our 25, and they did not separate positive and negative composites from each other.

While the overall strength composites of the Pacific feedback elements change, the asymmetry between them is largely preserved (Fig. 10). An exception is the SST-USTR feedback element (Fig. 10b), which displays varying ratios of the positive and negative strength composites.

In the Atlantic, all feedback elements vary substantially on decadal time scales (Fig. 11). Even when focusing on the important summer and winter seasons, the symmetries of the Bjerknes feedback elements change from decade to decade. Subsurface-surface cou-

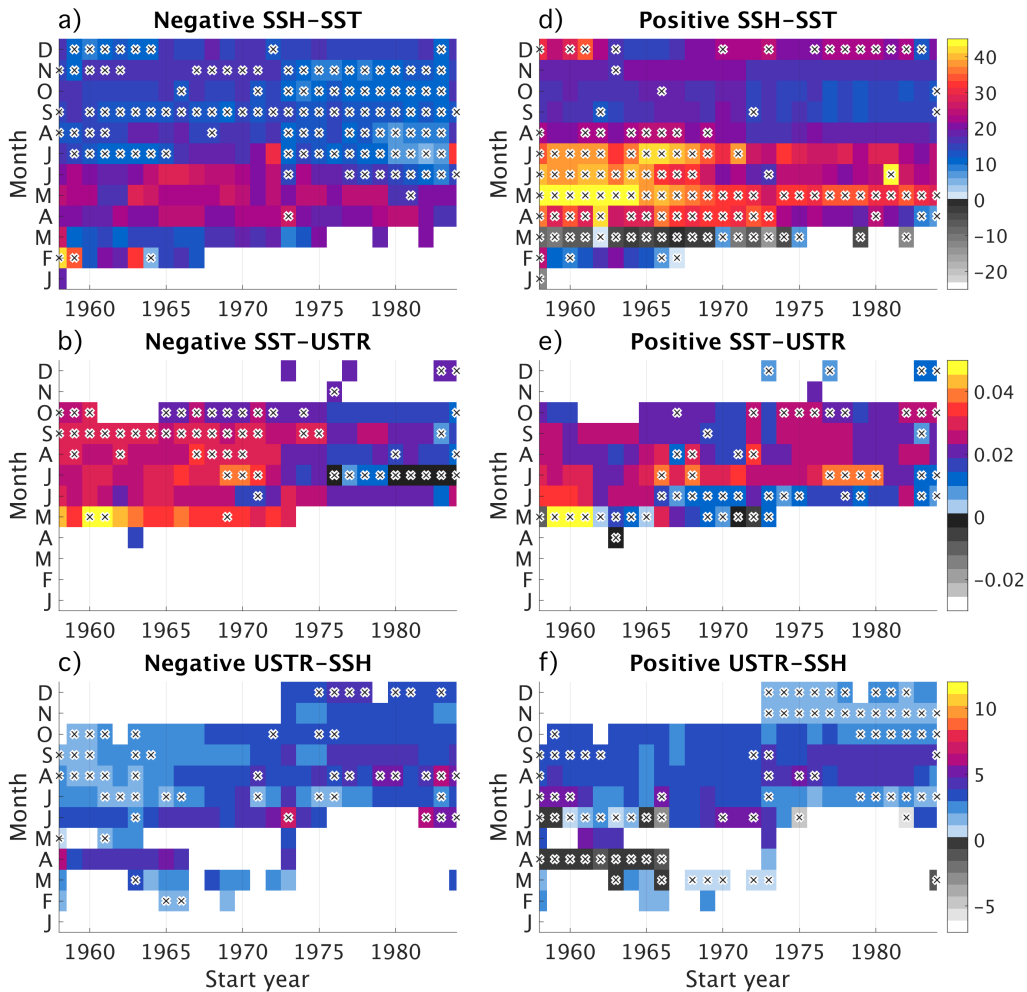


Figure 9: Decadal variations of the composites of the Pacific Bjerknes feedback elements, based on the ORAS4 dataset group for running sub-periods (*x*-axis, shown dates label the start of each analysis period) and each calendar month (*y*-axis). The left and right columns show variations of the negative (panels a-c), and positive composites (d-f). Rows show variations of the individual feedback elements, for the SSH-SST (a,d), SST-USTR (b,e), and USTR-SSH feedback elements (c,f). Composites have been diagnosed with respect to *Nino*_{3.4} for SSH and SST, and with respect to *Nino*₄ for USTR. Crosses indicate that the diagnosed feedback strength is significant (see text for details). Anomalies have been diagnosed with respect to the running analysis period. The width of the running window is 25 years.

pling, for example, was the dominant feedback element during the period 1993-2012 (Figs. 10d and 11a,d). On decadal time scales, this is not necessarily the case. The SSH-SST feedback element during early boreal summer was dominated by the positive composite in the 70s and 80s, and only recently started to draw more strongly from the negative composite. Similarly, the July feedback used to be strongly influenced by the negative composite, and only started to be dominated by the positive composite in the mid-80s. Subsurface-surface coupling in winter, too, has not always been exclusively supported by the negative composite. These shifting symmetries suggest that the relative contributions of positive and negative composites to the SSH-SST feedback element are highly variably on decadal time scales. In a similar fashion, the overall strengths and symme-

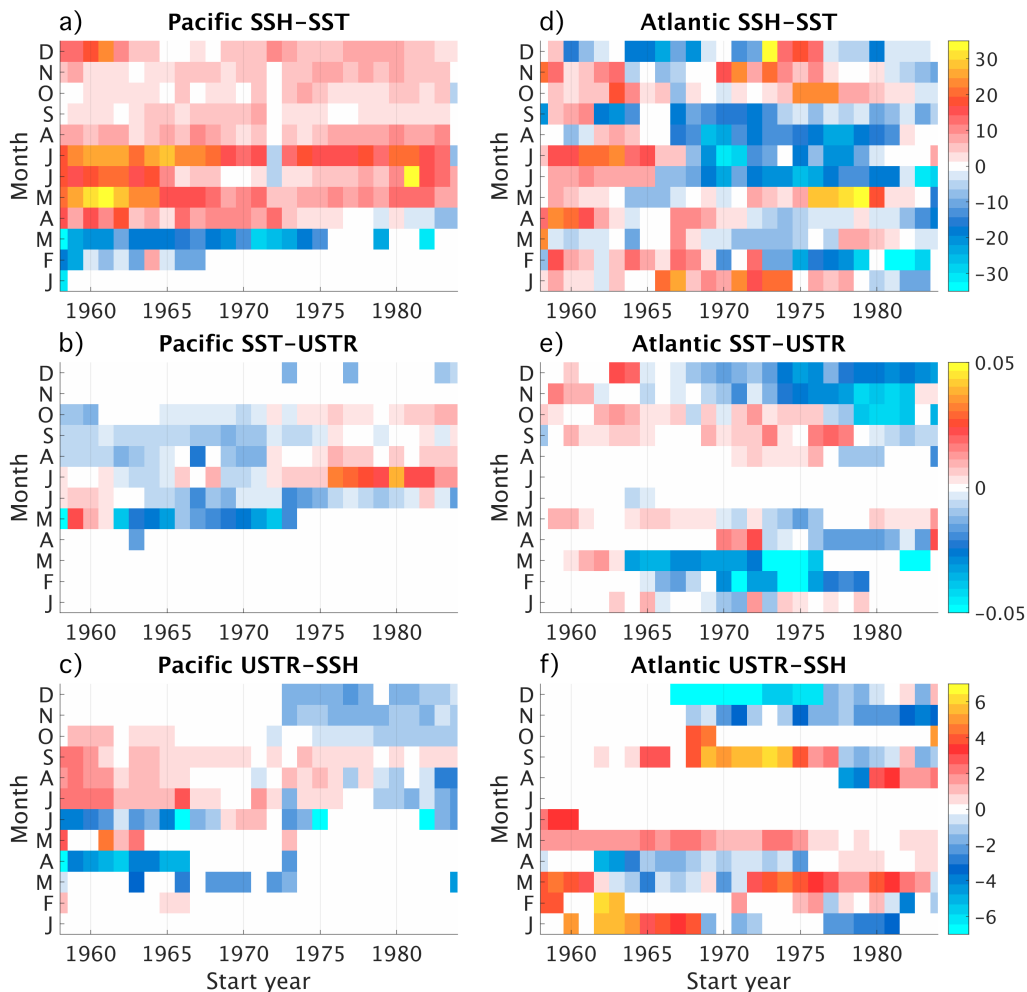


Figure 10: Similar to Fig. 9, but showing the difference between positive and negative composites in the Pacific (left column, panels a-c) and the Atlantic (right column, d-f), for the SSH-SST (a,d), SST-USTR (b,e), and USTR-SSH (c,f) feedback elements.

tries of the two wind-related feedback elements changed over the course of the past 50 years.

We conclude that the Atlantic Bjerknes feedback and its symmetry are non-stationary. Keep in mind, however, that the absolute numerical values shown here might be subject to large uncertainties, due to rather short analysis periods and inhomogeneities in the data available to the ORAS4 reanalysis. Hence, while our analysis clearly demonstrates that the Atlantic Bjerknes feedback does vary on decadal time scales, the magnitudes of these variations may not be well constrained by our data base.

An important consequence of our findings is that diagnosing the strength of the Atlantic Bjerknes feedback on the basis of a rather long dataset might obscure crucial, albeit non-stationary details, in the same manner that averaging over long time scales will effectively lose information on short-time scale processes.

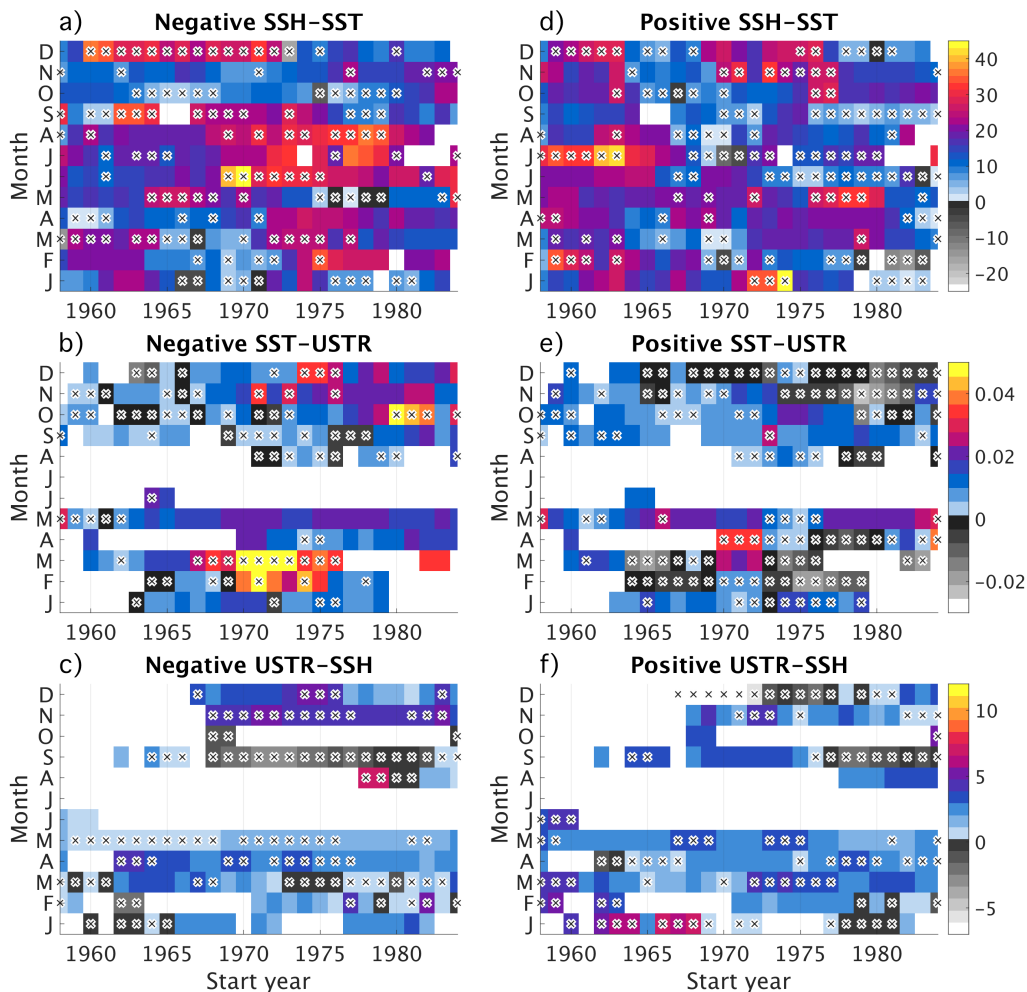


Figure 11: Same as Fig. 9, but for the Atlantic. Feedback strengths have been diagnosed with respect to *Atl3* for SSH and SST, and with respect to *WAtl* for USTR.

5 Summary and Discussion

5.1 Summary

We have studied the symmetry of the Atlantic and Pacific Bjerknes feedbacks, using robust regression to diagnose the strength of the three feedback elements that form the closed Bjerknes feedback loop – the SSH-SST, SST-USTR, and USTR-SSH feedbacks that relate to coupling between the subsurface and surface, SST and wind, and wind and thermocline depth, respectively. Our analysis of the Pacific agrees well with previous research and lends credibility to our results for the Atlantic.

During the recent period 1993-2012 in the Atlantic, asymmetries emerge for all feedback elements during boreal winter and summer, when the Atlantic Bjerknes feedback forms a closed positive feedback loop. During these months, the strengths of all feedback elements are positive, for both types of composites. While both positive and negative composites are strong during boreal summer, the positive composites are much weaker during boreal winter. The two wind-related feedback elements are weaker than their Pacific counterparts, and produce summer and winter asymmetries to a varying degree. The total Atlantic Bjerknes feedback is dominated by the negative strength composites in bo-

650 real winter, and shows mixed influences from positive and negative composites in sum-
651 mer.

652 Comparing our work with Lübbecke and McPhaden (2017)'s study suggested that
653 the results of a feedback analysis in the equatorial Atlantic are highly sensitive to the
654 chosen analysis period. Indeed, our ORAS4-based running analysis of the Atlantic Bjer-
655 knes feedback elements provides further evidence for the non-stationarity of the Atlantic
656 Bjerknnes feedback. One important result of our study is that conclusions drawn for feedback-
657 related issues in the tropical Atlantic will always have to explicitly consider the analy-
658 sis period that they are based on.

659 5.2 Discussion

660 Taking into account the proposed non-stationarity of the Atlantic Bjerknnes feed-
661 back, our study serves as a reminder that processes in the coupled equatorial Atlantic
662 climate system can unfold on substantially smaller spatiotemporal scales than their Pa-
663 cific counterparts. We concede that using even monthly mean data for our analysis might
664 be insufficient to resolve the rapid processes that establish the intricate variability in the
665 tropical Atlantic.

666 Another problem that we ran into are the very small sample sizes as soon as anal-
667 ysis periods are shorter than 30 years. For our analysis, we used period lengths between
668 20 and 25 years. Separating the data into positive and negative composites left us with
669 data pools that rarely exceeded the size of ten to twelve entries per analysis step. To re-
670 duce the arbitrariness of our results, we chose robust regression as our analysis method.
671 As our results have demonstrated, decreasing the temporal and spatial extent of our anal-
672 ysis domain reveals important details of the mechanisms that govern the tropical Atlantic.

673 A related issue is that our results concerning the stationarity of the Bjerknnes feed-
674 back elements rely on a single dataset, i.e. ORAS4, which in addition is a reanalysis. It
675 would be interesting to assemble additional datasets, preferentially based on direct ob-
676 servations, and repeat our analysis.

677 To conclude our study, we seek to consolidate the asymmetries that we detected
678 in the recent, OBS-based Pacific and Atlantic Bjerknnes feedback with the symmetry of
679 SST variability in the central equatorial ocean basins. Our analysis to this effect is based
680 on SST "events". To identify an SST event, we first calculate the anomalies of the time
681 series with respect to the linear trend and the seasonal cycle. For both positive and neg-
682 ative anomalies separately, we calculate the partial standard deviation. In either case,
683 we select all instances for which anomalies exceed 0.5 times the partial standard devi-
684 ation. These are potential contributions to events. We next identify periods during which
685 potential contributions have the same sign for at least three consecutive months. These
686 "persisting" anomalies form an SST event. For each event, the anomaly of the largest
687 magnitude provides the strength of the event. We diagnose events in the same 4° lon-
688 gitude $\times 4^\circ$ latitude boxes of SST data that we used for our previous analysis.

689 Figure 12 shows the average strength of positive and negative SST events along the
690 equatorial Pacific and Atlantic, in the same period that we used to diagnose our lagged
691 composite strengths in Section 3 (1993-2012). During boreal winter in the Pacific, the
692 well-known amplitude asymmetry emerges (Fig. 12a). East of $170^\circ W$ ($190^\circ E$), Pacific
693 warm events are substantially stronger than cold events, especially so in the Nino3.4 re-
694 gion. The difference between average warm and cold events can be as high as $1^\circ C$.

695 In contrast, SST events are much more symmetric in the Atlantic. This agrees with
696 Lübbecke and McPhaden (2017)'s findings. Summer Niños during the recent period seem
697 to have been slightly dominated by cold events (Fig. 12b), with a maximum difference
698 between negative and positive SST events of about $0.5^\circ C$. This corresponds to the asym-

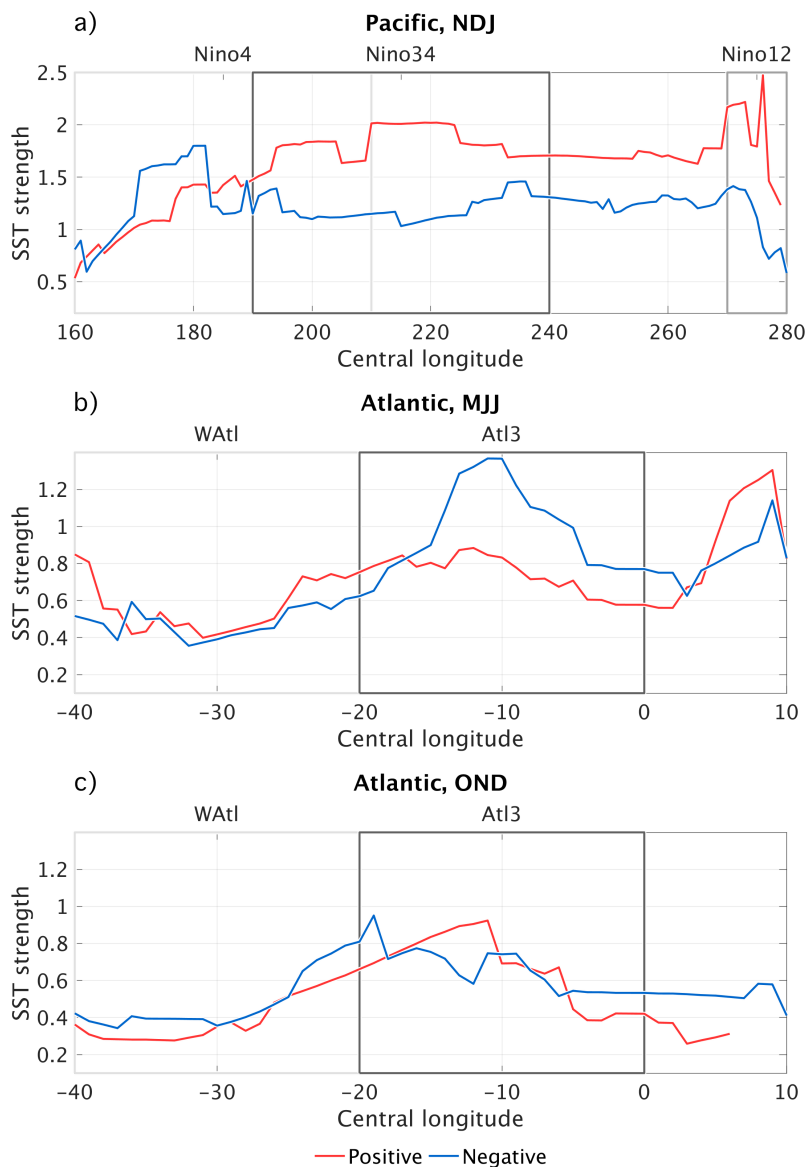


Figure 12: Zonal distribution of the ERSST-based average strength of positive (red) and negative (blue) SST events for the period 1993-2012 (see text for details on how SST events have been diagnosed). SST events have been considered along the equatorial Pacific when they occurred between November and January (NDJ, panel a), and along the equatorial Atlantic when they occurred between May and July (MJJ, b), or between October and December (OND, c). Note that because our analysis period is very short (to match the period for which we diagnosed the lagged, OBS-based feedback element strengths), the number of events diagnosed for each longitude box is smaller than ten. Note also that the y-axes span different strengths for the Pacific and Atlantic analysis. Overlaid rectangles indicate the Nino4, Nino3.4, and Nino1.2 (WAtl and Atl3) regions in the Pacific (Atlantic).

metry of subsurface-surface coupling that we identified in Fig. 5a, where the SSH-SST feedback element is clearly stronger for shallow thermoclines (associated with reduced SSTs) than for deep thermoclines (warm SSTs). Considering the total Bjerknes feedback

702 with respect to cold and warm SST conditions softens the relationship (cf. Fig. 7d-f).
703 While the total Bjerknes feedback was indeed stronger when diagnosed with respect to
704 cold SSTs in June, the response to warm SSTs dominated in May and July. (The ab-
705 solute magnitude of this asymmetry depends on which method is chosen to diagnose the
706 total feedback, cf. Section A.2 in the Appendix. All methods, however, agree on the neg-
707 ative composite dominating June, and the positive composite dominating July. This is-
708 sue again raises the question whether it is appropriate to weight all feedback elements
709 equally when calculating the total Bjerknes feedback.) Both measures – the strength of
710 subsurface-surface coupling by itself, including lags, and the estimate of the instantane-
711 ous total Bjerknes feedback – indicates a weak correspondence between the symmet-
712 ry of the (total) Bjerknes feedback and the observed, weak amplitude asymmetry.

713 In contrast, the Atlantic winter Niño is mostly symmetric (Fig. 12c), even though
714 the total Bjerknes feedback as well as the SSH-SST and USTR-SSH feedback elements
715 are clearly dominated by their negative composites during boreal winter (Figs. 7f, 5d,f).
716 While the (total) Bjerknes feedback is asymmetrical in winter, it does not project onto
717 the observed SST variability – indicating that the Bjerknes feedback plays a minor role
718 in establishing the Atlantic winter Niño. This in agreement with Dippe et al. (2018) who
719 have found that dynamical, Bjerknes feedback-related contributions to Atl3 SST vari-
720 ability do increase in winter, but are much smaller in magnitude than in summer. Rather
721 than being a dynamically driven phenomenon as in the Pacific, the Atlantic winter Niño
722 appears to be much more susceptible to atmospheric noise forcing.

723 Last, we briefly assess how stationary the symmetry of the Pacific and Atlantic Niños
724 are. Figure 13 shows how the strength of positive and negative SST events varied over
725 the past five decades, using again sliding analysis windows of a length of 25 years each,
726 considering both Pacific events in boreal winter, and Atlantic events in boreal summer.

727 In the Pacific, the basic asymmetry between warm and cold events did not change
728 over the past 50 years (Fig. 13a-c). However, how much warmer the warm events east
729 of $120^{\circ}W$ ($240^{\circ}E$) are than the corresponding cold events is indeed varying from decade
730 to decade. The strongest asymmetry so far occurred in the 1970s and 1980s, during a
731 warm phase of the Pacific Decadal Oscillation, with average warm events exceeding av-
732 erage cold events by more than $1.5^{\circ}C$.

733 In the Atlantic, general characteristics of equatorial SST events have not changed
734 dramatically over the past 50 years, while minor variations do occur (Fig. 13d-f). The
735 location of the strongest cold SST events, for example, appears to have slightly shifted
736 from the western into the central Atl3 region (Fig. 13d). Additionally, cold SST events
737 have become stronger within the last 30 years. Warm SST events, on the other hand,
738 have clearly weakened over the past 50 years (Fig. 13e), in agreement with Tokinaga and
739 Xie (2011). The resulting effect is that cold events in the eastern equatorial Atlantic dom-
740 inated the summer Niño during recent decades, while the 1960s and 1970s seem to have
741 seen stronger warm events (Fig. 13f). An interesting detail of this analysis is that asym-
742 metries identified in the Atl3 region do not extend homogeneously towards the eastern
743 edge of the basin. Rather, positive SST events become more pronounced close to the African
744 coast.

745 These findings complement our results on the decadal modulation of the Bjerknes
746 feedback's strength and could contribute to the understanding of decadal variability in
747 the tropical Pacific and Atlantic. In both ocean basins, a change in the characteristics
748 of the respective Niños has been noted in the 1970s. For the Pacific, this shift has been
749 related to the Pacific Decadal Oscillation (Mantua & Hare, 2002). The 1980s and 1990s
750 were characterized by strong eastern Pacific El Niño events, while the preceding and sub-
751 sequent decades featured weaker events that occurred more frequently and were more
752 often located in the central equatorial Pacific (An & Wang, 2000; Chung & Li, 2012).
753 In agreement with the 1976/77 climate shift, all Pacific Bjerknes feedback elements changed

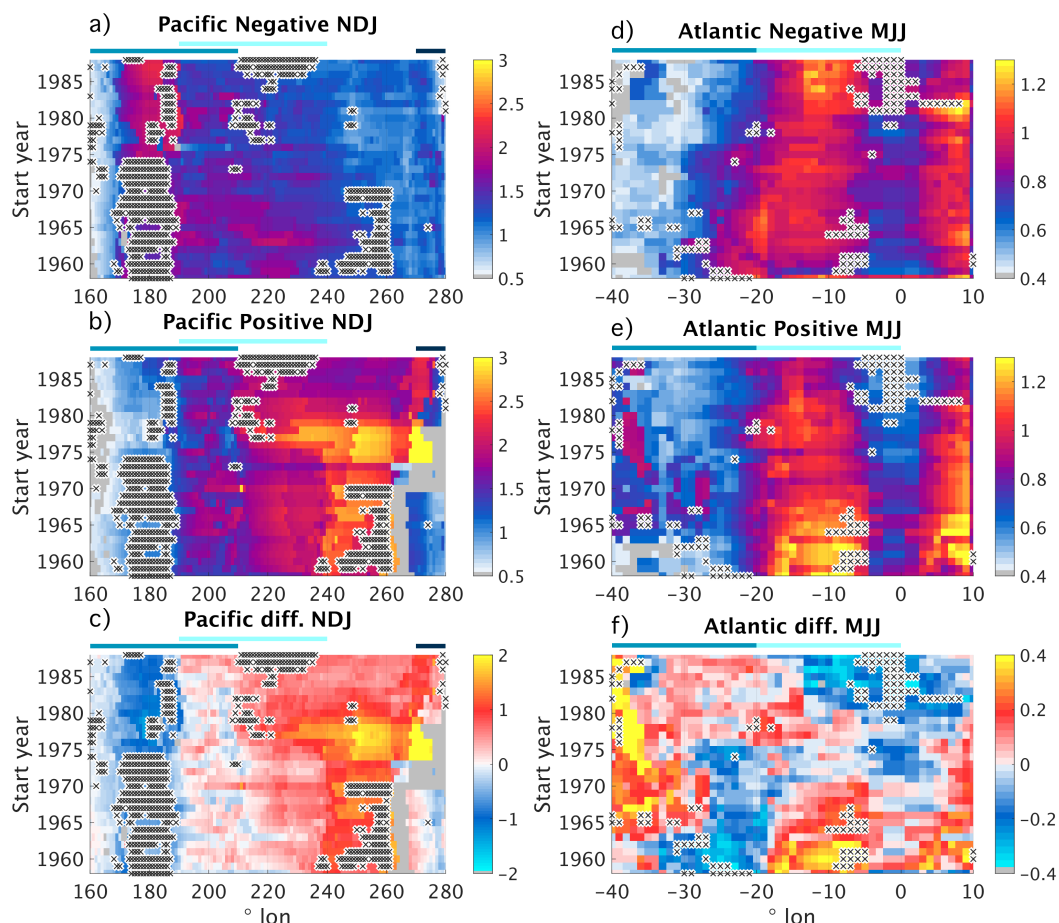


Figure 13: Decadal variations of ERSST-SST event strengths along the equator (x -axis) for running sub-periods (y -axis, shown dates label the start of each analysis period) in the Pacific (left column, panels a-c) and the Atlantic (right column, d-f). SST events have only been considered when they peaked in November-January (NDJ) and May-July (MJJ) in the Pacific and Atlantic, respectively. The left, middle, and right columns show the strength of negative and positive SST events, as well as their difference, respectively (see text for details on how SST events have been diagnosed). Black crosses indicate that average negative and positive event strengths are significantly different from each other, according to a Student t test and the significance level 0.1. The length of each sub-period is 25 years, and events have been diagnosed with respect to each sub-period.

in the 1970s (Fig. 9a-c), and the asymmetry between warm and cold events increased correspondingly (Fig. 13c).

For the tropical Atlantic, earlier studies on decadal time scales focused mainly on the variability of the interhemispheric SST gradient (Mehta & Delworth, 1995; Mehta, 1998; Wainer et al., 2008), while recent work started to address decadal variations in the eastern equatorial Atlantic SST variability with bearings on the Atlantic Niño. Losada and Rodríguez-Fonseca (2016) describe differences in the spatial pattern of the Atlantic Niño before and after the 1970s, with positive SST anomalies restricted to the eastern equatorial Atlantic in the earlier and a more basin-wide SST signal in the later period. Additionally, Tokinaga and Xie (2011) find a weakening of SST variability in the eastern equatorial Atlantic over the time period 1950 to 2009. These changes are roughly

765 reflected in the weakening of the SSH-SST feedback element's positive composite (Fig.
766 11d) and the associated weakening of the warm events (Fig. 13e).

767 Overall, we have shown that the Atlantic Bjerknes feedback appears to be config-
768 ured in subtly different ways for positive and negative Atlantic Niño events, both dur-
769 ing summer and winter. While these asymmetries project weakly onto the symmetry of
770 summer SST events, the winter Niño is much more susceptible to other influences. Both
771 the Atlantic Bjerknes feedback and the symmetry of the Atlantic Niño appear to vary
772 on decadal time scales.

773 A Appendix

774 A.1 Using the same lags for positive and negative composites

775 In the main text, we presented composites of the Bjerknes feedback elements and,
776 as discussed in the "Methods" section, included feedback lags that we previously diag-
777 nosed for our full anomaly time series, disregarding the sign of the forcing variable. Here,
778 we assess whether using these lags enhances our feedback strengths as expected and whether
779 it affects positive and negative composites equally. We do this by repeating our regres-
780 sion analysis, but this time using a constant lag of 0 months for each feedback element
781 ("instantaneous feedback elements"), at all locations and during all months. We then
782 subtract the lagged feedback elements from the instantaneous feedback elements to as-
783 sess when including lags into our analysis enhances the composite of the feedback ele-
784 ment (negative difference). Note that the positive and negative composites that we use
785 are identical in both cases, because they are based on the forcing variable of each feed-
786 back element. It is the offset in time of the response variable that differs between the
787 two cases.

788 Figures A.1 and A.2 show the difference between the instantaneous and the lagged
789 feedbacks. Including feedback lags into our analysis does enhance the composites of the
790 Bjerknes feedback elements in general. Calculating the mean across all pixels contribut-
791 ing to Figs. A.1 and A.2 yields, both in the Atlantic and the Pacific, negative values for
792 all feedback elements and both composites, except for the positive composite of the At-
793 lantic USTR-SSH feedback element. However, while the overall effect is in agreement with
794 our goals, including the lags can have unexpected local effects.

795 In the Pacific, including lags into our analysis generally enhances the strength of
796 the feedback composites (Fig. A.1), with three notable exceptions: First, the negative
797 SSH-SST composite appears to be degraded by lags to the east of the Niño3.4 region for
798 the entire year (Fig. A.1a). This indicates that subsurface-surface coupling operates in
800 a slightly different manner for negative Pacific Niño events, which in turn is perhaps re-
801 lated to the different average thermocline depths associated with warm and cold Pacific
802 Niños. Second, the negative SST-USTR feedback element composite is degraded by lags
803 during the spring barrier. This, however, is of no practical concern, since the overall cou-
804 pling during boreal spring in any case is decreased. Third, in a similar fashion, the pos-
805 itive USTR-SSH feedback element during the spring barrier clearly suffers when incor-
806 porating lags.

806 Figure A.2 shows that the impact of lags on Atlantic feedback strengths is less straight
807 forward than in the Pacific. While lags generally enhance the feedback strengths, they
808 can have severely detrimental effects in certain regions and seasons. Three notable cases
809 are: First, similar to the Pacific, the lags of the SSH-SST feedback element differ from
810 each other; unlike in the Pacific, they do so during the crucial month of May (Fig. 2a,d
811 of the main text). Here, lags strongly decrease the positive composite of the SSH-SST
812 feedback element. The overall effect of this degradation, however, is small, since the cor-
813 responding lagged negative composite is clearly enhanced by the incorporation of lags.
814 The overall May asymmetry between the positive and negative composites of the SSH-

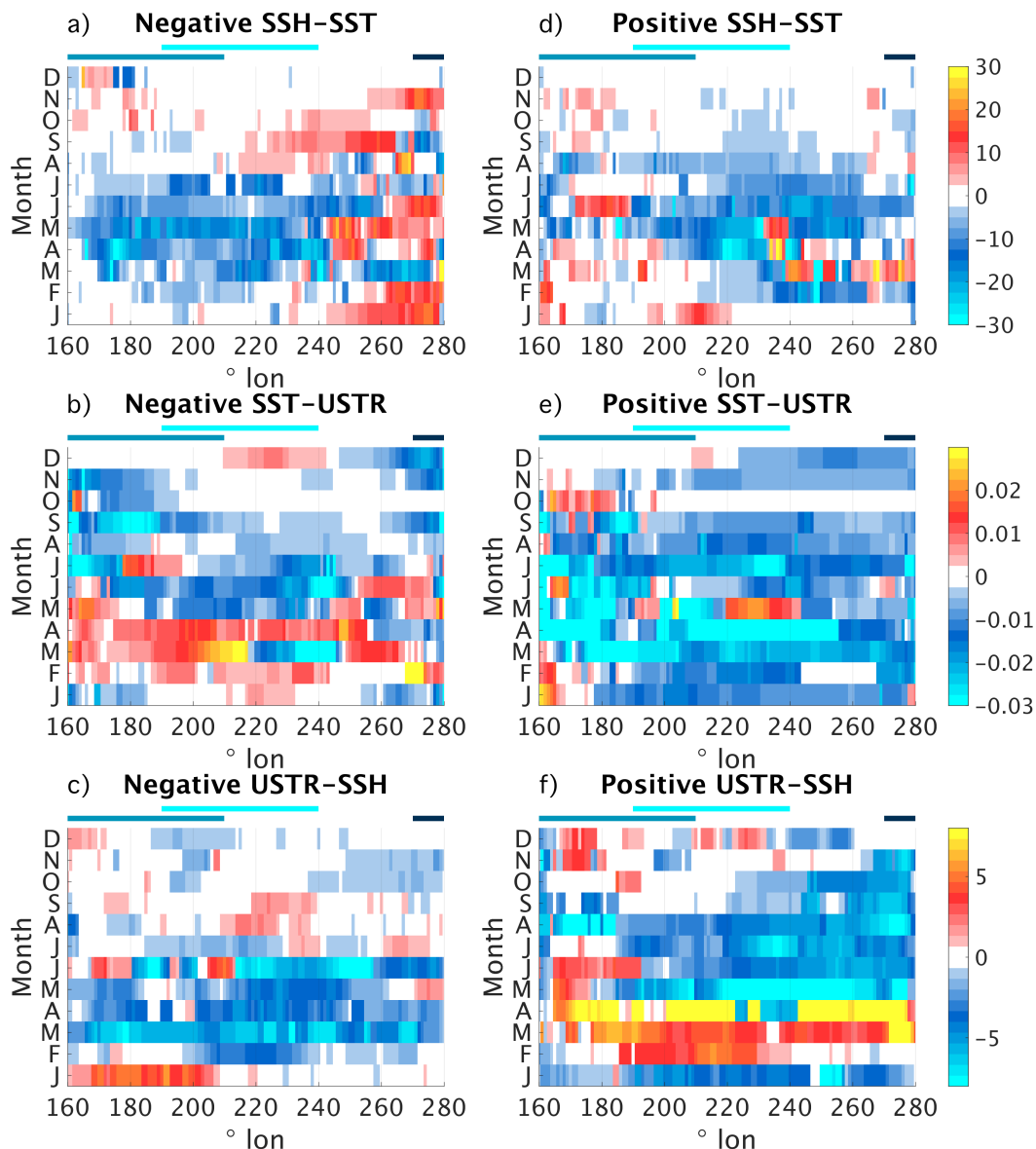


Figure A.1: OBS-based comparison between lagged and instantaneous feedback element composites in the Pacific, along the equator (x -axis) and stratified into calendar months (y -axis). The instantaneous feedback elements have been diagnosed in the same manner as the lagged feedback elements shown in the main text, but using a constant lag of 0 months when performing robust regression. Positive values indicate that the instantaneous composites are stronger than the lagged composites. Coloured bars below the title indicate the zonal extent of the Nino4, Nino3.4, and Nino1.2 regions blue, light blue, and dark blue, respectively.

815 SST feedback element remains intact. Second, the negative SST-USTR feedback element
 16 composite suffers when using lags in June and July (Fig. A.2b). These months, however,
 17 are characterized by weakly negative lags (Fig. 2e of the main text) and we expect that
 818 they do not contribute substantially to the closed Atlantic Bjerknes feedback. Third, in
 819 a similar fashion, the August degradations of both the positive and the negative USTR-
 20 SSH feedback element composites are of no practical concern.

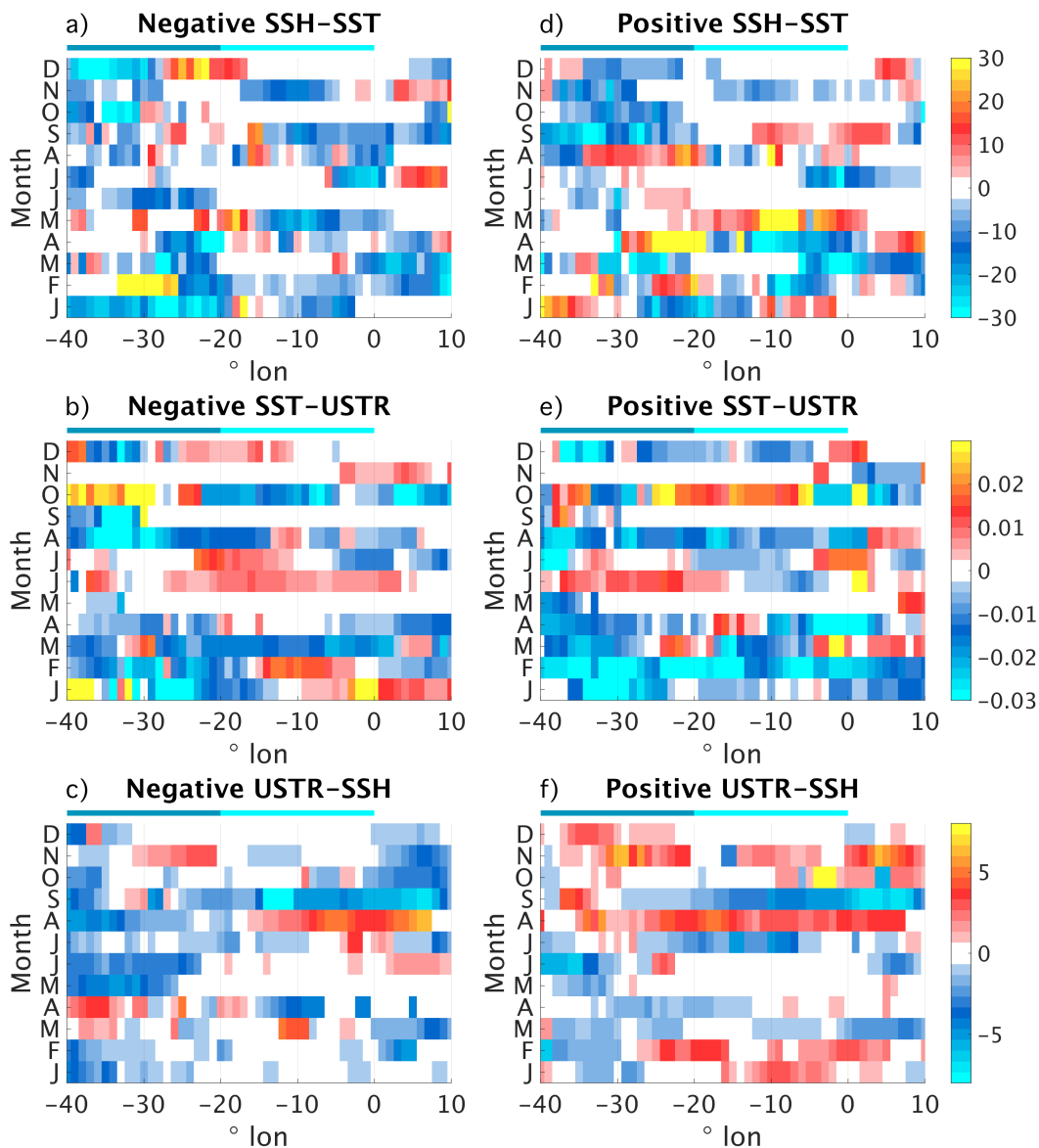


Figure A.2: Same as Fig. A.1, but for the Atlantic. Overlaid coloured rectangles indicate the zonal extent of the WAtl and Atl3 regions.

Overall, we conclude that using a constant lag for positive and negative feedback element strength composites does, in general, enhance the strength of the feedbacks as expected. When exceptions occur, they are usually related to negative lags that are of little importance for the closed Bjerknes feedback.

Nevertheless, this simple comparison serves to demonstrate again how diverse the mechanisms are that produce the variability of the Atlantic and Pacific Niños, and that it may not be justified to make equivalent assumptions for warm and cold events.

A.2 On the sensitivity of the total feedback to different diagnosis methods

In addition to the SST-based total feedback shown in the main text, we present three ancillary manifestations of the total Bjerknes feedback in Figs. A.3-A.5.

We diagnose the total Bjerknes feedback in two ways, depending on which subset of our data we select to calculate the strength of the three feedback elements contributing to the total feedback composites.

1. “*Constant-composite*” total feedbacks (panels a-b, d-e in Figs. A.3 to A.5): Composites of the individual Bjerknes feedback are identical. This is the method that was used to diagnose the SST-based total feedback shown in the main text. Total feedbacks of this class are directly linked to a single variable. The SST-based total feedbacks are a measure of the strength of the total feedback *when SST anomalies are either positive or negative*. Likewise, negative/positive USTR-based and SSH-based total feedback composites are associated with westerly/easterly wind stress anomalies and shallower/deeper thermocline depths, respectively.
2. “*Variable-composite*” total feedbacks (panels c,f in Figs. A.3 to A.5): For each feedback element, we use individual, “native” composites that depend on the specific feedback element. This method is congruent with the way we diagnosed our lagged feedback elements in Section 3.1 of the main text. Composites for the SSH-SST, SST-USTR, and USTR-SSH feedback elements are based on the sign of SSH, SST, and USTR anomalies, respectively. Again, this means that positive composites of any two feedback elements do not necessarily share the same base data.

In the Pacific, results are consistent between different manifestations of the total Bjerknes feedback (panels a-c of Figs. A.3 to A.5). Seasonalities of positive and negative total feedback composites are well comparable for all manifestations, as are the relative strengths. This highlights the large-scale character of the Pacific Niño, showing that SSH, SST, and USTR vary largely synchronously when measured at the same calendar months during periods when the total Bjerknes feedback is strong. On the other hand, constant-composite feedbacks can be twice as strong as the corresponding variable-composite feedbacks, according to our simple measure. This perhaps indicates that using constant composites prevents compensation effects between the three individual feedback elements. Providing consistent composites for all feedback elements in the constant-composite case emphasizes interactions between all three variables, while the variable-composite case focuses on interactions of only two variables, ignoring the third link in the Bjerknes feedback loop.

In the Atlantic, results are largely consistent for different manifestations of the total Bjerknes feedback (panels d-f of Figs. A.3-A.5d-f). Irrespective of the compositing type, total feedbacks are stronger when they are associated with negative anomalies in boreal winter, and weaker in summer. As in the Pacific, details differ between the three constant-composite manifestations, and the variable-composite manifestation produces weaker total feedbacks. A prominent example are the positive composites of the constant-composite manifestations in July. For this calendar month, the total feedback is pronounced for deep thermoclines, moderately strong for warm SSTs, and effectively absent for easterly wind stress anomalies. However, as our base data pool only spans 20 years in total and we subdivide these further into positive and negative composites, we expect that the details of our analysis are subject to large uncertainties.

Overall, qualitative results are consistent when comparing different manifestations of the total Bjerknes feedback, lending some credibility to our method. While details differ for the three constant-composite feedbacks, results are much more sensitive to the

choice of either constant or variable composites when diagnosing the individual feedback elements contributing to the total feedback.

Acknowledgments

This study has been supported by the German Ministry for Education and Research (BMBF) through MiKlip2, subproject 01LP1517D (ATMOS-MODINI) and SACUS (03G0837A), and by the European Union 7th Framework Programme (FP7 2007–2013) under Grant agreement 603521 PREFACE project. RJG is also grateful for continuing support from GEOMAR. The data used in this study can be obtained GEOMAR's OPeNDAP Service at <https://data.geomar.de>. Help is provided at the bottom of the page.

References

- An, S.-I., & Wang, B. (2000). Interdecadal Change of the Structure of the ENSO Mode and Its Impact on the ENSO Frequency. *Journal of Climate*, 13(12), 2044–2055. Retrieved from [https://doi.org/10.1175/1520-0442\(2000\)013\(12\)2044:ICOTSO.0.CO;2](https://doi.org/10.1175/1520-0442(2000)013(12)2044:ICOTSO.0.CO;2)
- Ashok, K., & Yamagata, T. (2009). The El Niño with a difference. *Nature*, 461(May), 481–484. doi: 10.1038/461481a
- Balmaseda, M. A., Mogensen, K., & Weaver, A. T. (2012). Evaluation of the ECMWF ocean reanalysis system ORAS4. *Quarterly Journal of the Royal Meteorological Society*, 139(674), 1132–1161. Retrieved from <https://doi.org/10.1002/qj.2063> doi: 10.1002/qj.2063
- Bjerknes, J. (1966). A possible response of the atmospheric Hadley circulation to equatorial anomalies of ocean temperature. *Tellus*, 18(4), 820–829. Retrieved from <https://www.tandfonline.com/doi/full/10.3402/tellusa.v18i4.9712> doi: 10.3402/tellusa.v18i4.9712
- Bjerknes, J. (1969). Atmospheric Teleconnections From The Equatorial Pacific. *Monthly Weather Review*, 97(3), 163–172. Retrieved from [http://journals.ametsoc.org/doi/abs/10.1175/1520-0493\(1969\)097\(03\)163:ATFTEP.3.CO;2](http://journals.ametsoc.org/doi/abs/10.1175/1520-0493(1969)097(03)163:ATFTEP.3.CO;2) doi: 10.1175/1520-0493(1969)097(03)163:ATFTEP.3.CO;2
- Burls, N. J., Reason, C. J. C., Penven, P., & Philander, S. G. (2011). Similarities between the tropical Atlantic seasonal cycle and ENSO: An energetics perspective. *Journal of Geophysical Research: Oceans*, 116(C11), C11010. Retrieved from <http://dx.doi.org/10.1029/2011JC007164> doi: 10.1029/2011JC007164
- Burls, N. J., Reason, C. J. C., Penven, P., & Philander, S. G. (2012). Energetics of the Tropical Atlantic Zonal Mode. *Journal of Climate*, 25(21), 7442–7466. Retrieved from <http://dx.doi.org/10.1175/JCLI-D-11-00602.1> doi: 10.1175/JCLI-D-11-00602.1
- Cane, M. A. (1984). Modeling Sea Level During El Niño. *Journal of Physical Oceanography*, 14(12), 1864–1874. Retrieved from [http://dx.doi.org/10.1175/1520-0485\(1984\)014\(12\)1864:MSLDEN.0.CO;2](http://dx.doi.org/10.1175/1520-0485(1984)014(12)1864:MSLDEN.0.CO;2)
- Capotondi, A., Wittenberg, A. T., Newman, M., Di Lorenzo, E., Yu, J.-Y., Braconnot, P., ... Yeh, S.-W. (2015). Understanding ENSO Diversity. *Bulletin of the American Meteorological Society*, 96(6), 921–938. Retrieved from <https://doi.org/10.1175/BAMS-D-13-00117.1> doi: 10.1175/BAMS-D-13-00117.1
- Chen, D., Lian, T., Fu, C., Cane, M. A., Tang, Y., Murtugudde, R., ... Zhou, L. (2015). Strong influence of westerly wind bursts on El Niño diversity. *Nature*

- 928 *Geoscience*, 8(5), 339–345. Retrieved from <http://dx.doi.org/10.1038/ngeo2399>
929 <http://10.0.4.14/ngeo2399>
- 930 Chung, P.-H., & Li, T. (2012). Interdecadal Relationship between the Mean
931 State and El Niño Types. *Journal of Climate*, 26(2), 361–379. Re-
932 trieved from <https://doi.org/10.1175/JCLI-D-12-00106.1> doi:
933 10.1175/JCLI-D-12-00106.1
- 934 Cobb, K. M., Westphal, N., Sayani, H. R., Watson, J. T., Di Lorenzo, E., Cheng,
935 H., ... Charles, C. D. (2013). Highly Variable El Niño–Southern Oscillation
936 Throughout the Holocene. *Science*, 339(6115), 67 LP – 70. Retrieved from
937 <http://science.sciencemag.org/content/339/6115/67.abstract>
- 938 Dee, D. P., Uppala, S. M., Simmons, A. J., Berrisford, P., Poli, P., Kobayashi, S., ...
939 Vitart, F. (2011). The ERA-Interim reanalysis: Configuration and performance
940 of the data assimilation system. *Quarterly Journal of the Royal Meteorological
941 Society*, 137(656), 553–597. doi: 10.1002/qj.828
- 942 Delworth, T. L., & Mann, M. E. (2000). Observed and simulated multidecadal
943 variability in the Northern Hemisphere. *Climate Dynamics*, 16(9), 661–
944 676. Retrieved from <https://doi.org/10.1007/s003820000075> doi:
945 10.1007/s003820000075
- 946 Deppenmeier, A.-L., Haarsma, R. J., & Hazeleger, W. (2016). The Bjerknes feed-
947 back in the tropical Atlantic in CMIP5 models. *Climate Dynamics*, 1–17. Re-
948 trieved from <http://dx.doi.org/10.1007/s00382-016-2992-z> doi: 10.1007/
949 s00382-016-2992-z
- 950 DiNezio, P. N., & Deser, C. (2014). Nonlinear Controls on the Persistence of La
951 Niña. *Journal of Climate*, 27(19), 7335–7355. Retrieved from [https://doi
952 .org/10.1175/JCLI-D-14-00033.1](https://doi.org/10.1175/JCLI-D-14-00033.1) doi: 10.1175/JCLI-D-14-00033.1
- 953 Ding, H., Greatbatch, R. J., Latif, M., Park, W., & Gerdes, R. (2013). Hindcast
954 of the 1976/77 and 1998/99 Climate Shifts in the Pacific. *Journal of Climate*,
955 26(19), 7650–7661. Retrieved from [http://journals.ametsoc.org/doi/abs/
956 10.1175/JCLI-D-12-00626.1](http://journals.ametsoc.org/doi/abs/10.1175/JCLI-D-12-00626.1) doi: 10.1175/JCLI-D-12-00626.1
- 957 Dippe, T., Greatbatch, R. J., & Ding, H. (2018). On the relationship between
958 Atlantic Niño variability and ocean dynamics. *Climate Dynamics*, 51(1), 597–
959 612. Retrieved from <https://doi.org/10.1007/s00382-017-3943-z> doi:
960 10.1007/s00382-017-3943-z
- 961 Dommenges, D., Bayr, T., & Frauen, C. (2013). Analysis of the non-linearity in the
962 pattern and time evolution of El Niño southern oscillation. *Climate Dynamics*,
963 40(11), 2825–2847. Retrieved from [https://doi.org/10.1007/s00382-012-
964 -1475-0](https://doi.org/10.1007/s00382-012-1475-0) doi: 10.1007/s00382-012-1475-0
- 965 Duan, W., & Wei, C. (2013). The ‘spring predictability barrier’ for ENSO pre-
966 dictions and its possible mechanism: results from a fully coupled model. *Inter-
967 national Journal of Climatology*, 33(5), 1280–1292. Retrieved from [http://dx
968 .doi.org/10.1002/joc.3513](http://dx.doi.org/10.1002/joc.3513) doi: 10.1002/joc.3513
- 969 Gill, A. E. (1980). Some simple solutions for heat-induced tropical circulation.
970 *Quarterly Journal of the Royal Meteorological Society*, 106(449), 447–462. Re-
971 trieved from <http://doi.wiley.com/10.1002/qj.49710644905> doi: 10.1002/
972 qj.49710644905
- 973 Graham, N. E. (1994). Decadal-scale climate variability in the tropical and North
974 Pacific during the 1970s and 1980s: observations and model results. *Climate
975 Dynamics*, 10(3), 135–162. Retrieved from [https://doi.org/10.1007/
976 BF00210626](https://doi.org/10.1007/BF00210626) doi: 10.1007/BF00210626
- 977 Holland, P. W., & Welsch, R. E. (1977). Robust regression using iteratively
978 reweighted least-squares. *Communications in Statistics - Theory and
979 Methods*, 6(9), 813–827. Retrieved from [http://dx.doi.org/10.1080/
980 03610927708827533](http://dx.doi.org/10.1080/03610927708827533) doi: 10.1080/03610927708827533
- 981 Hu, Z.-Z., Kumar, A., Huang, B., Zhu, J., Zhang, R.-H., & Jin, F.-F. (2017). Asym-
982 metric evolution of El Niño and La Niña: the recharge/discharge processes and

- 983 role of the off-equatorial sea surface height anomaly. *Climate Dynamics*, 49(7),
 984 2737–2748. Retrieved from <https://doi.org/10.1007/s00382-016-3498-4>
 985 doi: 10.1007/s00382-016-3498-4
- 986 Hu, Z.-Z., Kumar, A., Ren, H.-L., Wang, H., L'Heureux, M., & Jin, F.-F. (2012).
 987 Weakened Interannual Variability in the Tropical Pacific Ocean since 2000.
 988 *Journal of Climate*, 26(8), 2601–2613. Retrieved from [https://doi.org/](https://doi.org/10.1175/JCLI-D-12-00265.1)
 989 [10.1175/JCLI-D-12-00265.1](https://doi.org/10.1175/JCLI-D-12-00265.1) doi: 10.1175/JCLI-D-12-00265.1
- 990 Huang, B., Thorne, P. W., Banzon, V. F., Boyer, T., Chepurin, G., Lawrimore,
 991 J. H., ... Zhang, H.-M. (2017). Extended Reconstructed Sea Surface Tem-
 992 perature, Version 5 (ERSSTv5): Upgrades, Validations, and Intercomparisons.
 993 *Journal of Climate*, 30(20), 8179–8205. Retrieved from [https://doi.org/](https://doi.org/10.1175/JCLI-D-16-0836.1)
 994 [10.1175/JCLI-D-16-0836.1](https://doi.org/10.1175/JCLI-D-16-0836.1) doi: 10.1175/JCLI-D-16-0836.1
- 995 Huber, P. J., & Ronchetti, E. M. (2009). *Robust Statistics* (Second Edi ed.). Wiley.
- 996 Hummels, R., Dengler, M., & Bourlès, B. (2013). Seasonal and regional variabil-
 997 ity of upper ocean diapycnal heat flux in the Atlantic cold tongue. *Progress in*
 998 *Oceanography*, 111, 52–74. doi: 10.1016/j.pocean.2012.11.001
- 999 Jin, F. F., Kim, S. T., & Bejarano, L. (2006). A coupled-stability index for ENSO.
 1000 *Geophysical Research Letters*, 33(23). doi: 10.1029/2006GL027221
- 1001 Keenlyside, N. S., & Latif, M. (2007). Understanding Equatorial Atlantic Interan-
 1002 nual Variability. *Journal of Climate*, 20(1), 131–142. Retrieved from [http://](http://dx.doi.org/10.1175/JCLI3992.1)
 1003 dx.doi.org/10.1175/JCLI3992.1 doi: 10.1175/JCLI3992.1
- 1004 Knight, J. R., Folland, C. K., & Scaife, A. A. (2006). Climate impacts of
 1005 the Atlantic Multidecadal Oscillation. *Geophysical Research Letters*,
 1006 33(17). Retrieved from <https://doi.org/10.1029/2006GL026242> doi:
 1007 [10.1029/2006GL026242](https://doi.org/10.1029/2006GL026242)
- 1008 Levine, A. F. Z., & Jin, F. F. (2017). A simple approach to quantifying the
 1009 noise-ENSO interaction. Part I: Deducing the state-dependency of the wind-
 1010 stress forcing using monthly mean data. *Climate Dynamics*, 48(1), 1–18.
 1011 Retrieved from <http://dx.doi.org/10.1007/s00382-015-2748-1> doi:
 1012 [10.1007/s00382-015-2748-1](https://doi.org/10.1007/s00382-015-2748-1)
- 1013 Levine, A. F. Z., & McPhaden, M. J. (2016). How the July 2014 easterly wind
 1014 burst gave the 2015–2016 El Niño a head start. *Geophysical Research Let-*
 1015 *ters*, 43(12), 6503–6510. Retrieved from [http://dx.doi.org/10.1002/](http://dx.doi.org/10.1002/2016GL069204)
 1016 [2016GL069204](http://dx.doi.org/10.1002/2016GL069204) doi: 10.1002/2016GL069204
- 1017 Li, J., Xie, S.-P., Cook, E. R., Morales, M. S., Christie, D. A., Johnson, N. C., ...
 1018 Fang, K. (2013). El Niño modulations over the past seven centuries. *Na-*
 1019 *ture Climate Change*, 3, 822. Retrieved from [http://dx.doi.org/10.1038/](http://dx.doi.org/10.1038/nclimate1936)
 1020 [nclimate1936](http://dx.doi.org/10.1038/nclimate1936)[http://www.nature.com/](http://www.nature.com/articles/nclimate1936#supplementary-information)
 1021 [articles/nclimate1936#supplementary-information](http://www.nature.com/articles/nclimate1936#supplementary-information)
- 1022 Losada, T., & Rodríguez-Fonseca, B. (2016). Tropical atmospheric response to
 1023 decadal changes in the Atlantic Equatorial Mode. *Climate Dynamics*, 47(3-4),
 1024 1211–1224. doi: 10.1007/s00382-015-2897-2
- 1025 Lübbecke, J. F., Burls, N. J., Reason, C. J. C., & McPhaden, M. J. (2014). Vari-
 1026 ability in the South Atlantic Anticyclone and the Atlantic Niño Mode. *Journal*
 1027 *of Climate*, 27(21), 8135–8150. Retrieved from [http://dx.doi.org/10.1175/](http://dx.doi.org/10.1175/JCLI-D-14-00202.1)
 1028 [JCLI-D-14-00202.1](http://dx.doi.org/10.1175/JCLI-D-14-00202.1) doi: 10.1175/JCLI-D-14-00202.1
- 1029 Lübbecke, J. F., & McPhaden, M. J. (2013). A comparative stability analysis of At-
 1030 lantic and Pacific Niño modes. *Journal of Climate*, 26(16), 5965–5980. doi: 10
 1031 .1175/JCLI-D-12-00758.1
- 1032 Lübbecke, J. F., & McPhaden, M. J. (2017). Symmetry of the Atlantic Niño
 1033 mode. *Geophysical Research Letters*, 44(2), 965–973. Retrieved from [http://](http://doi.wiley.com/10.1002/2016GL071829)
 1034 doi.wiley.com/10.1002/2016GL071829 doi: 10.1002/2016GL071829
- 1035 Mantua, N. J., & Hare, S. R. (2002). The Pacific Decadal Oscillation. *Journal*
 1036 *of Oceanography*, 58(1), 35–44. Retrieved from [https://doi.org/10.1023/A:](https://doi.org/10.1023/A:1015820616384)
 1037 [1015820616384](https://doi.org/10.1023/A:1015820616384) doi: 10.1023/A:1015820616384

- 1038 Martín-Rey, M., Polo, I., Rodríguez-Fonseca, B., Losada, T., & Lazar, A. (2017).
 1039 Is There Evidence of Changes in Tropical Atlantic Variability Modes under
 1040 AMO Phases in the Observational Record? *Journal of Climate*, *31*(2), 515–
 1041 536. Retrieved from <https://doi.org/10.1175/JCLI-D-16-0459.1> doi:
 1042 10.1175/JCLI-D-16-0459.1
- 1043 Mehta, V. M. (1998). Variability of the Tropical Ocean Surface Temperatures
 1044 at Decadal–Multidecadal Timescales. Part I: The Atlantic Ocean. *Journal*
 1045 *of Climate*, *11*(9), 2351–2375. Retrieved from [https://doi.org/10.1175/
 1046 1520-0442\(1998\)011{\\%}3C2351:V0TTOS{\\%}3E2.0.COhttp://0.0.0.2](https://doi.org/10.1175/1520-0442(1998)011{\\%}3C2351:V0TTOS{\\%}3E2.0.COhttp://0.0.0.2) doi:
 1047 10.1175/1520-0442(1998)011{\\%}3C2351:V0TTOS{\\%}3E2.0.CO;2
- 1048 Mehta, V. M., & Delworth, T. (1995). Decadal Variability of the Tropical At-
 1049 lantic Ocean Surface Temperature in Shipboard Measurements and in a
 1050 Global Ocean-Atmosphere Model. *Journal of Climate*, *8*(2), 172–190. Re-
 1051 trieved from [https://doi.org/10.1175/1520-0442\(1995\)008{\\%}3C0172:
 1052 DVOTTA{\\%}3E2.0.COhttp://0.0.0.2](https://doi.org/10.1175/1520-0442(1995)008{\\%}3C0172:DVOTTA{\\%}3E2.0.COhttp://0.0.0.2) doi: 10.1175/1520-0442(1995)008{\\%}3C0172:
 1053 DVOTTA{\\%}3E2.0.CO;2
- 1054 Minobe, S. (1997). A 50–70 year climatic oscillation over the North Pacific and
 1055 North America. *Geophysical Research Letters*, *24*(6), 683–686. Retrieved from
 1056 <https://doi.org/10.1029/97GL00504> doi: 10.1029/97GL00504
- 1057 Minobe, S. (2000). Spatio-temporal structure of the pentadecadal variability over
 1058 the North Pacific. *Progress in Oceanography*, *47*(2), 381–408. Retrieved from
 1059 <http://www.sciencedirect.com/science/article/pii/S0079661100000422>
 1060 doi: [https://doi.org/10.1016/S0079-6611\(00\)00042-2](https://doi.org/10.1016/S0079-6611(00)00042-2)
- 1061 Okumura, Y., & Xie, S. P. (2006). Some overlooked features of tropical Atlantic
 1062 climate leading to a new Nino-like phenomenon. *Journal of Climate*, *19*(22),
 1063 5859–5874.
- 1064 Rebert, J. P., Donguy, J. R., Eldin, G., & Wyrtki, K. (1985). Relations between
 1065 sea level, thermocline depth, heat content, and dynamic height in the tropical
 1066 Pacific Ocean. *Journal of Geophysical Research: Oceans*, *90*(C6), 11719–
 1067 11725. Retrieved from <https://doi.org/10.1029/JC090iC06p11719> doi:
 1068 10.1029/JC090iC06p11719
- 1069 Richter, I., Behera, S. K., Masumoto, Y., Taguchi, B., Sasaki, H., & Yamagata,
 1070 T. (2013). Multiple causes of interannual sea surface temperature variabil-
 1071 ity in the equatorial Atlantic Ocean. *Nature Geoscience*, *6*(1), 43–47. Re-
 1072 trieved from <http://www.nature.com/doi/finder/10.1038/ngeo1660> doi:
 1073 10.1038/ngeo1660
- 1074 Schlesinger, M. E., & Ramankutty, N. (1994). An oscillation in the global climate
 1075 system of period 65–70 years. *Nature*, *367*, 723. Retrieved from [http://dx
 1076 .doi.org/10.1038/367723a0](http://dx.doi.org/10.1038/367723a0)<http://10.0.4.14/367723a0>
- 1077 Smith, T. M., & Reynolds, R. W. (2003). Extended Reconstruction of Global
 1078 Sea Surface Temperatures Based on COADS Data (1854–1997). *Journal of*
 1079 *Climate*, *16*(10), 1495–1510. Retrieved from [https://doi.org/10.1175/
 1080 1520-0442-16.10.1495](https://doi.org/10.1175/1520-0442-16.10.1495) doi: 10.1175/1520-0442-16.10.1495
- 1081 Street, J. O., Carroll, R. J., & Ruppert, D. (1988). A Note on Computing
 1082 Robust Regression Estimates via Iteratively Reweighted Least Squares.
 1083 *The American Statistician*, *42*(2), 152–154. Retrieved from [https://
 1084 www.tandfonline.com/doi/abs/10.1080/00031305.1988.10475548](https://www.tandfonline.com/doi/abs/10.1080/00031305.1988.10475548) doi:
 1085 10.1080/00031305.1988.10475548
- 1086 Takahashi, K., & Dewitte, B. (2016). Strong and moderate nonlinear El Niño
 1087 regimes. *Climate Dynamics*, *46*(5), 1627–1645. Retrieved from [https://
 1088 doi.org/10.1007/s00382-015-2665-3](https://doi.org/10.1007/s00382-015-2665-3) doi: 10.1007/s00382-015-2665-3
- 1089 Takahashi, K., Montecinos, A., Goubanova, K., & Dewitte, B. (2011). ENSO
 1090 regimes: Reinterpreting the canonical and Modoki El Niño. *Geophysical*
 1091 *Research Letters*, *38*(10). Retrieved from [http://dx.doi.org/10.1029/
 1092 2011GL047364](http://dx.doi.org/10.1029/2011GL047364) doi: 10.1029/2011GL047364

- 1093 Timmermann, A., An, S.-I., Kug, J.-S., Jin, F.-F., Cai, W., Capotondi, A.,
 1094 ... Zhang, X. (2018). El Niño–Southern Oscillation complexity. *Nature*,
 1095 *559*(7715), 535–545. Retrieved from <https://doi.org/10.1038/s41586-018-0252-6> doi: 10.1038/s41586-018-0252-6
- 1096 Tokinaga, H., & Xie, S.-P. (2011). Weakening of the equatorial Atlantic cold tongue
 1097 over the past six decades. *Nature Geoscience*, *4*(4), 222–226. Retrieved from
 1098 <http://dx.doi.org/10.1038/ngeo1078> doi: 10.1038/ngeo1078
- 1099 Torrence, C., & Webster, P. J. (1998). The annual cycle of persistence in the El
 1100 Niño/Southern Oscillation. *Quarterly Journal of the Royal Meteorological*
 1101 *Society*, *124*(550), 1985–2004. Retrieved from <https://doi.org/10.1002/qj.49712455010> doi: 10.1002/qj.49712455010
- 1102 Trenberth, K. E., & Hurrell, J. W. (1994). Decadal atmosphere-ocean variations in
 1103 the Pacific. *Climate Dynamics*, *9*(6), 303–319. Retrieved from <https://doi.org/10.1007/BF00204745> doi: 10.1007/BF00204745
- 1104 Uppala, S. M., Kållberg, W. P., Simmons, J. A., Andrae, U., Costa, B., Fiorino,
 1105 M., ... Woollen, J. (2006). The ERA-40 re-analysis. *Quarterly Journal*
 1106 *of the Royal Meteorological Society*, *131*(612), 2961–3012. Retrieved from
 1107 <https://doi.org/10.1256/qj.04.176> doi: 10.1256/qj.04.176
- 1108 Wainer, I., Servain, J., & Clauzet, G. (2008). Is the decadal variability in the trop-
 1109 ical Atlantic a precursor to the NAO? *Annales geophysicae: atmospheres, hy-*
 1110 *dro-spheres and space sciences*, *26*(12), 4075.
- 1111 Wengel, C., Latif, M., Park, W., Harlaß, J., & Bayr, T. (2018). Seasonal
 1112 ENSO phase locking in the Kiel Climate Model: The importance of the
 1113 equatorial cold sea surface temperature bias. *Climate Dynamics*. Re-
 1114 trievied from <https://doi.org/10.1007/s00382-017-3648-3> doi:
 1115 10.1007/s00382-017-3648-3
- 1116 Xie, S.-P., Tanimoto, Y., Noguchi, H., & Matsuno, T. (1999). How and why cli-
 1117 mate variability differs between the tropical Atlantic and Pacific. *Geophysical*
 1118 *Research Letters*, *26*(11), 1609–1612. Retrieved from <http://dx.doi.org/10.1029/1999GL900308> doi: 10.1029/1999GL900308
- 1119 Yeh, S.-w., Kug, J.-s., Dewitte, B., Kwon, M.-h., Kirtman, B. P., & Jin, F.-f.
 1120 (2009). El Niño in a changing climate. *Nature*, *461*(7263), 511–4. Re-
 1121 trievied from <http://www.ncbi.nlm.nih.gov/pubmed/19779449> doi:
 1122 10.1038/nature08316
- 1123 Zebiak, S. E., & Cane, M. A. (1987). A Model El Niño–Southern Oscillation.
 1124 *Monthly Weather Review*, *115*(10), 2262–2278. Retrieved from [https://doi.org/10.1175/1520-0493\(1987\)115<2262:AMENO%3E2.0.CO;2](https://doi.org/10.1175/1520-0493(1987)115<2262:AMENO%3E2.0.CO;2) doi: 10.1175/1520-0493(1987)115<2262:AMENO%3E2.0.CO;2
- 1125 Zheng, F., Fang, X.-H., Yu, J.-Y., & Zhu, J. (2014). Asymmetry of the Bjerknes
 1126 positive feedback between the two types of El Niño. *Geophysical Research*
 1127 *Letters*, *41*(21), 7651–7657. Retrieved from <http://dx.doi.org/10.1002/2014GL062125> doi: 10.1002/2014GL062125
- 1128 Zhu, J., Kumar, A., & Huang, B. (2015). The relationship between thermo-
 1129 cline depth and SST anomalies in the eastern equatorial Pacific: Season-
 1130 ality and decadal variations. *Geophysical Research Letters*, *42*(11), 4507–
 1131 4515. Retrieved from <http://dx.doi.org/10.1002/2015GL064220> doi:
 1132 10.1002/2015GL064220

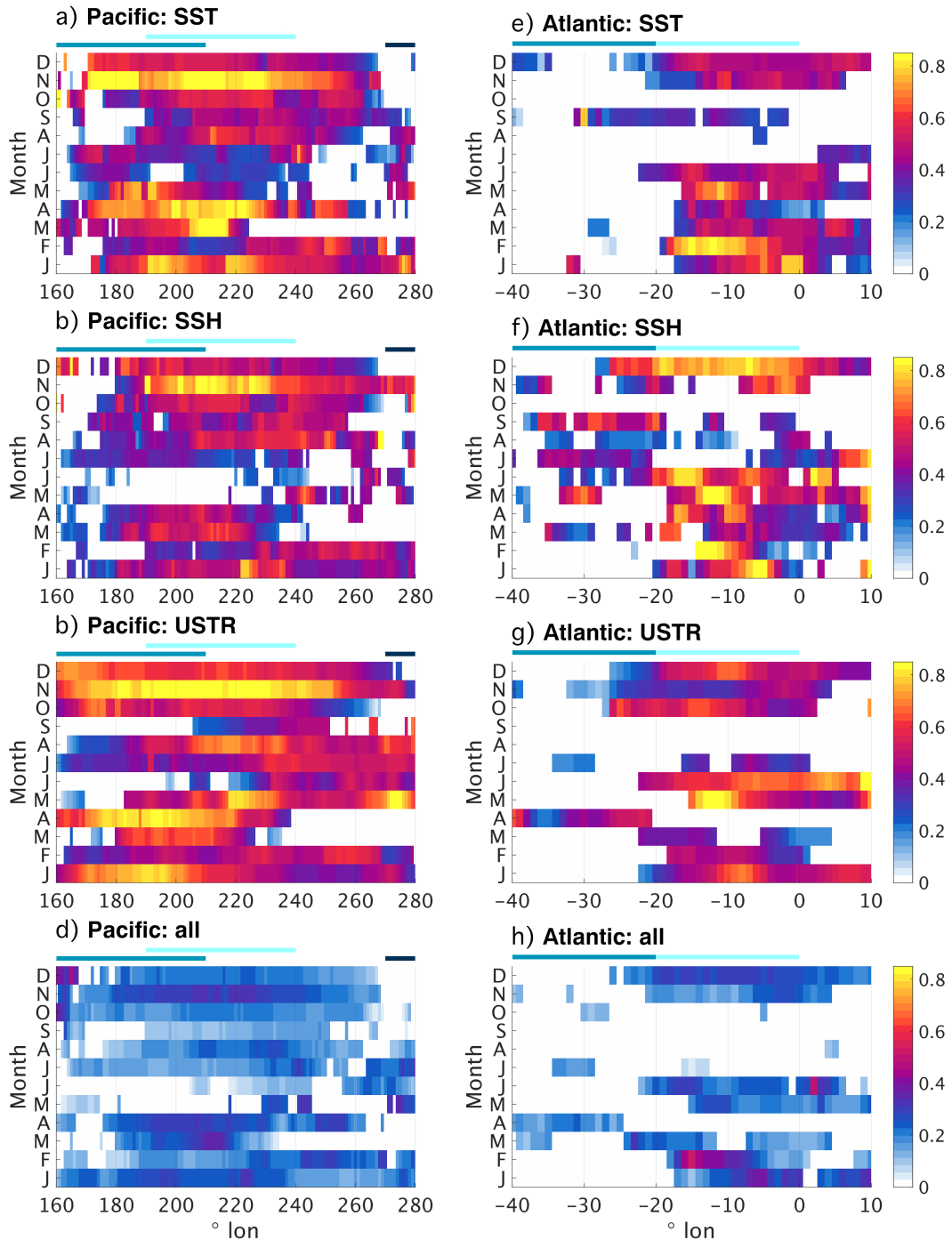


Figure A.3: OBS-based comparison of different manifestations of the negative composite of the total Bjerknes feedback in the Pacific (left column, panels a-d) and the Atlantic (right column, e-h) for the period 1993-2012. All panels show total feedbacks along the equator (x-axis) and stratified into calendar months (y-axis). The first, second, third, and fourth rows show the negative composites of the total Bjerknes feedback using constant composites based on SST (a,e; these are the same as in the main text), SSH (b,f), constant composites based on USTR (c,g), and variable composites (d,h) (see text for details on the differences between the manifestations). Recall that the SST/SSH/USTR-based total feedback composites are a measure of the total Bjerknes feedback for when the SST/thermocline/zonal wind stress in the western ocean basin is warmer/deeper/more easterly (positive anomalies) or cooler/shallower/more westerly (negative anomalies) than on average. White indicates that at least one of the feedback elements contributing to the composite of the total feedback was negative. Coloured bars below the title indicate the zonal extent of the Nino4, Nino3.4, and Nino1.2 (WAtl and ATL3) regions in blue, light blue, and dark blue (blue and light blue) in the Pacific (Atlantic), respectively.

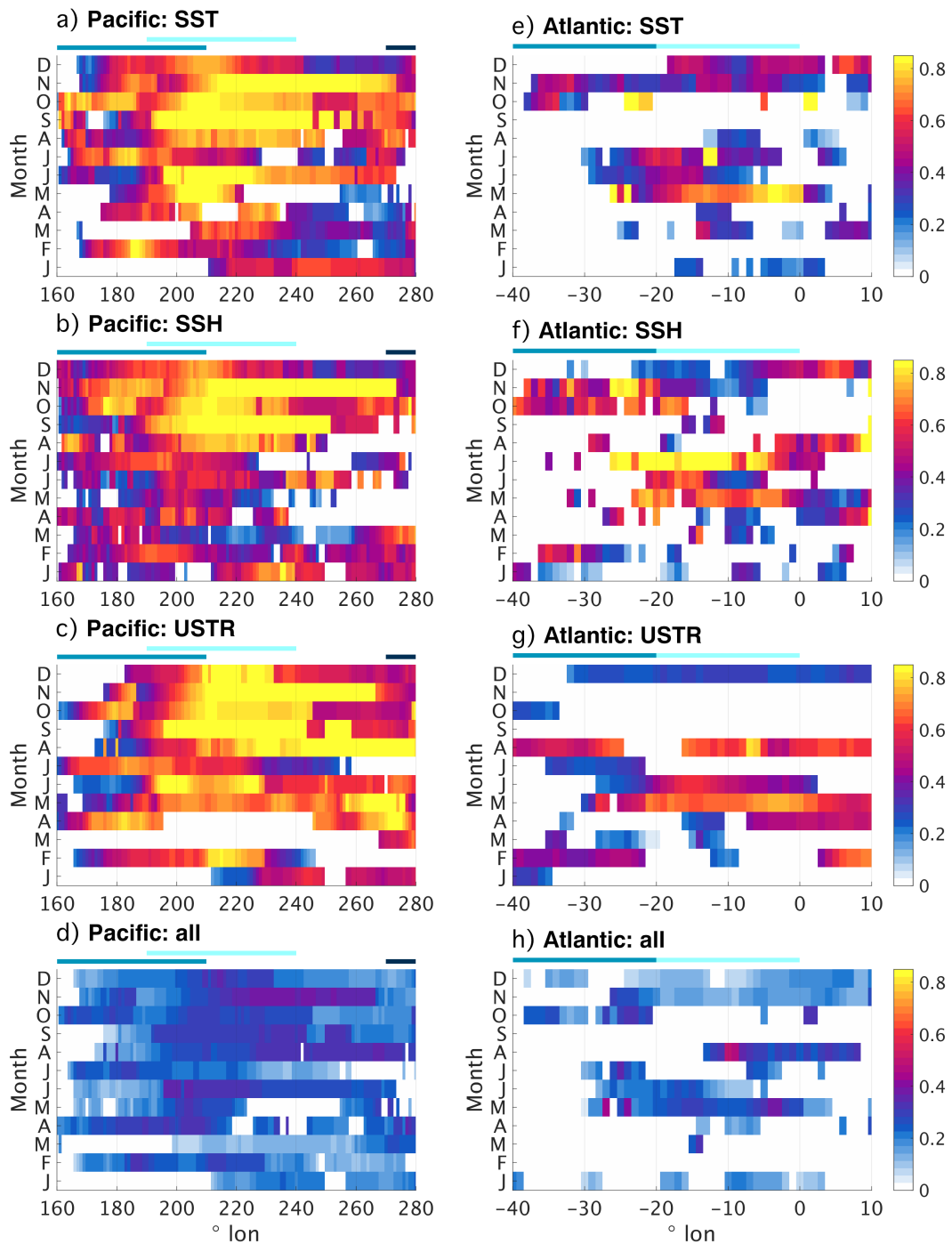


Figure A.4: Same as Fig. SA.3, but for manifestations of the positive composites of the total Bjerknes feedback.

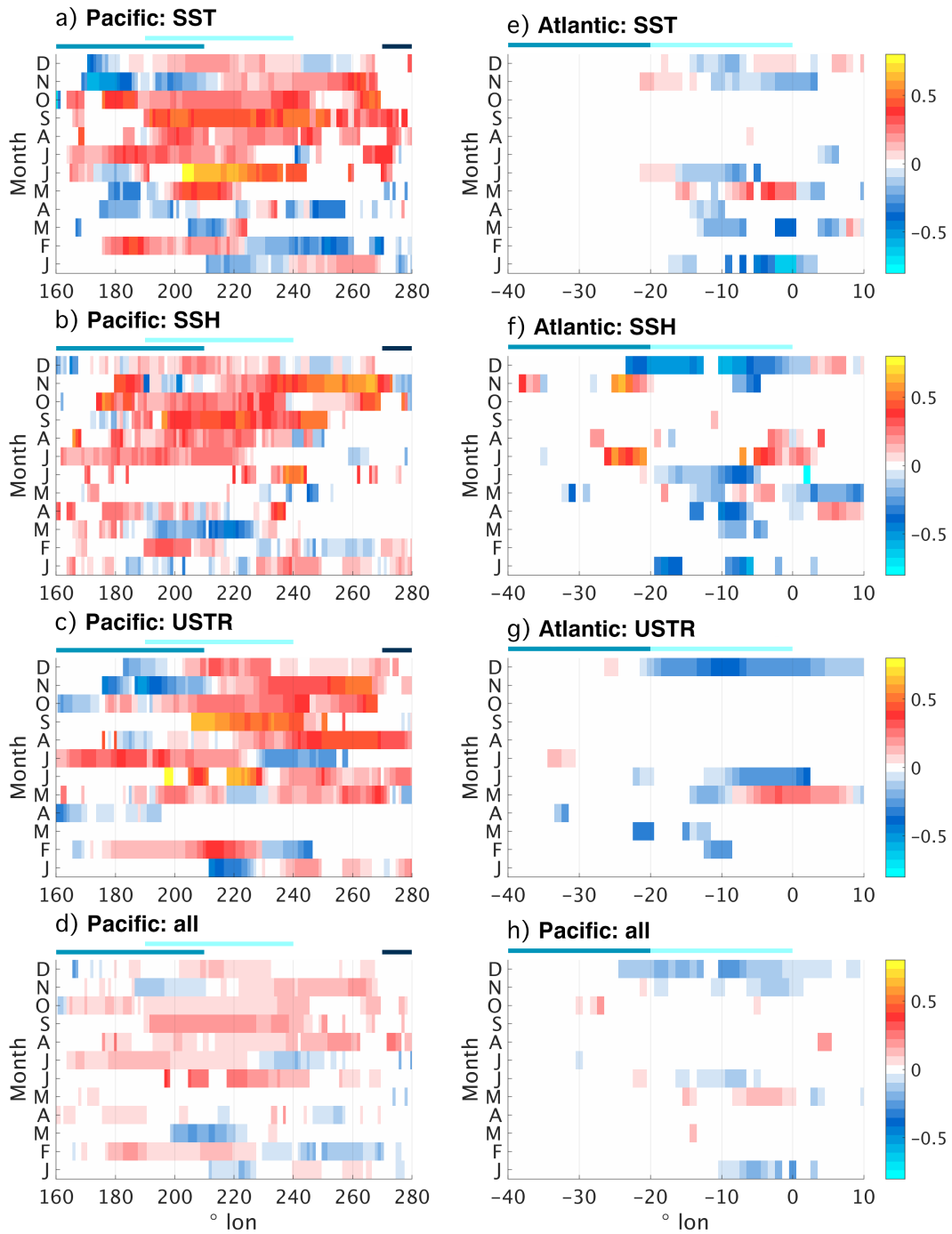
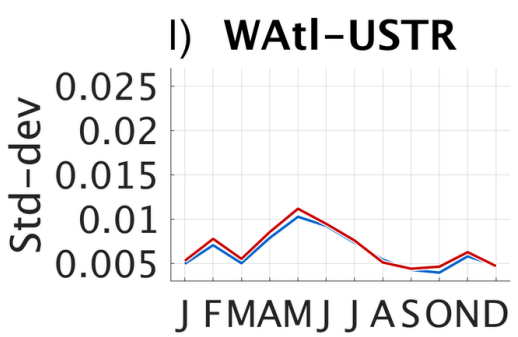
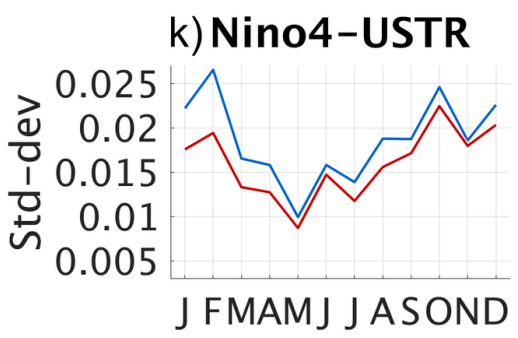
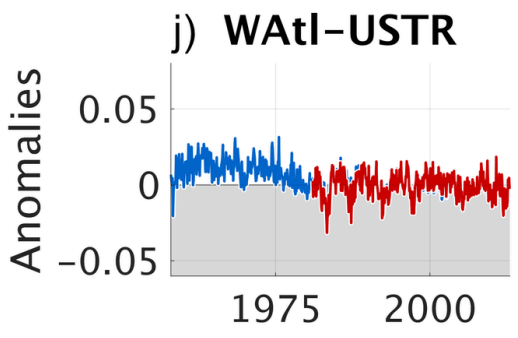
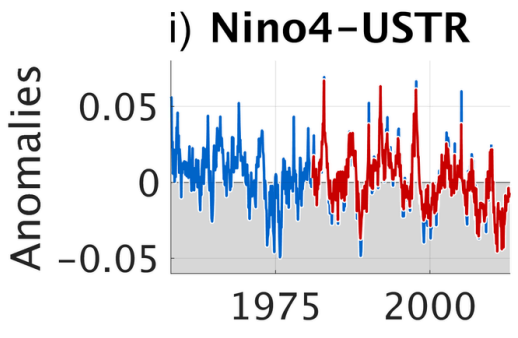
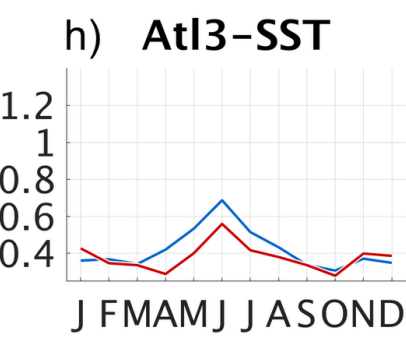
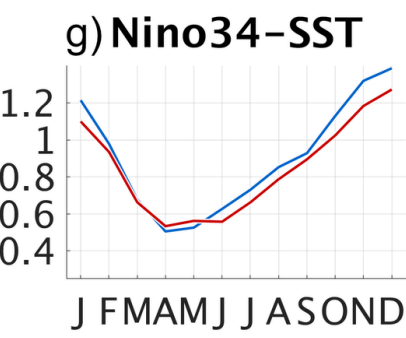
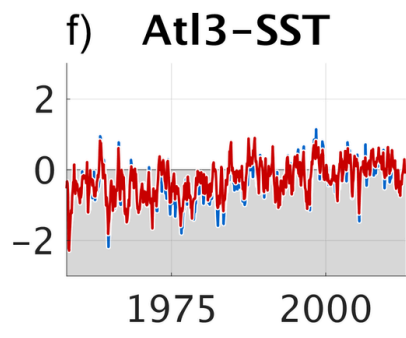
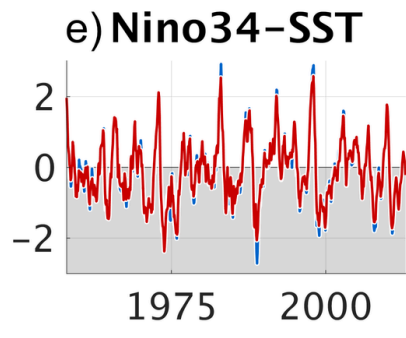
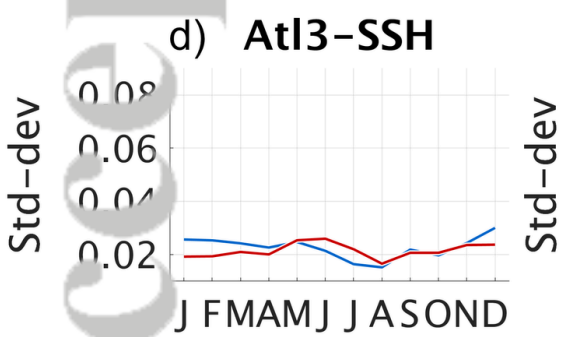
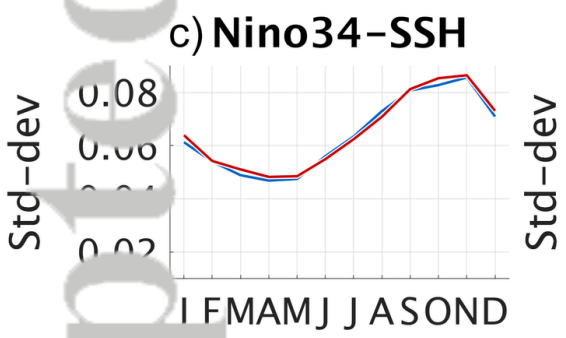
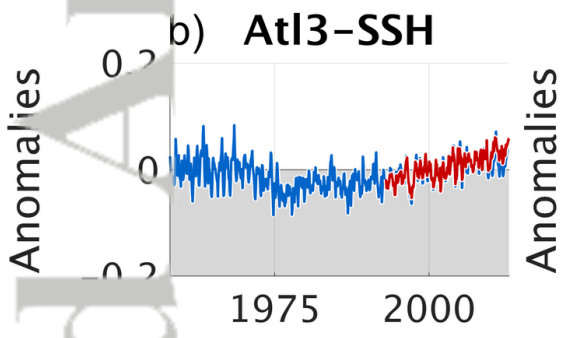
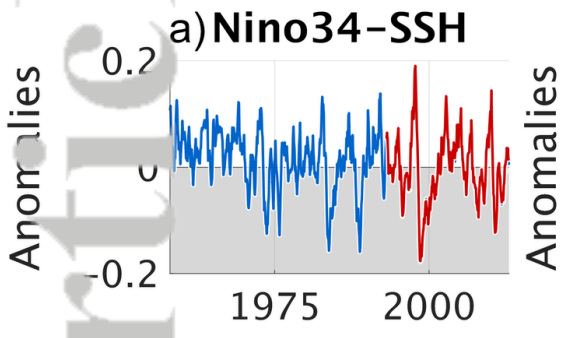
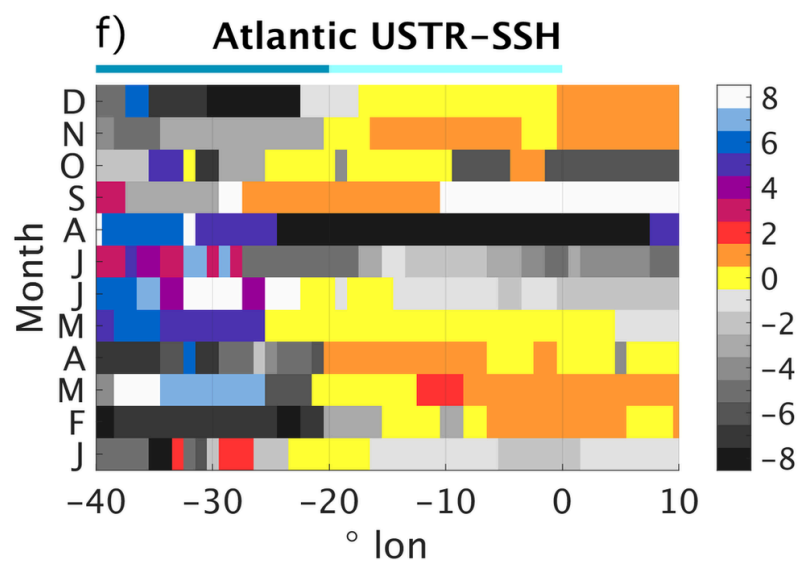
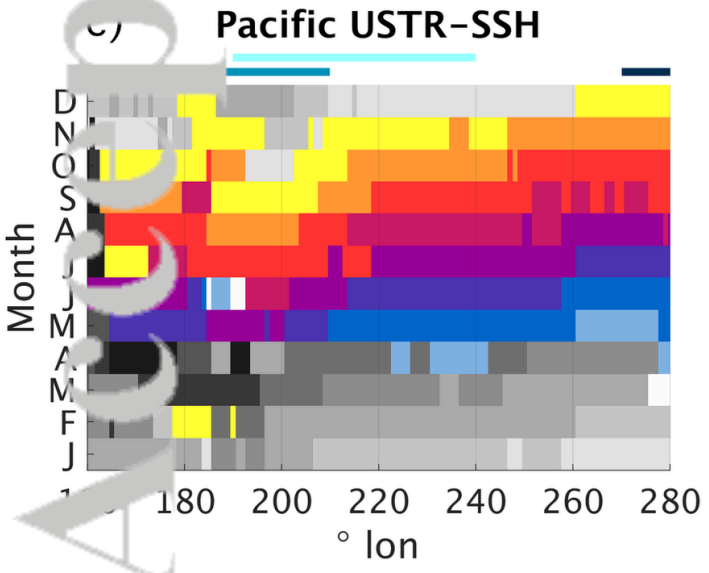
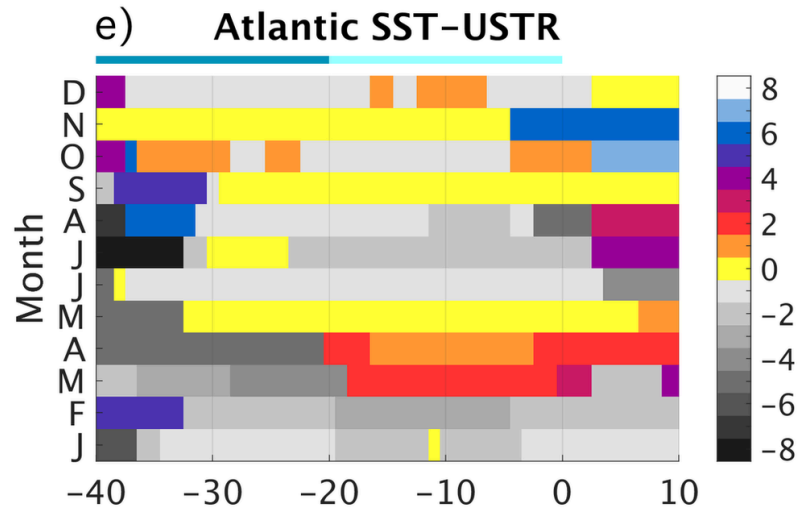
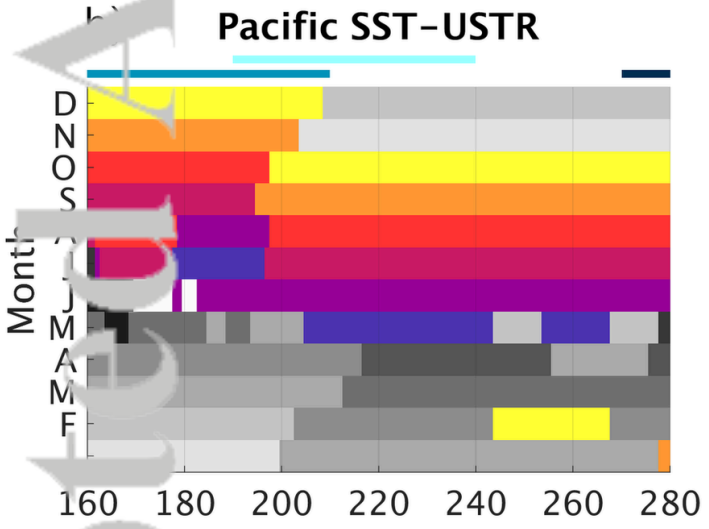
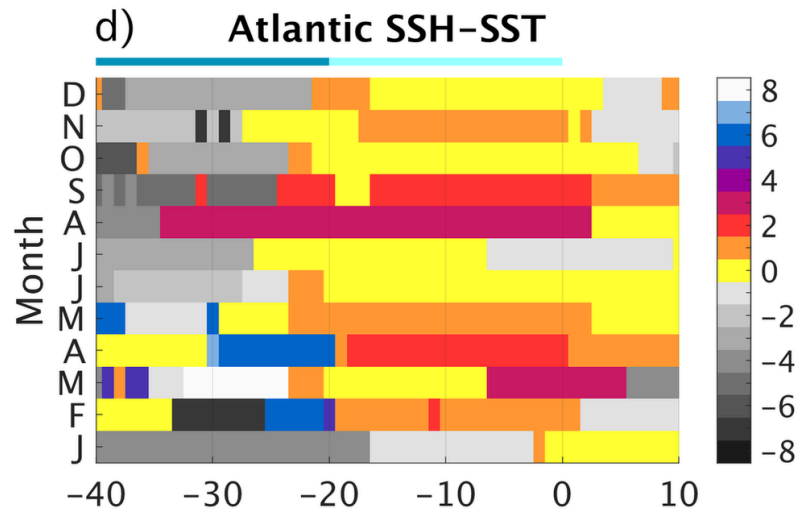
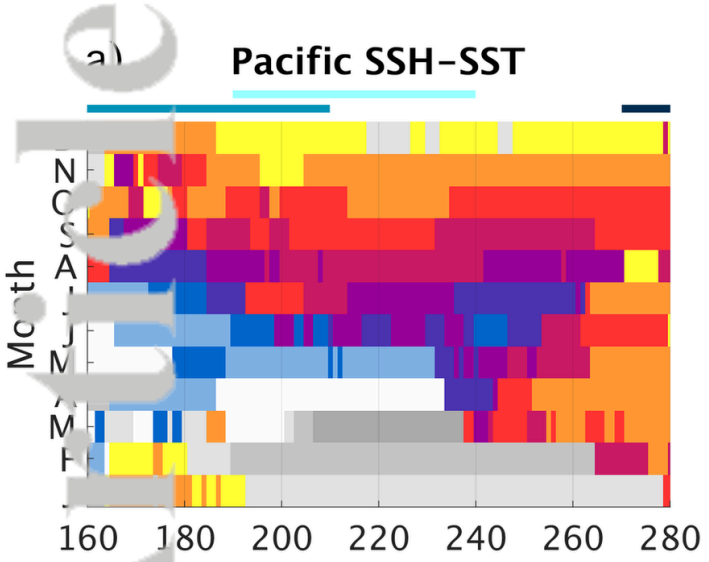


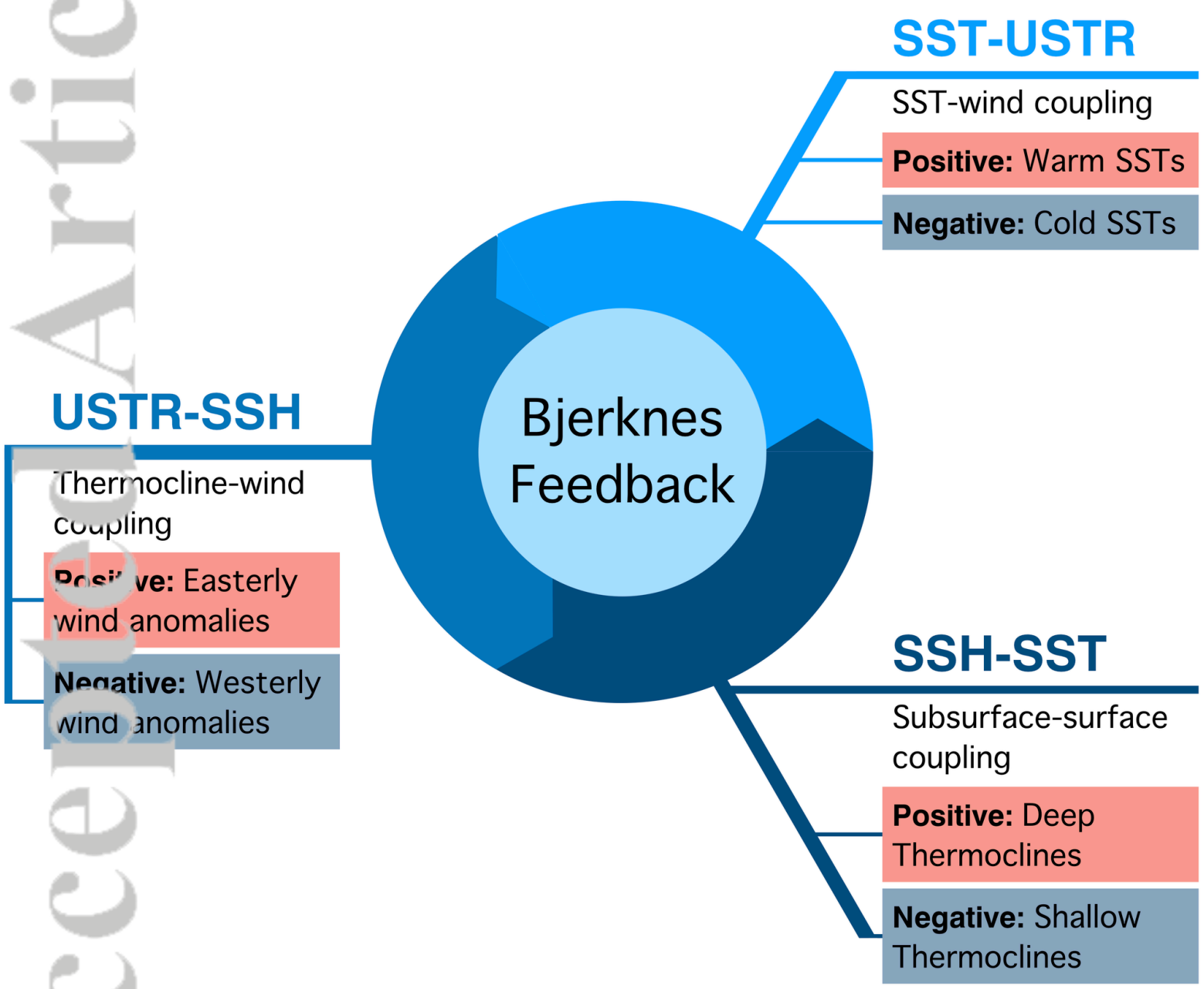
Figure A.5: Same as Fig. SA.3, but for the difference between the positive and negative composites of different manifestations of the total Bjerknes feedback.



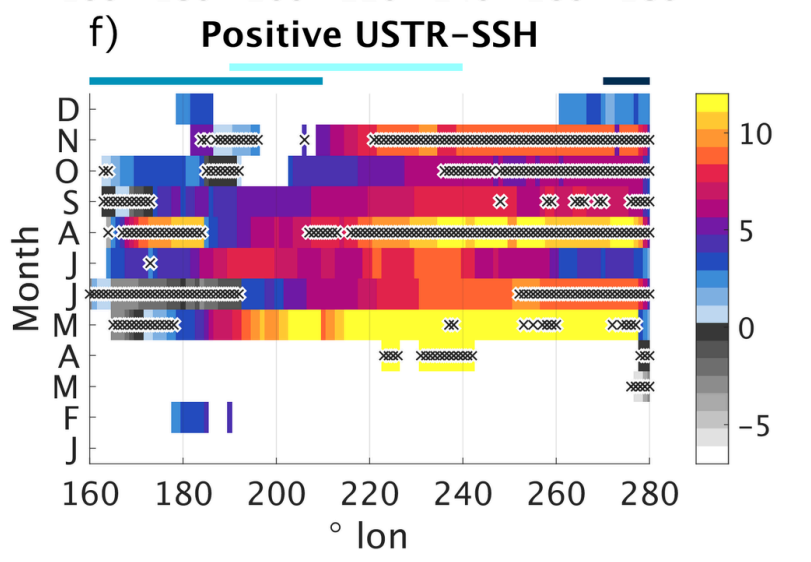
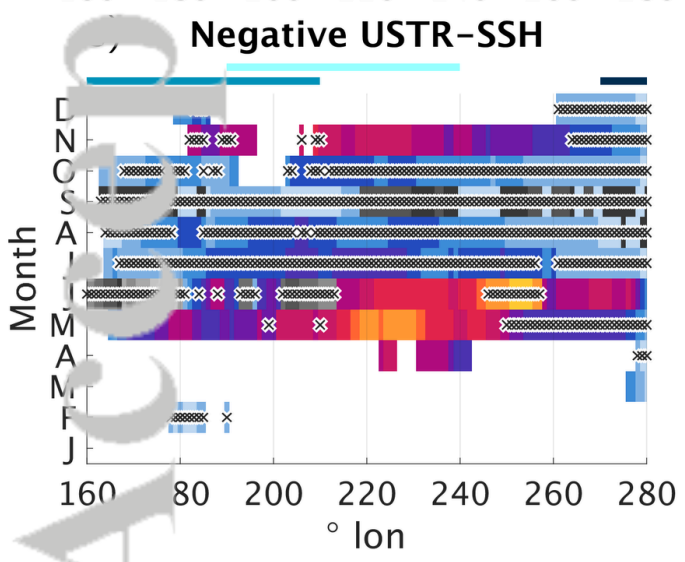
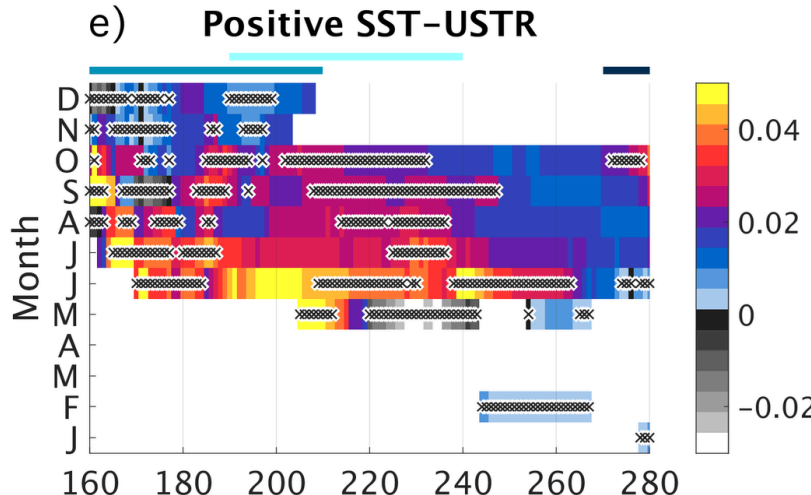
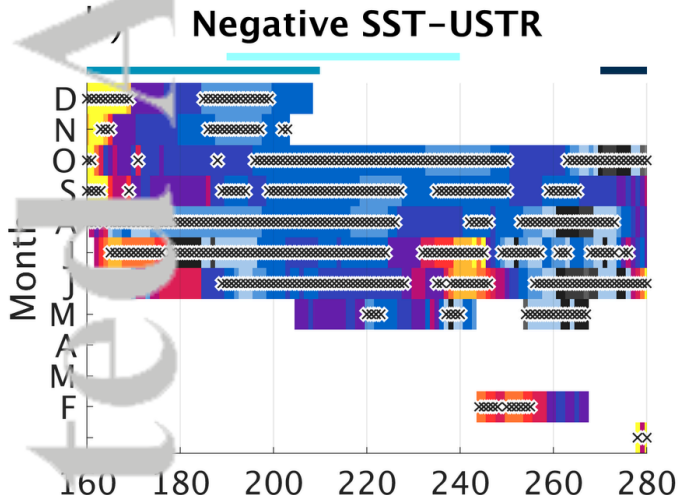
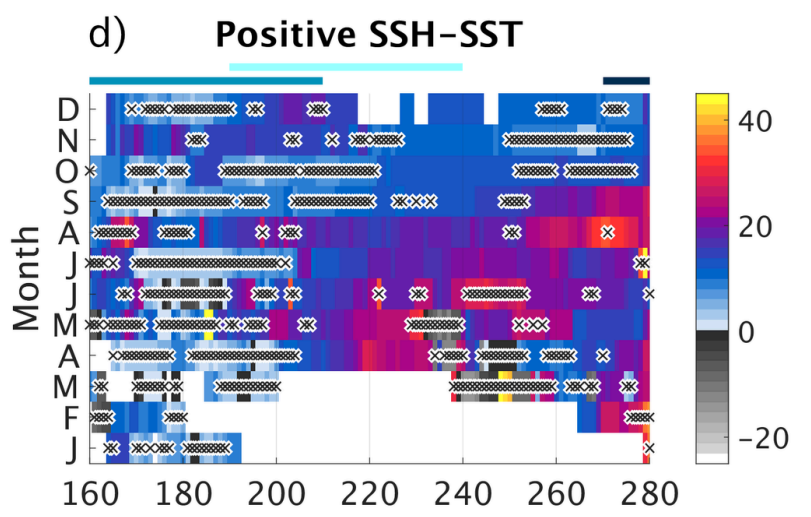
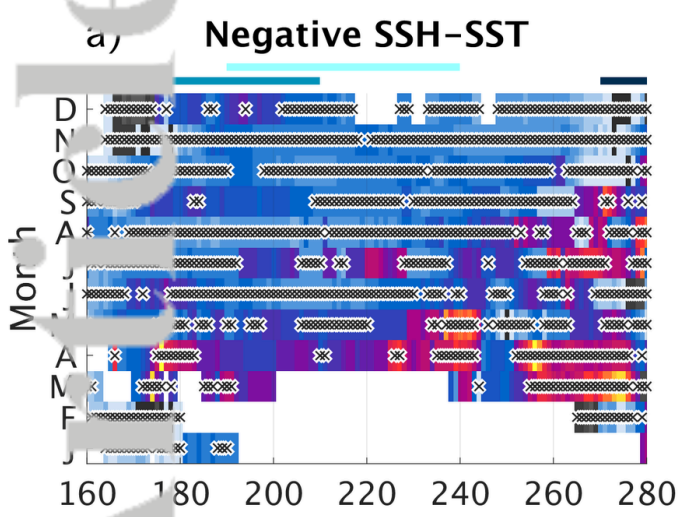
2018JC014700-f01-z-AA.png



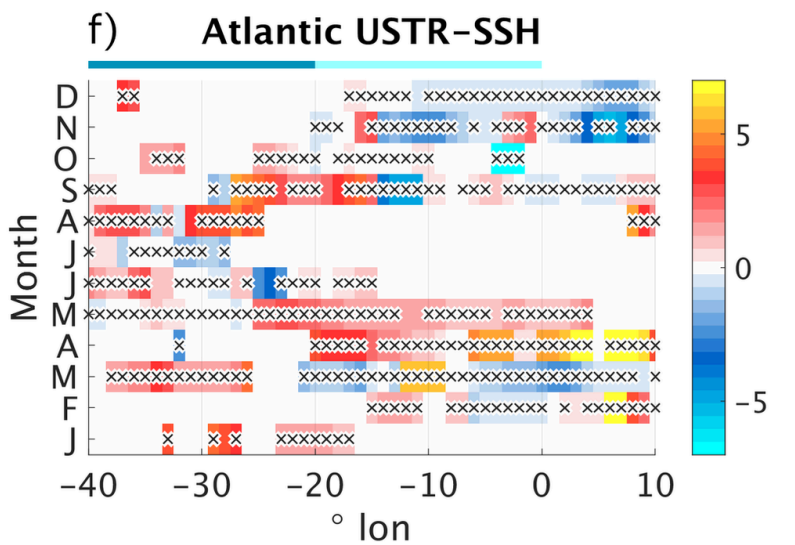
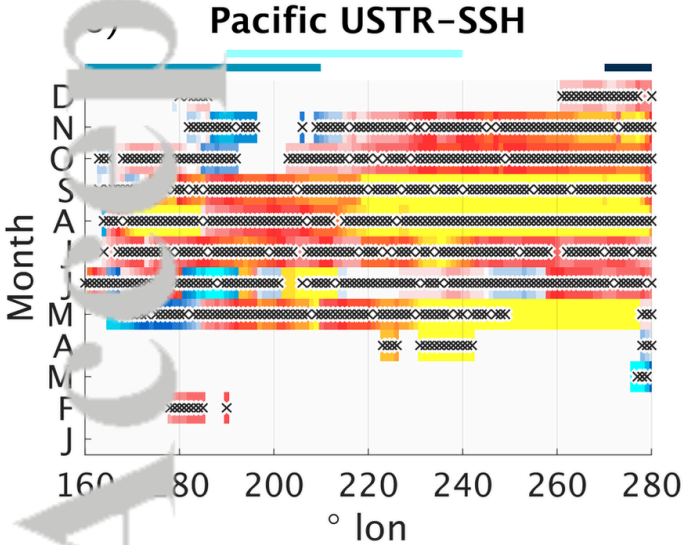
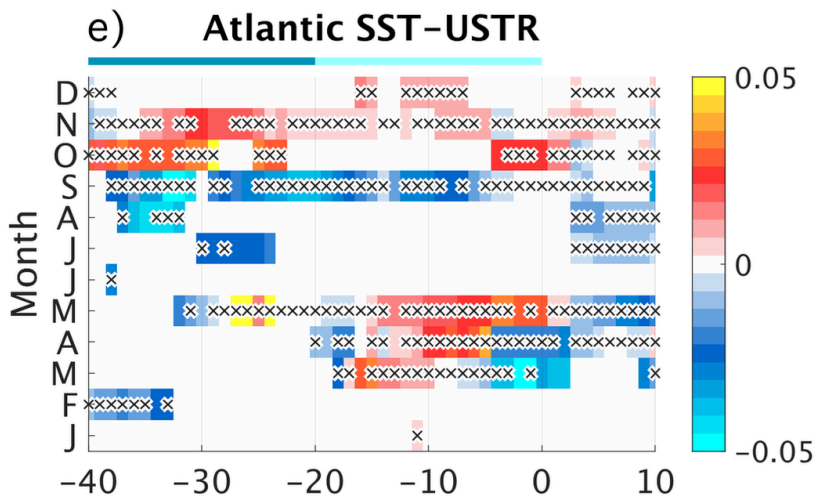
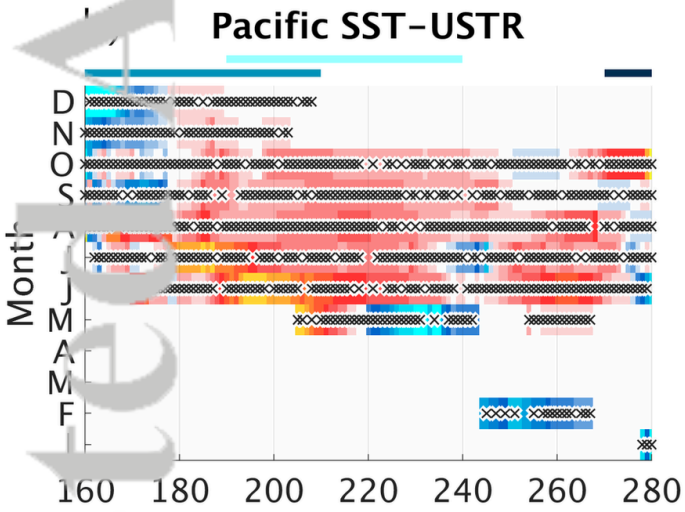
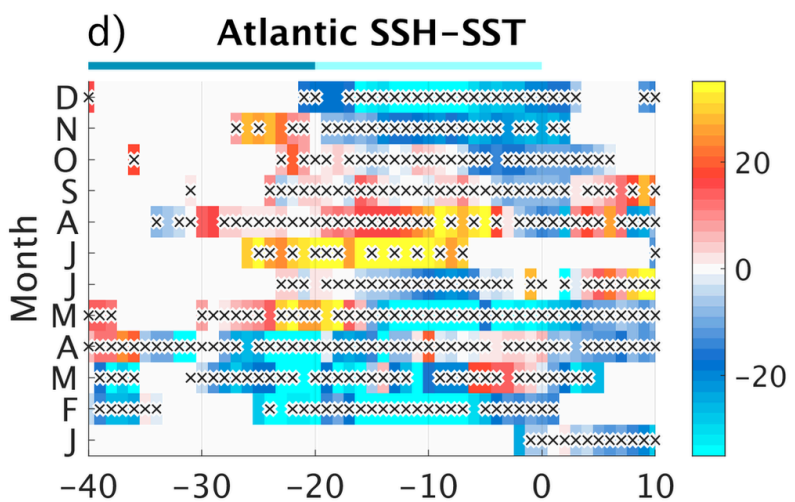
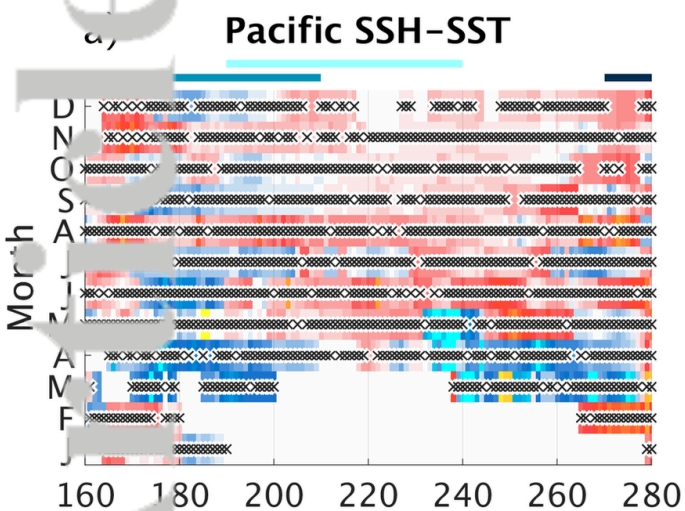
2018JC014700-f02-z_AA.png



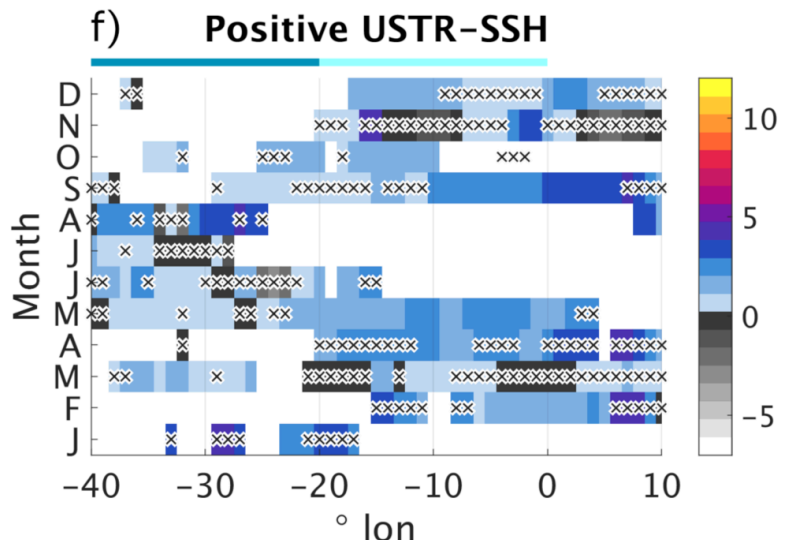
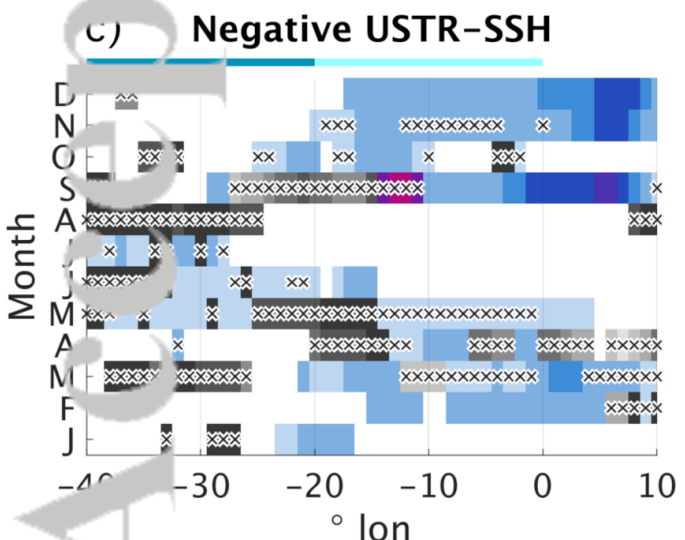
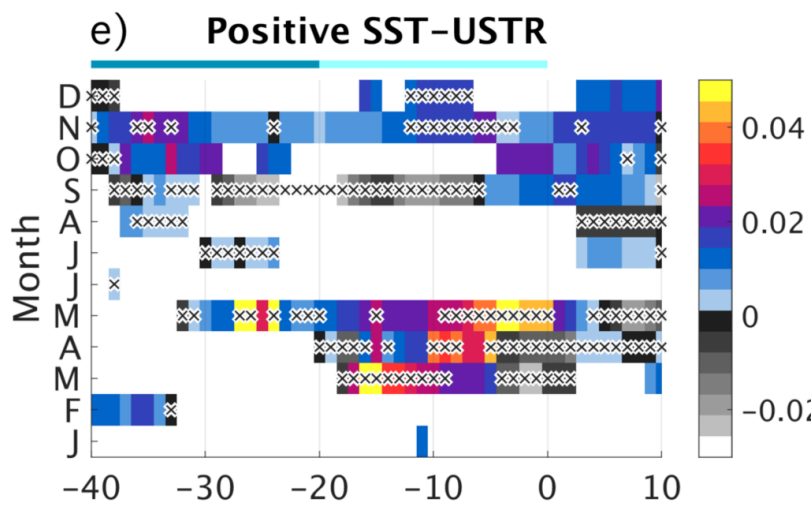
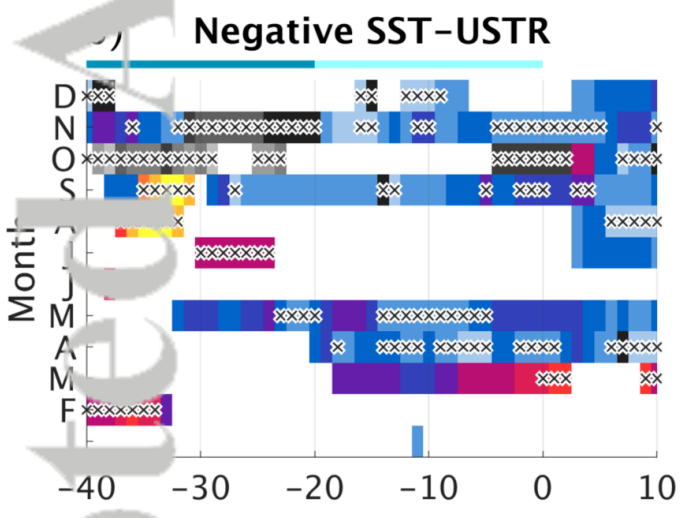
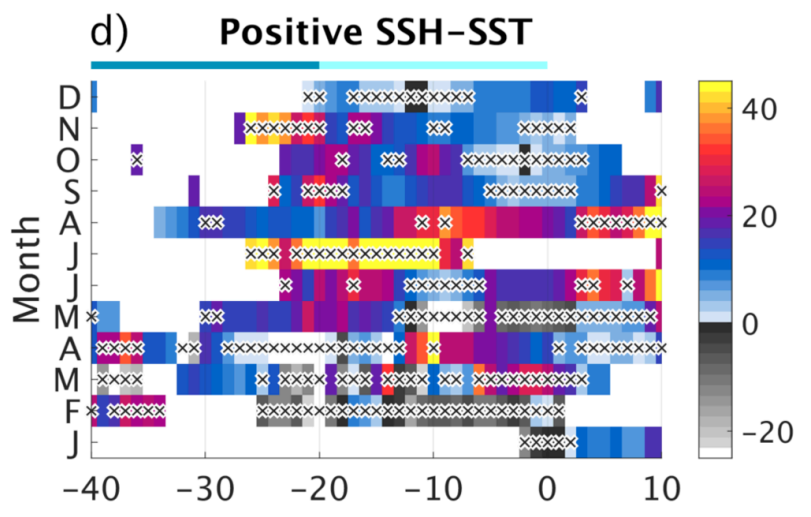
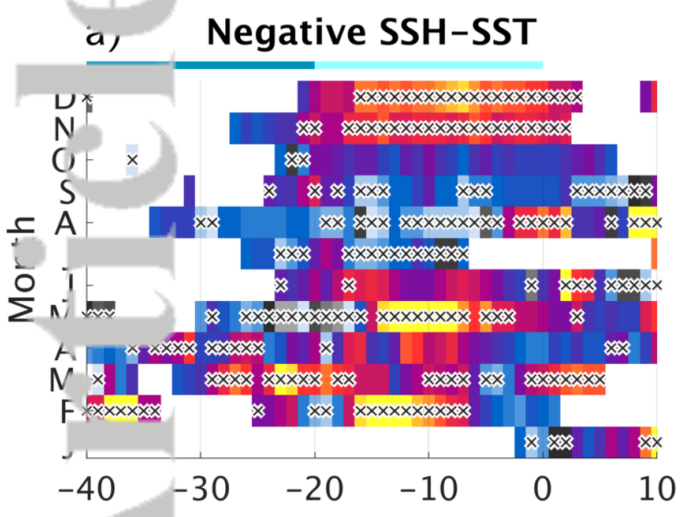
2018JC014700-f03-z-AA.png



2018JC014700-f04-z-AA.png

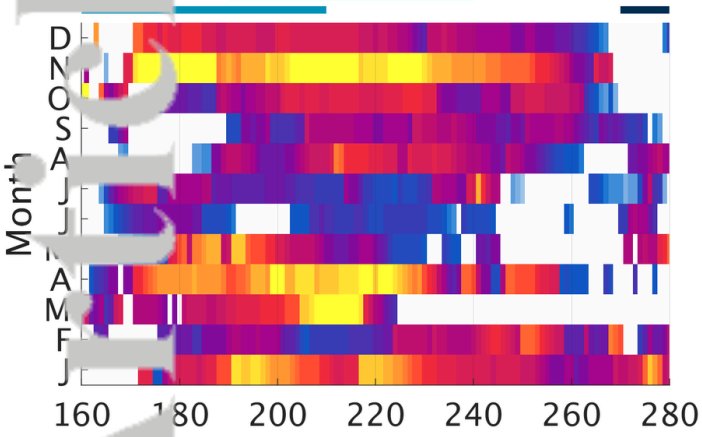


2018JC014700-f05-z_AA.png

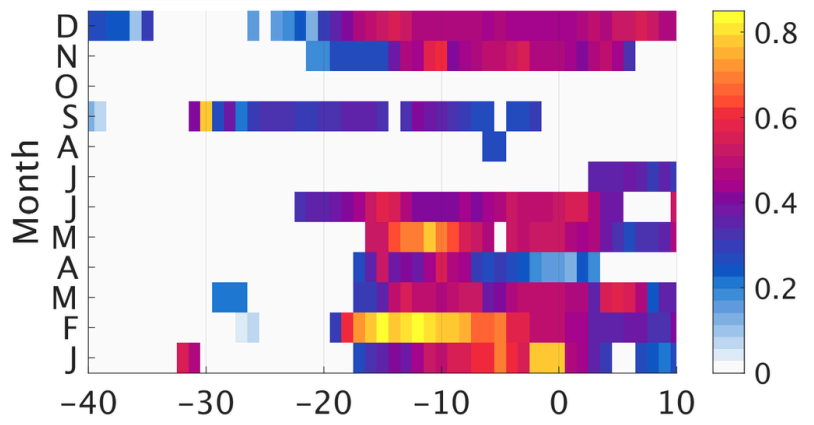


2018JC014700-f06-z-AA.png

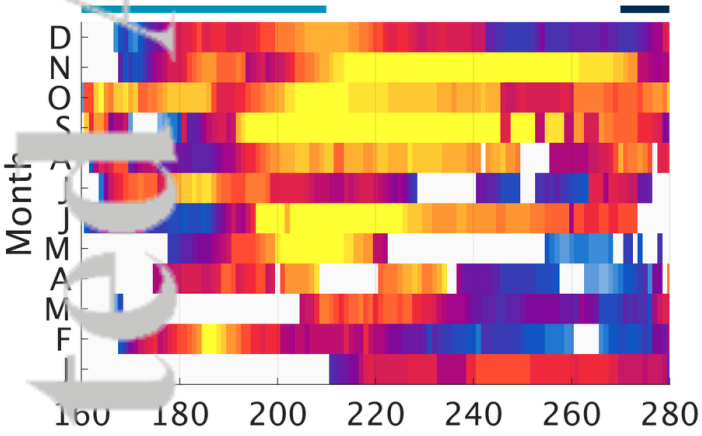
a) Pacific: negative



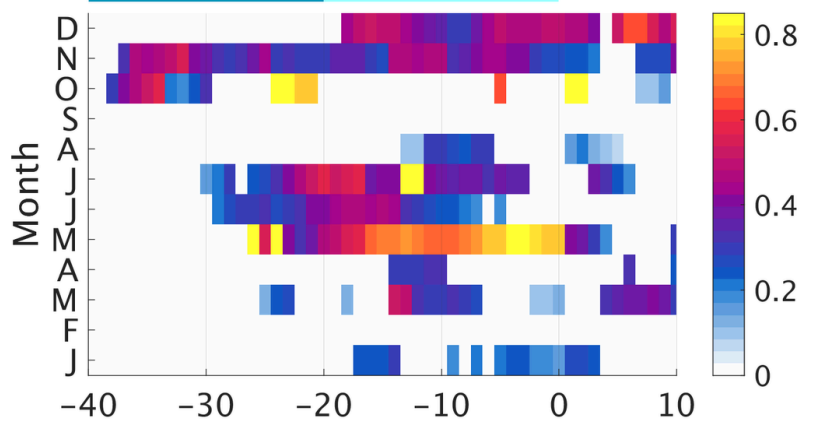
d) Atlantic: negative



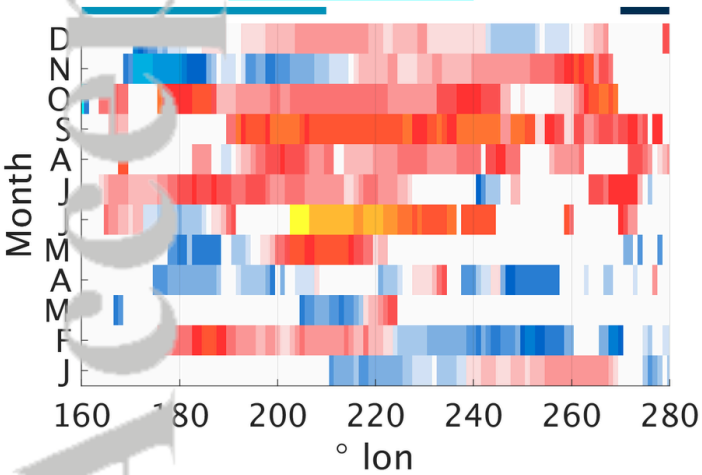
b) Pacific: positive



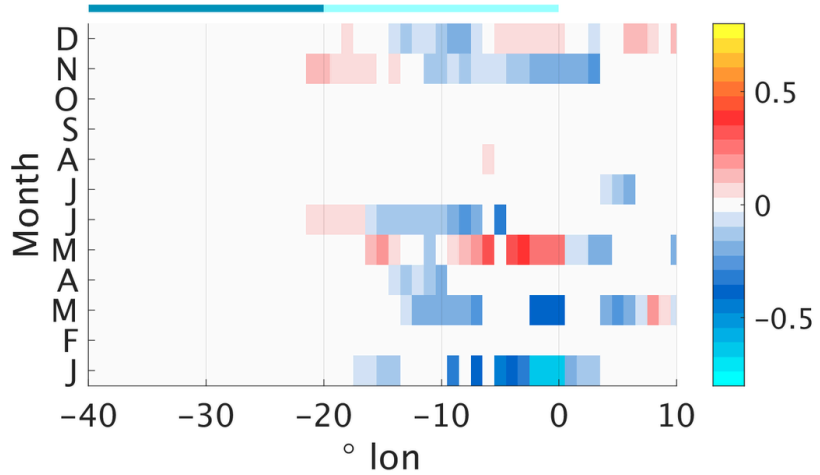
e) Atlantic: positive



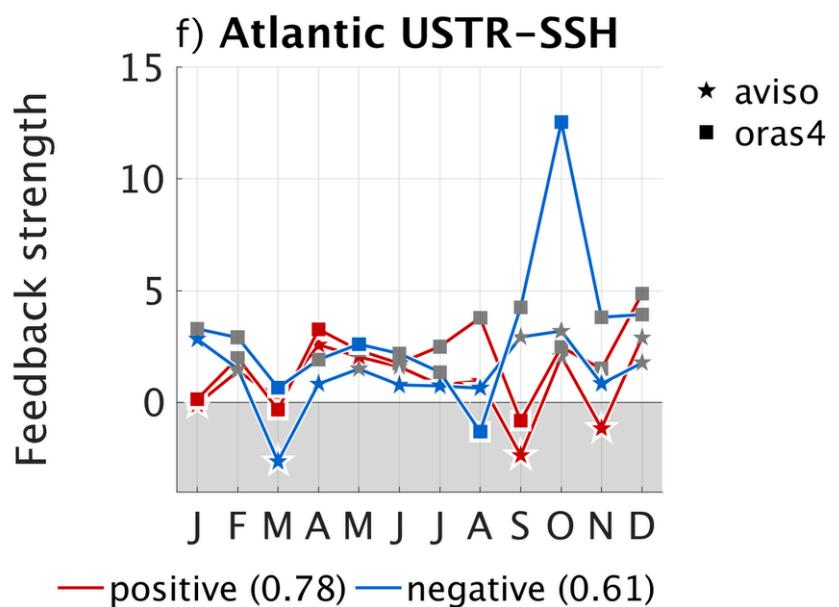
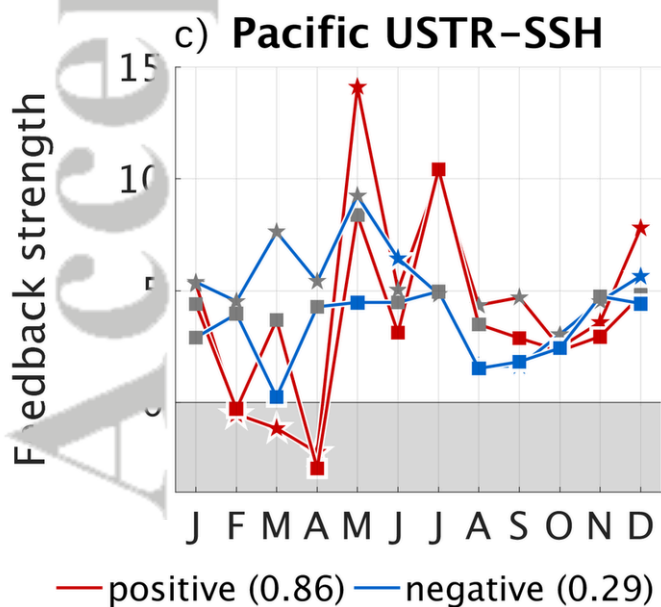
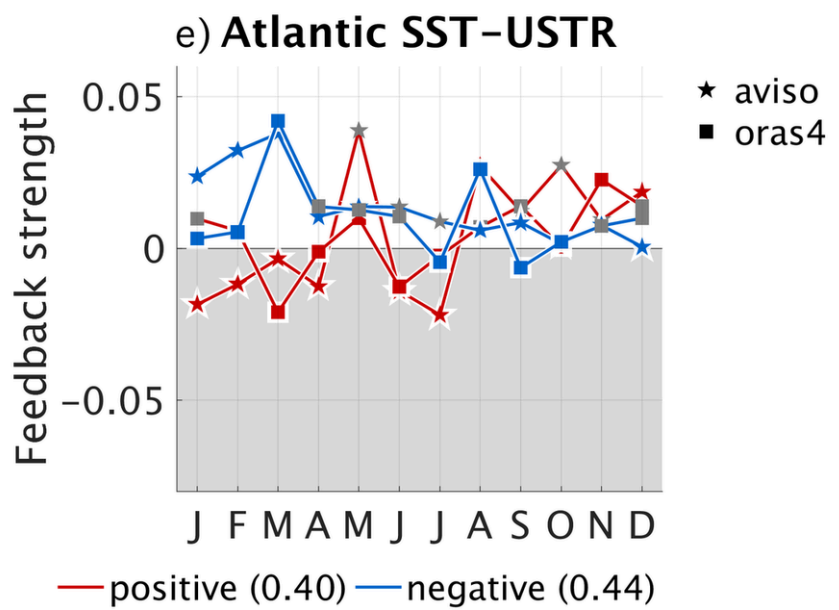
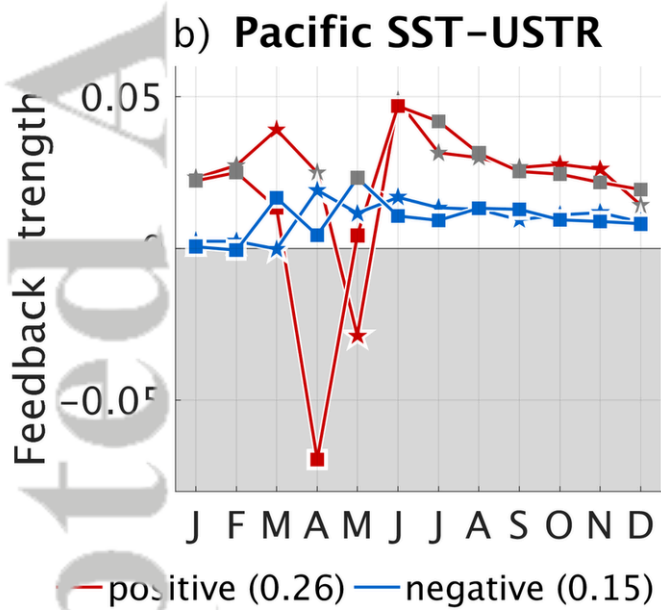
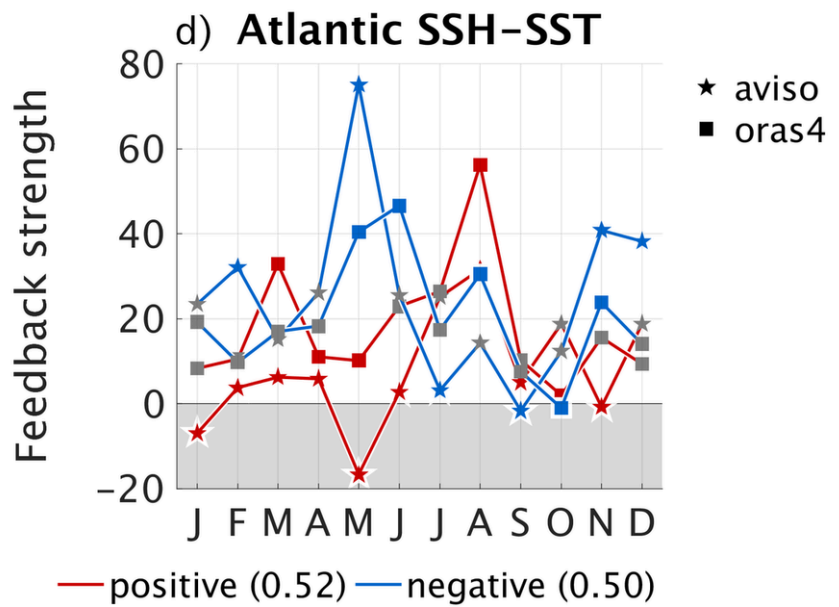
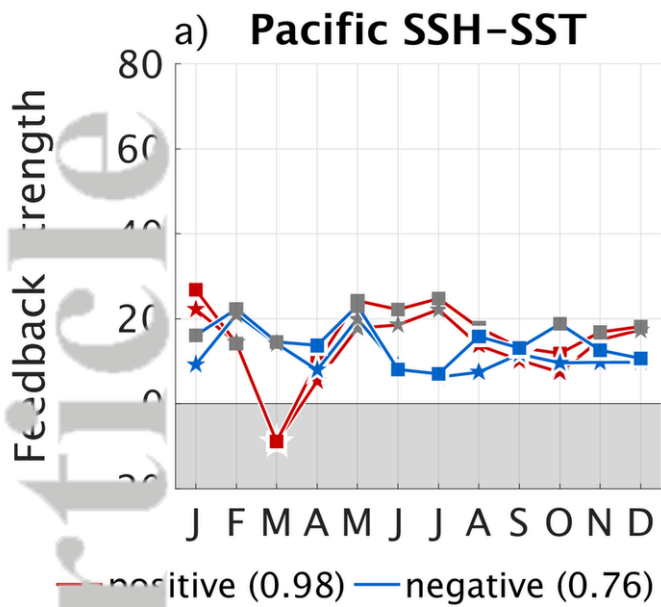
c) Pacific: difference



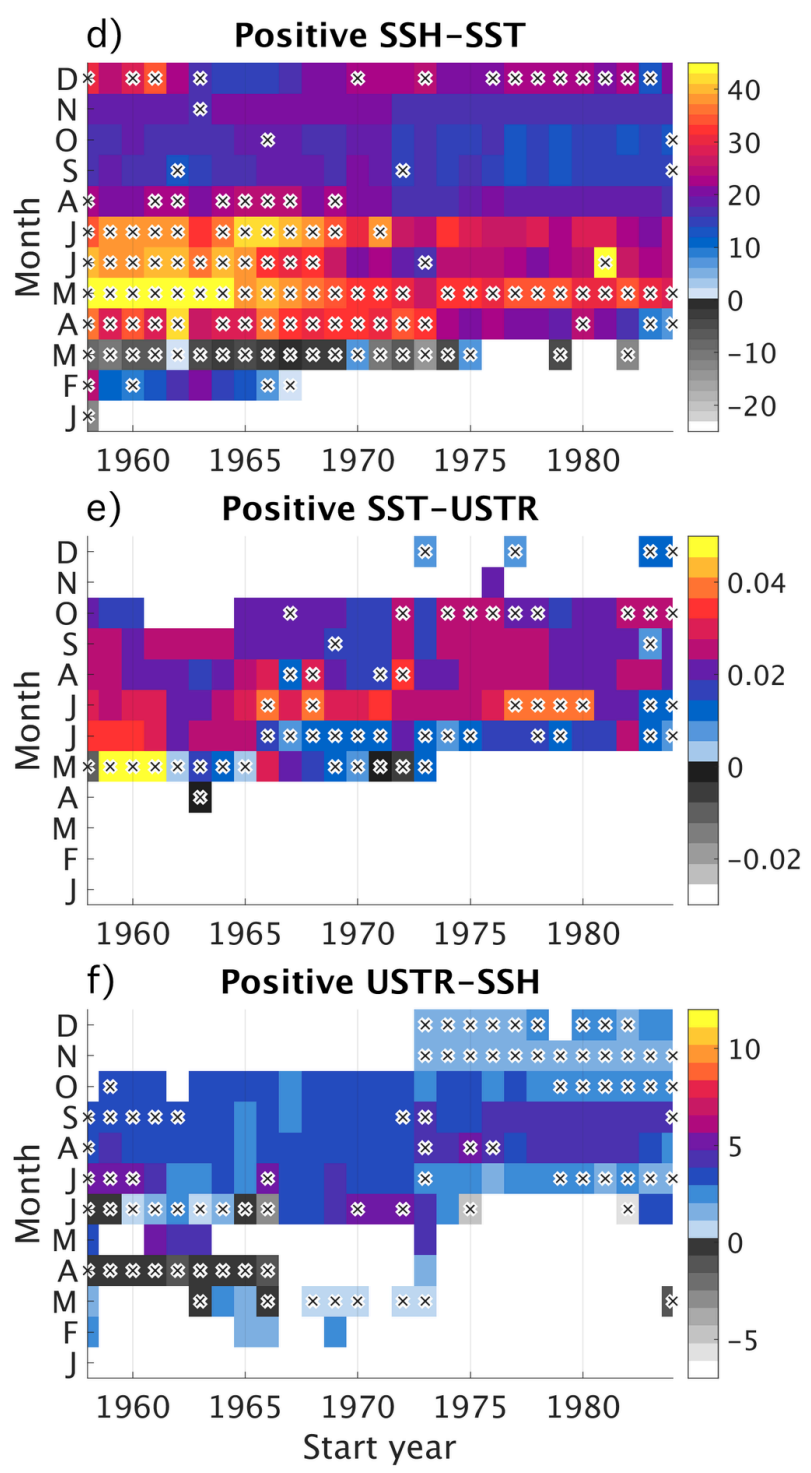
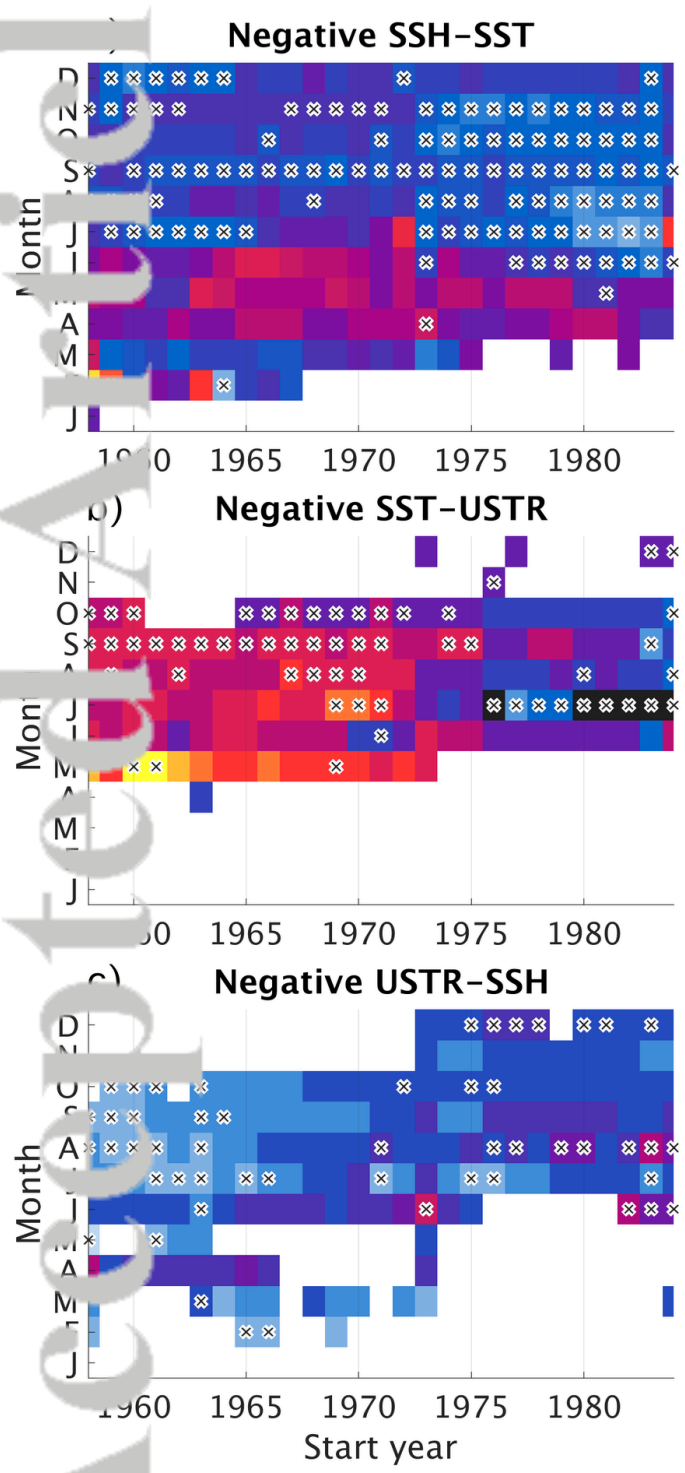
f) Atlantic: difference



2018JC014700-f07-z_AA.png

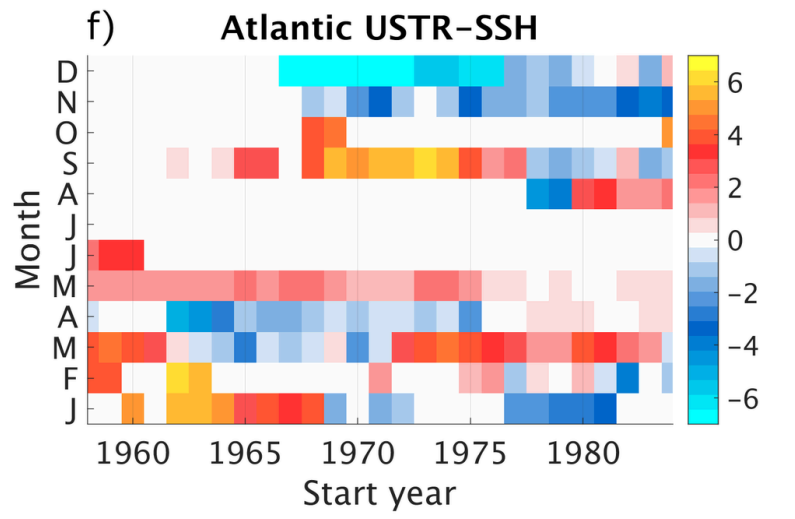
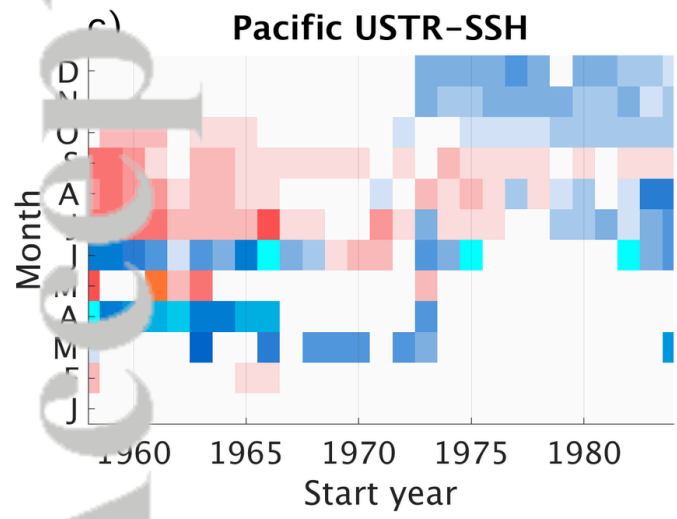
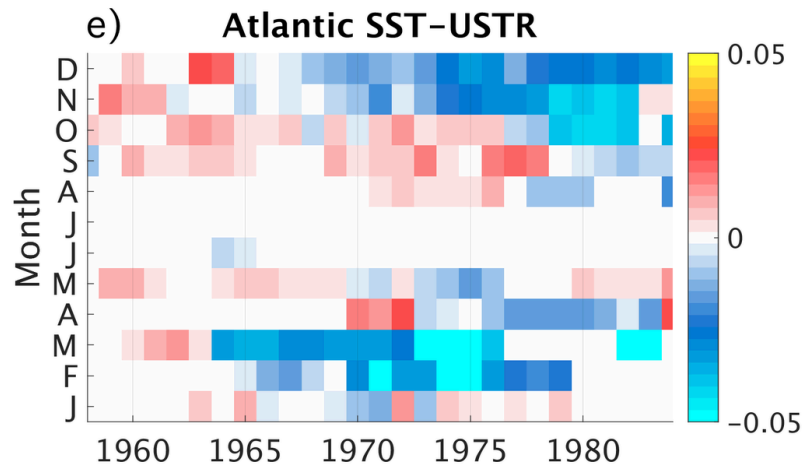
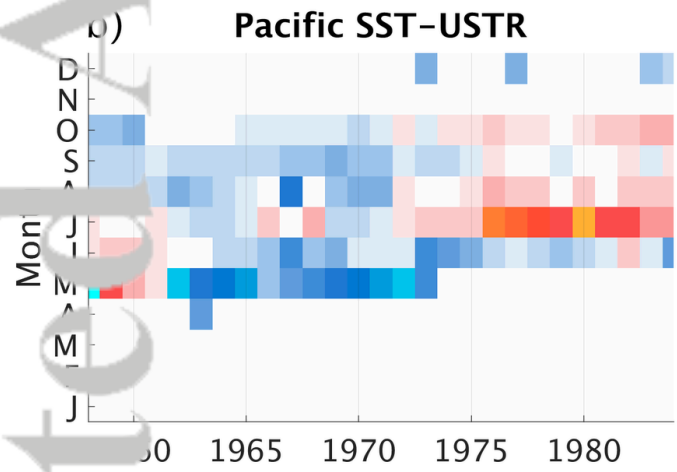
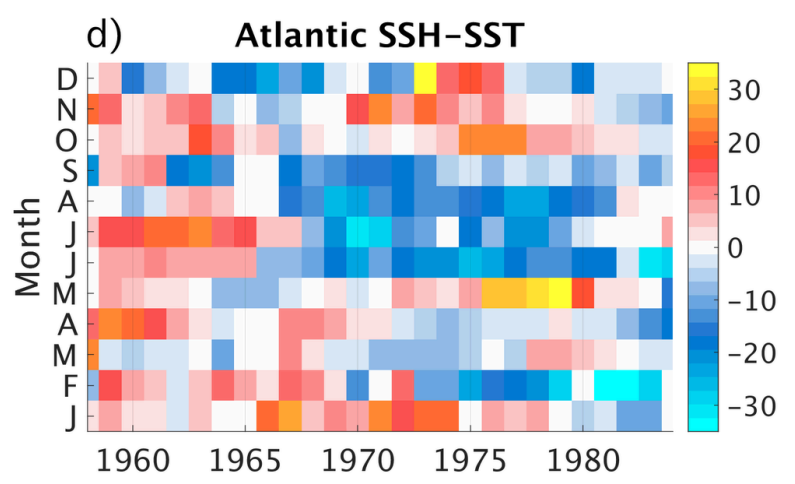
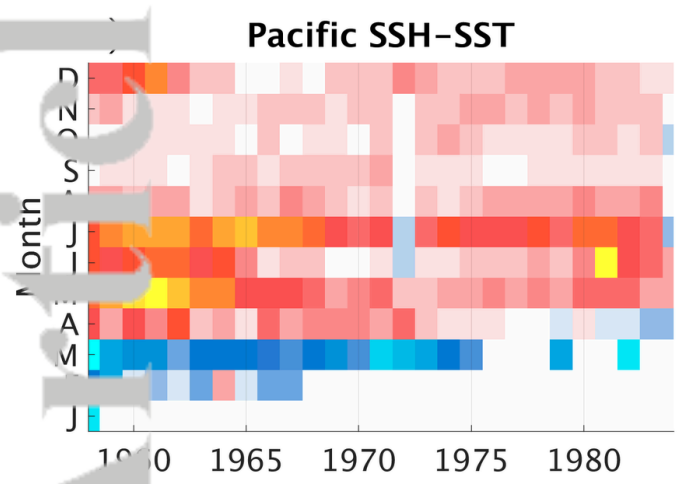


Accepted Article

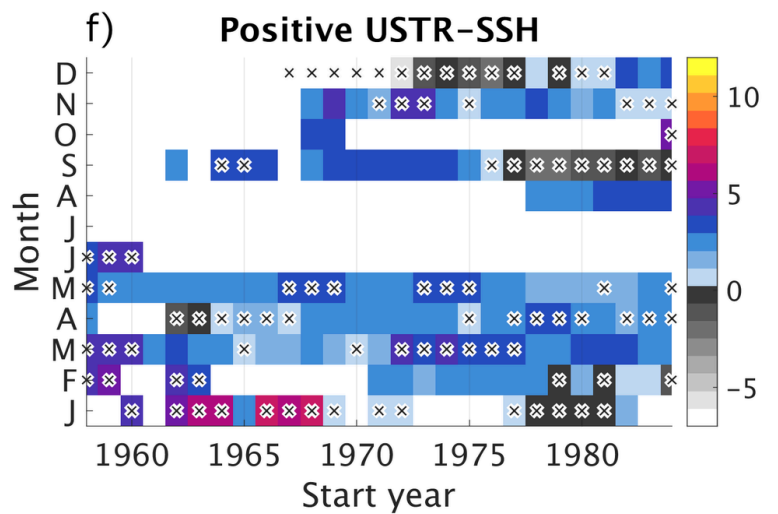
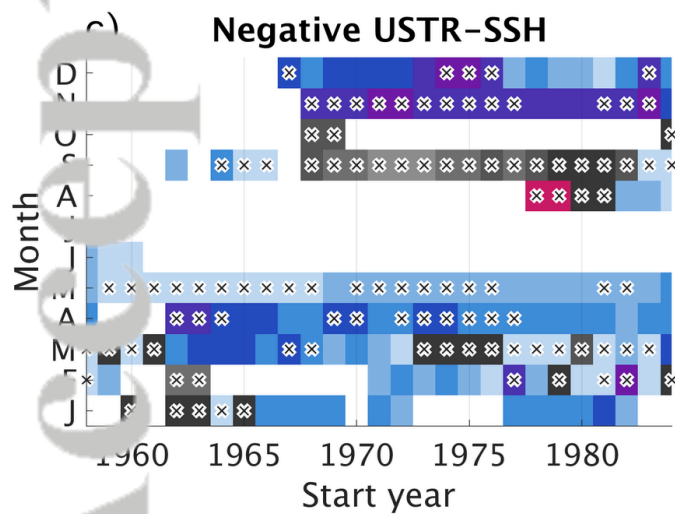
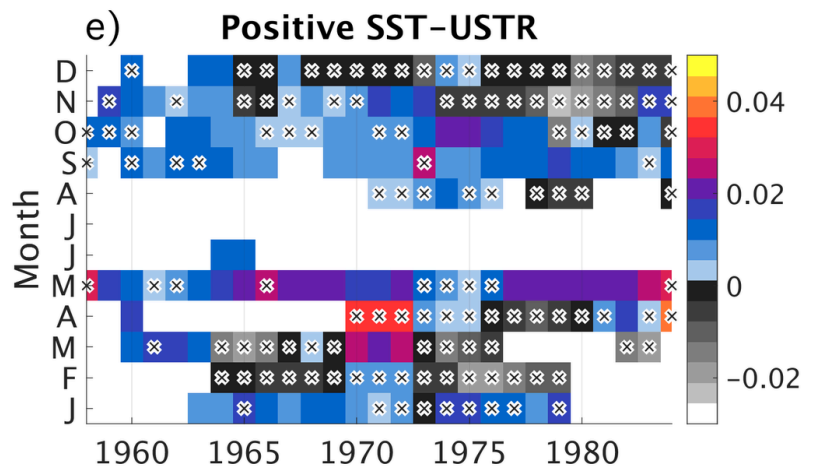
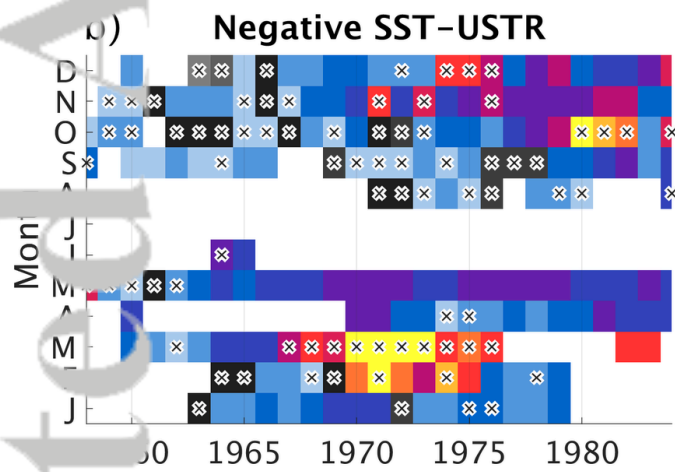
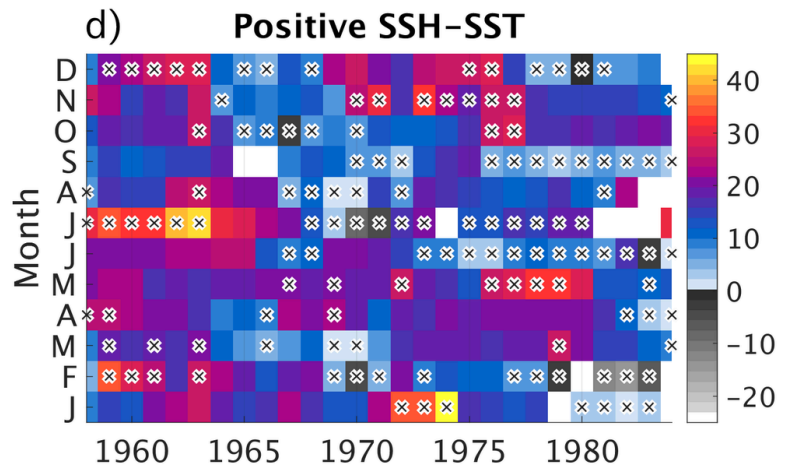
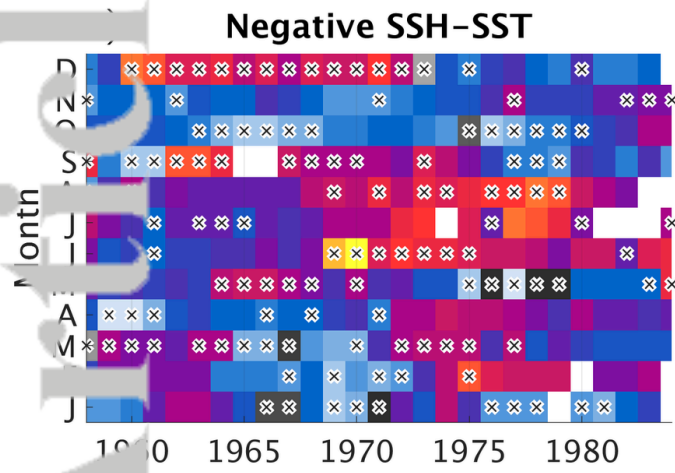


2018JC014700-f09-z_AA.png

Accepted Article

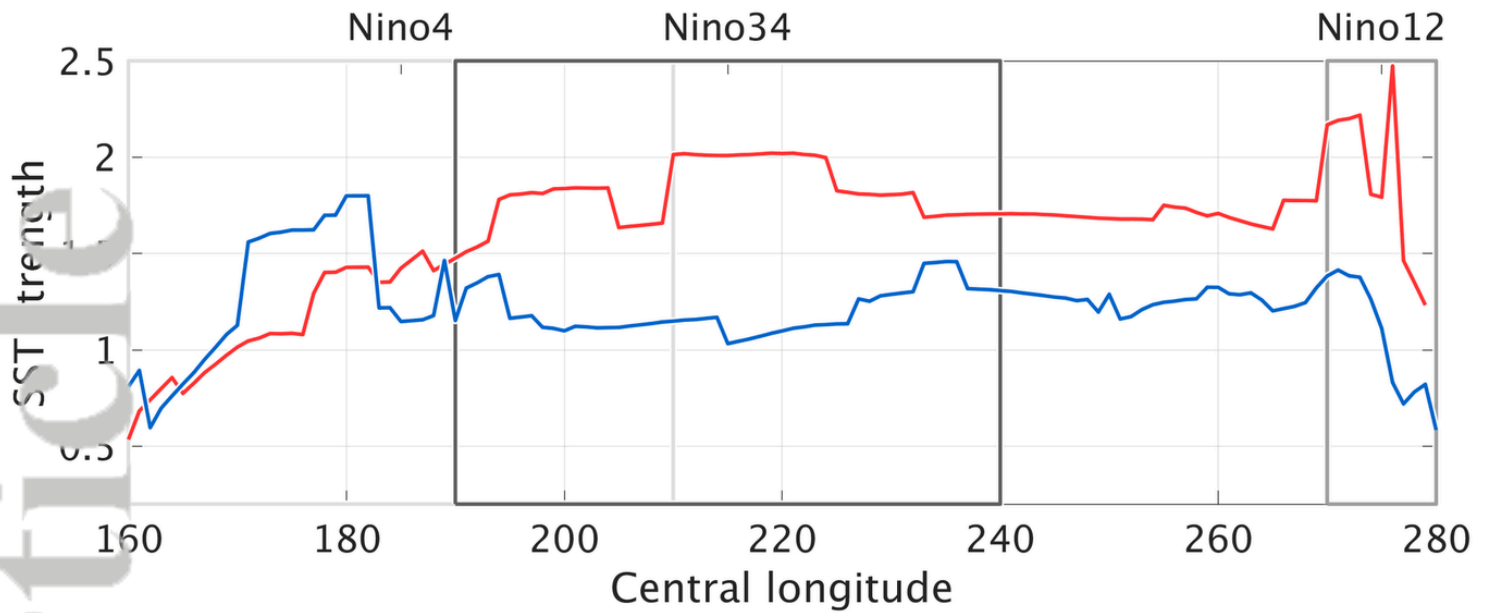


2018JC014700-f10-z_AA.png

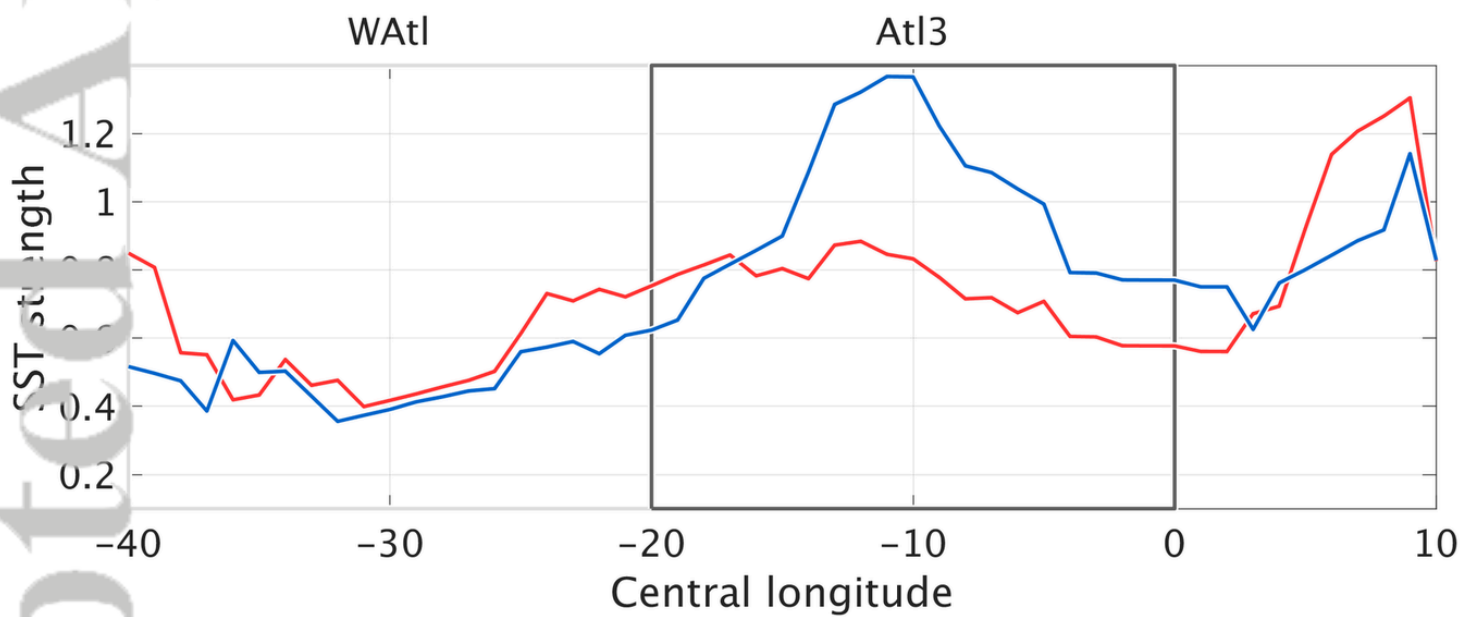


2018JC014700-f11-z_AA.png

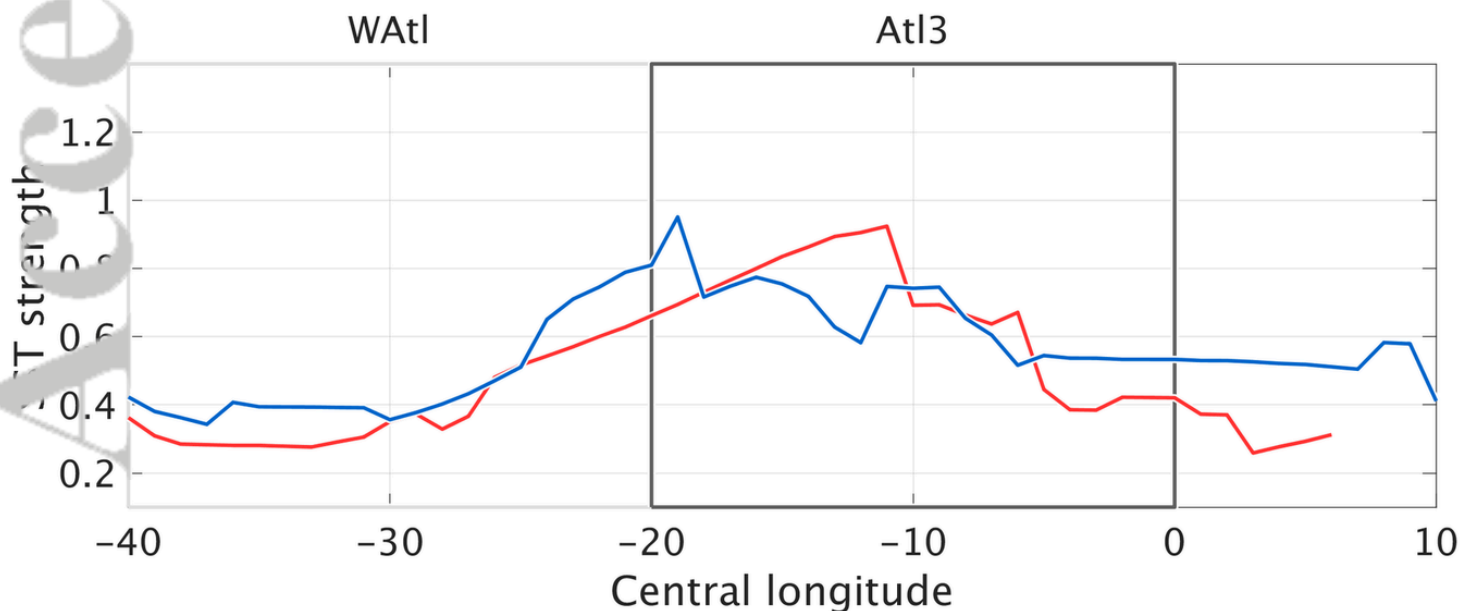
a)

Pacific, NDJ

b)

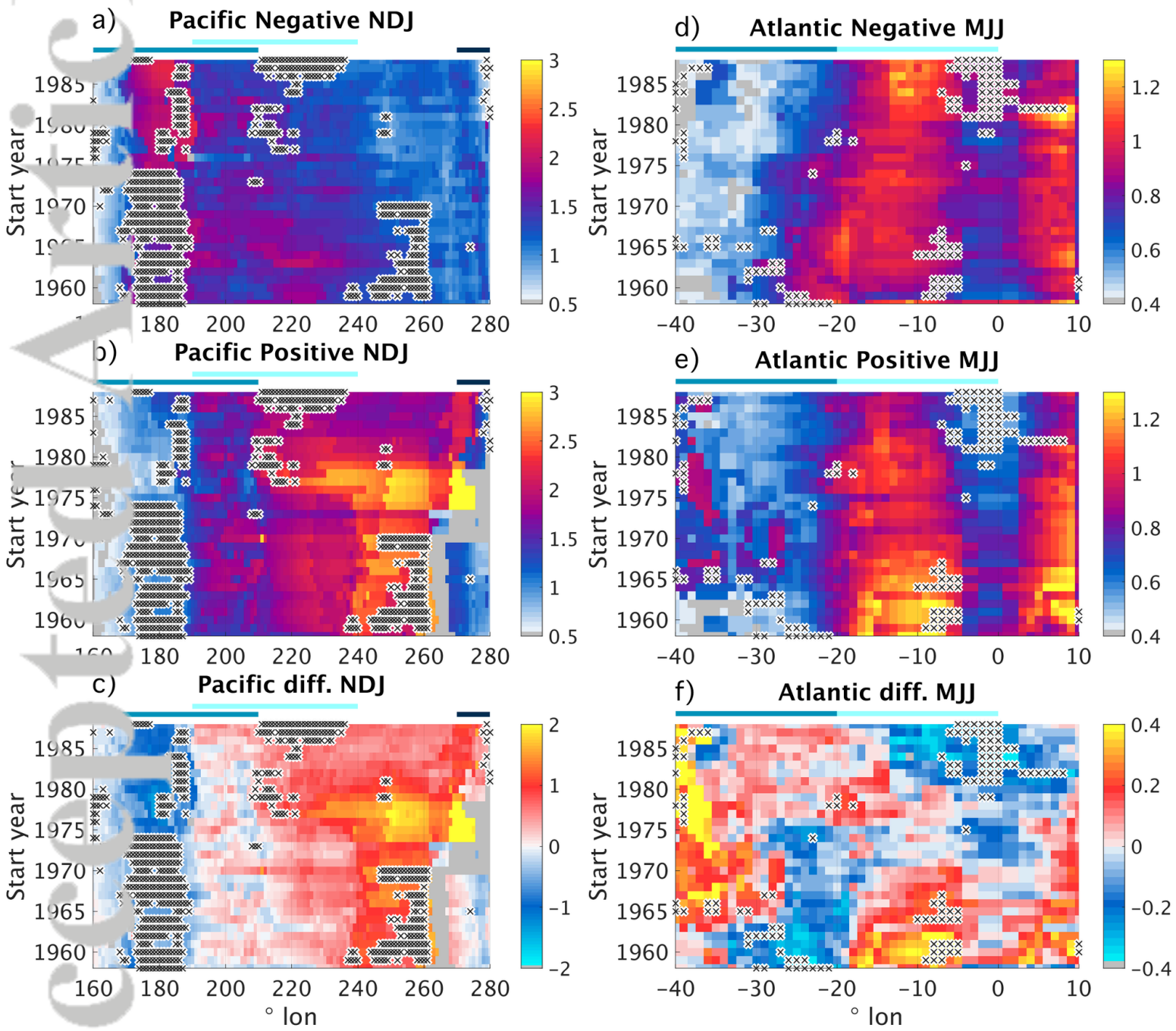
Atlantic, MJJ

c)

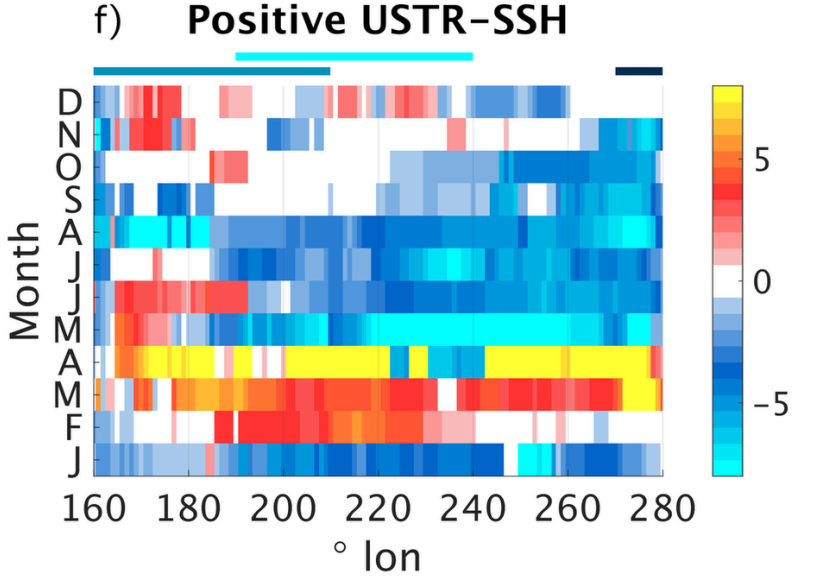
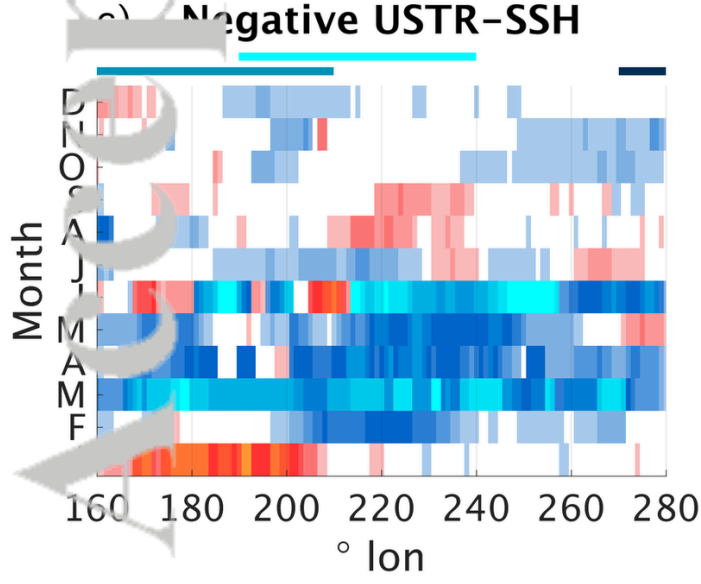
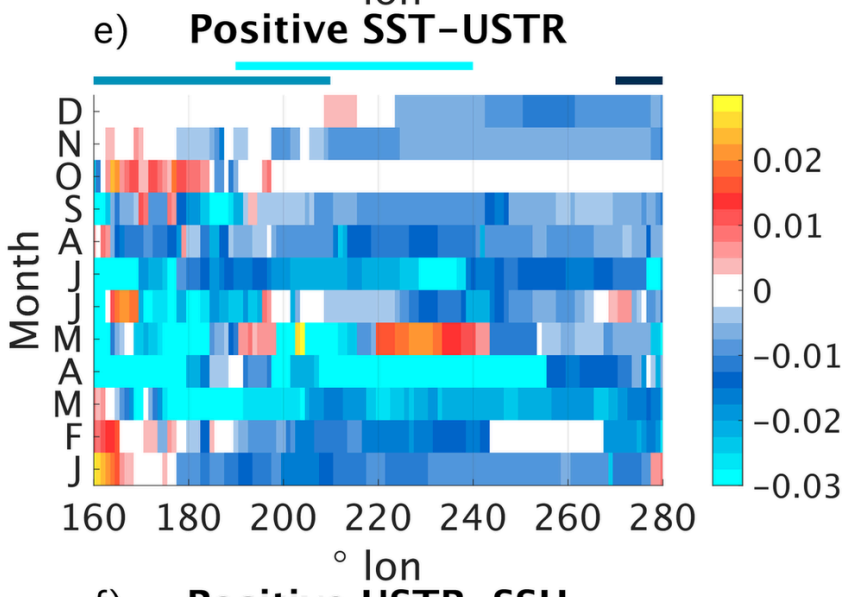
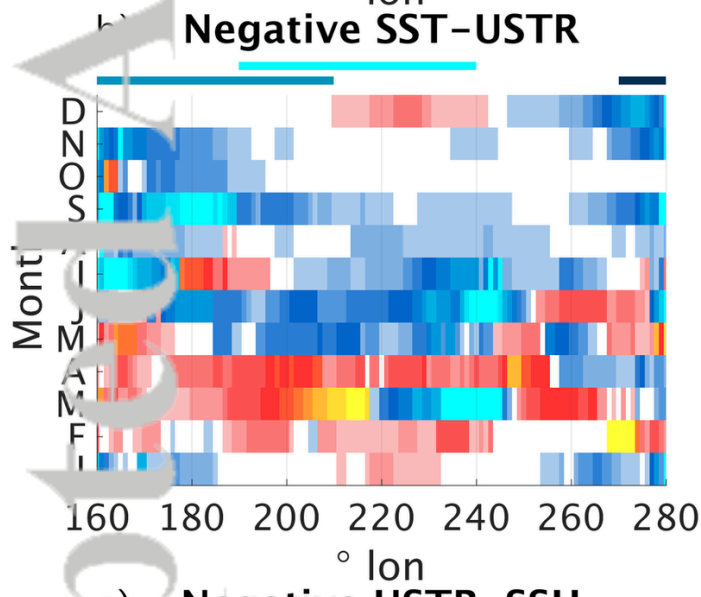
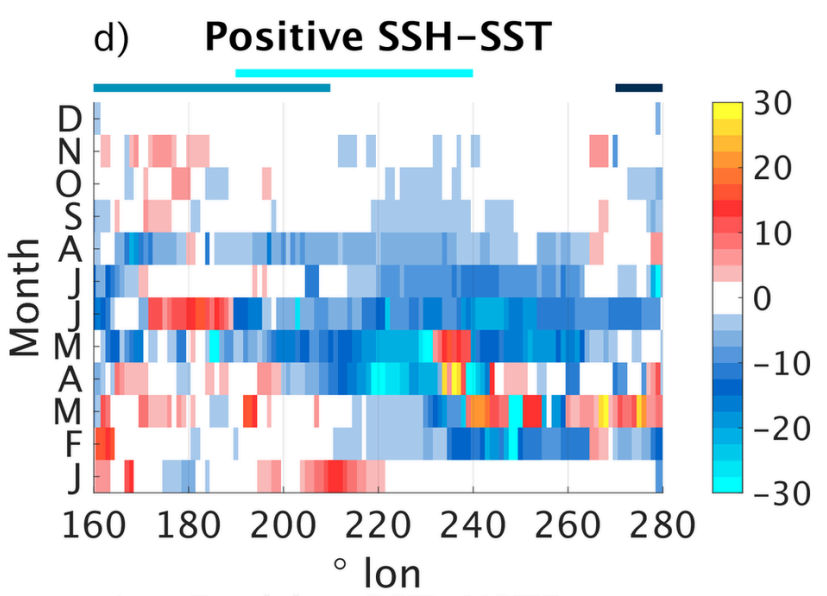
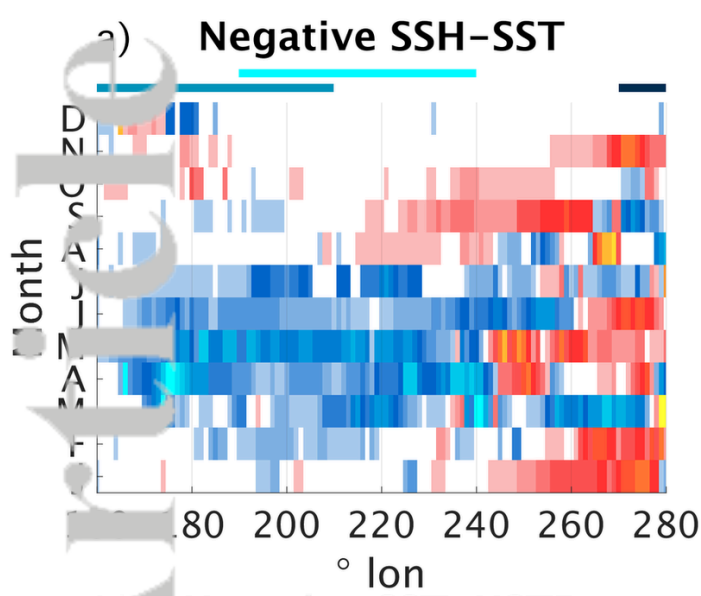
Atlantic, OND

— Positive — Negative

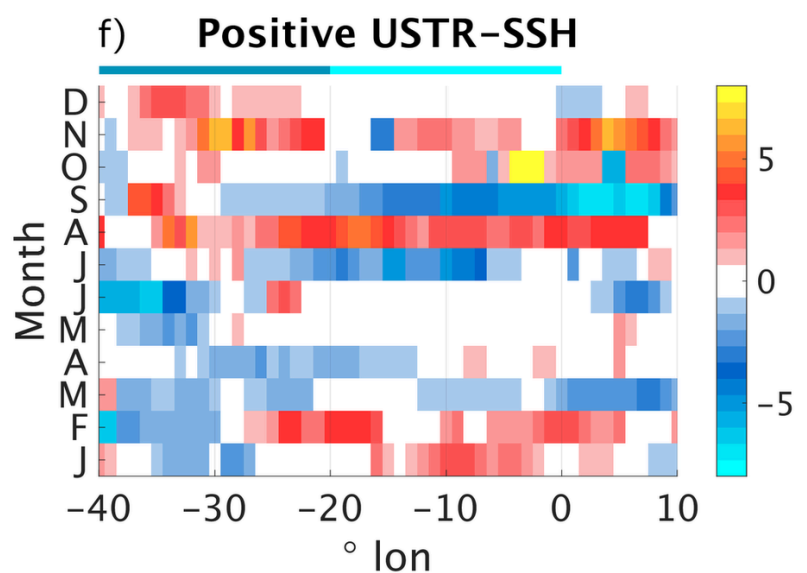
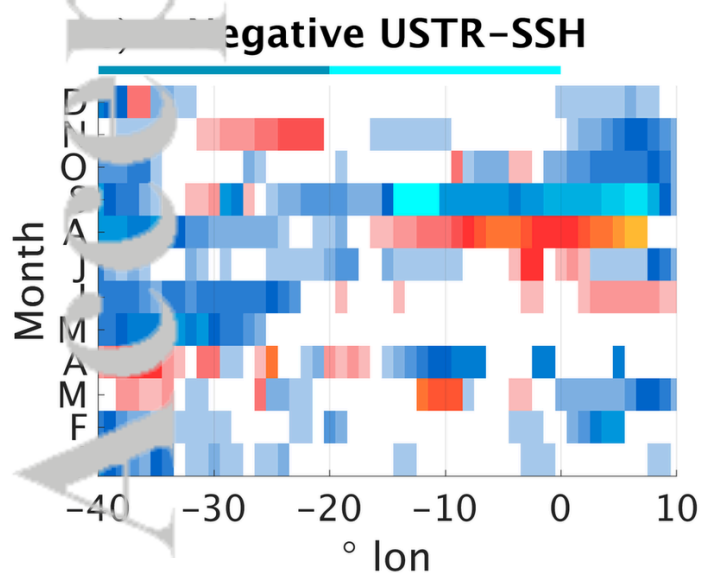
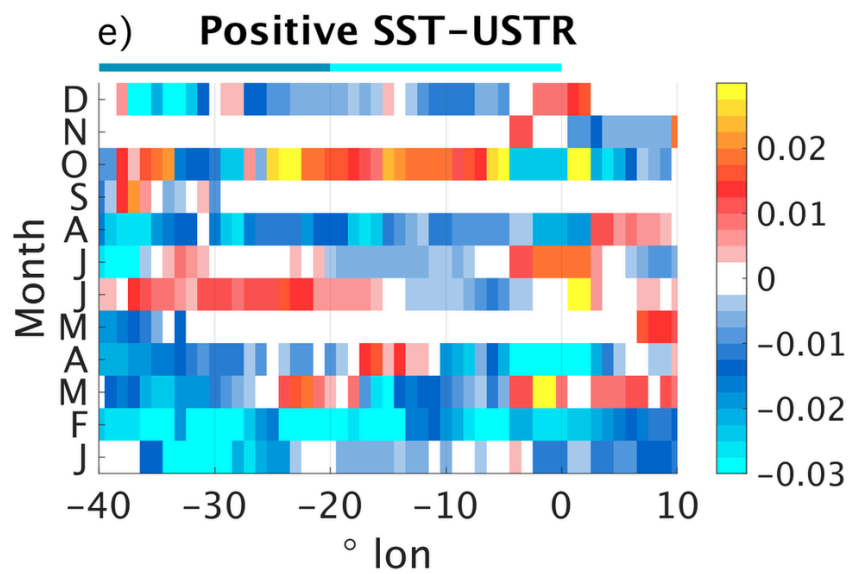
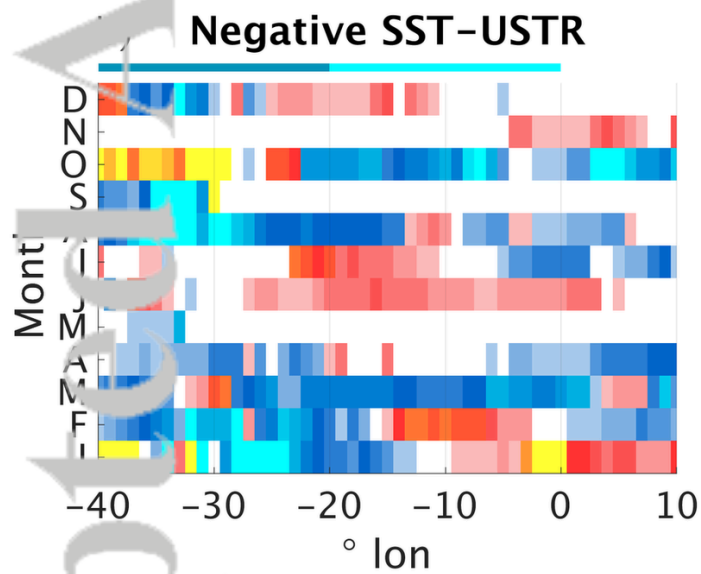
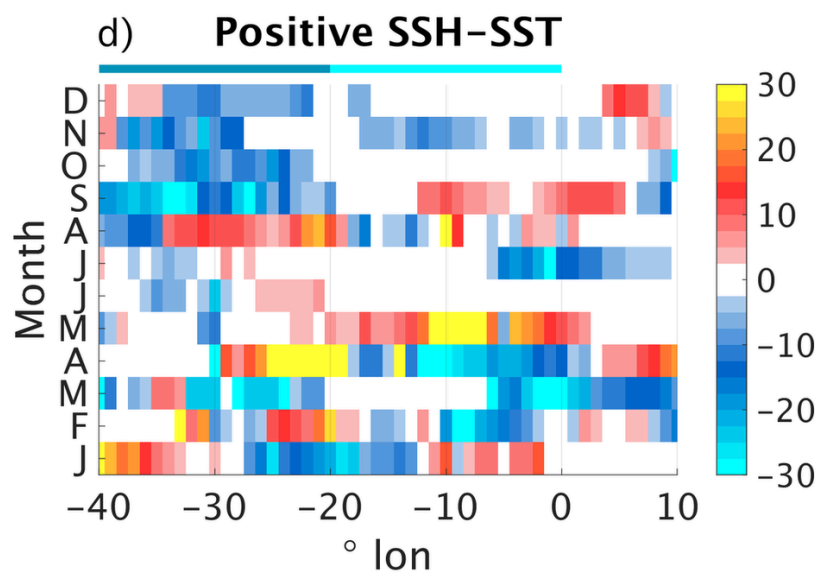
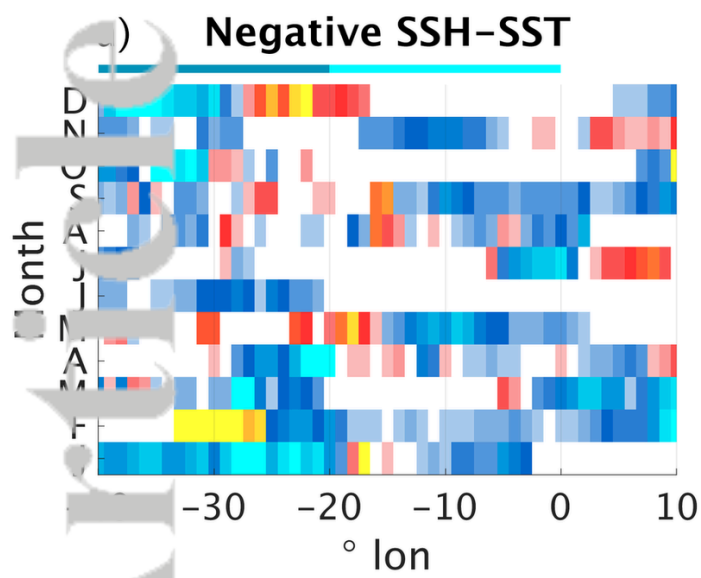
Accepted Article



2018JC014700-f13-z_AA.png

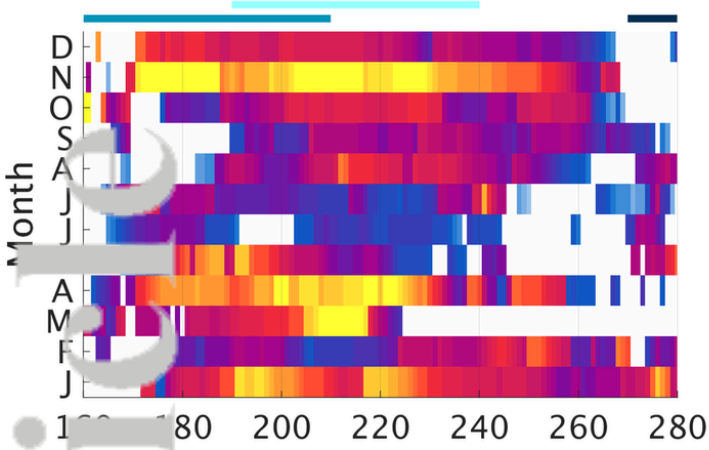


2018JC014700-f14-z-AA.png

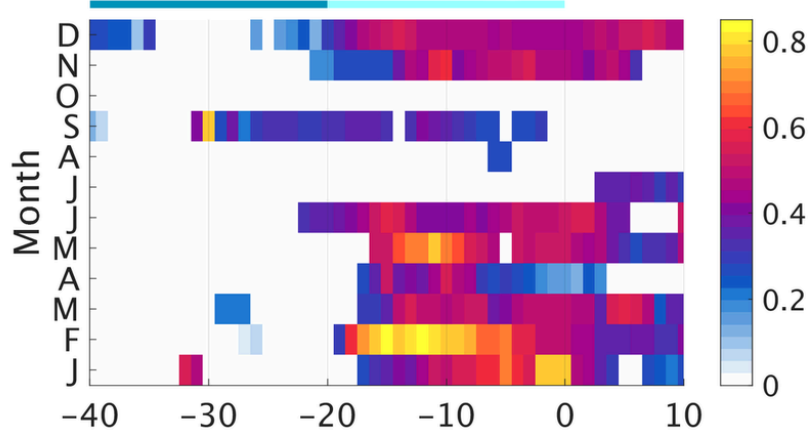


2018JC014700-f15-z-AA.png

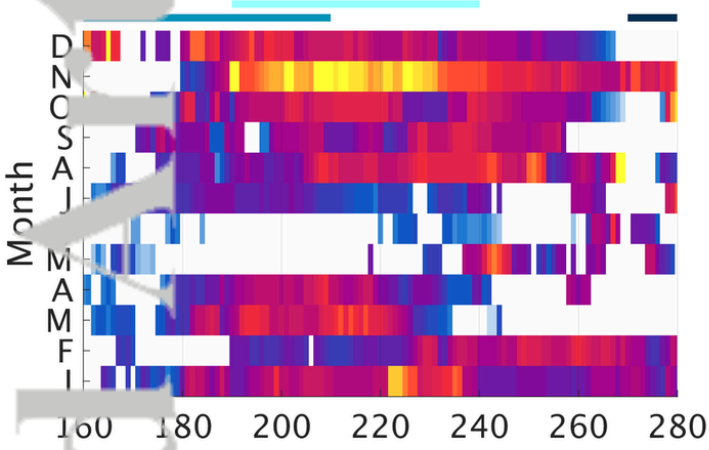
a) Pacific: SST



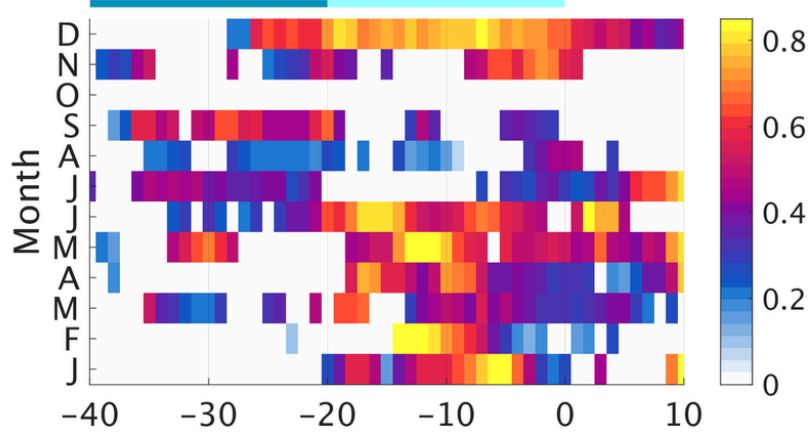
e) Atlantic: SST



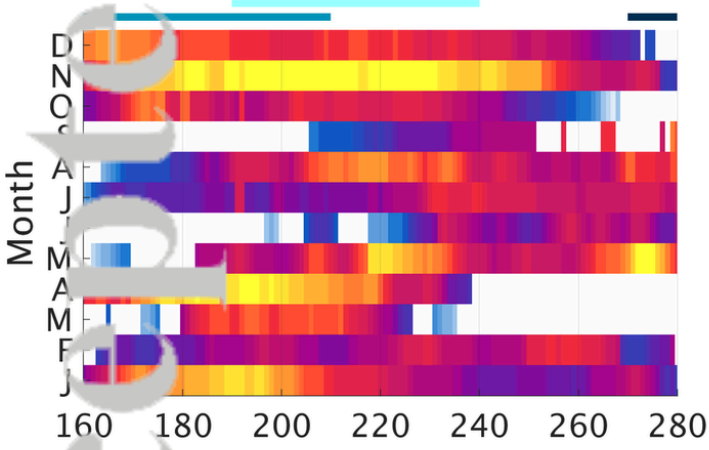
b) Pacific: SSH



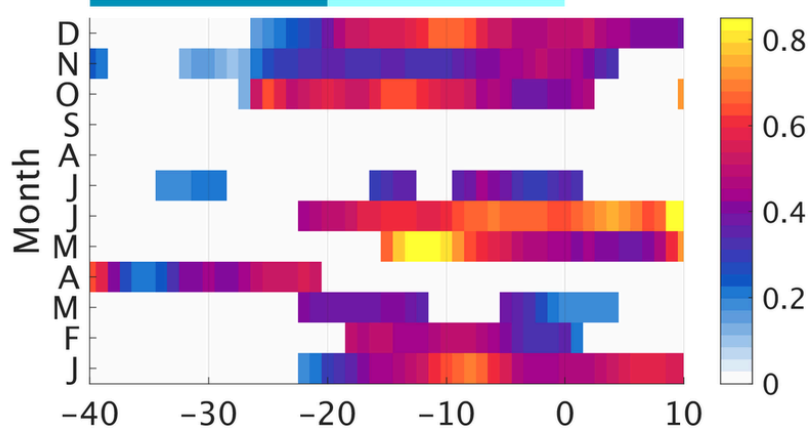
f) Atlantic: SSH



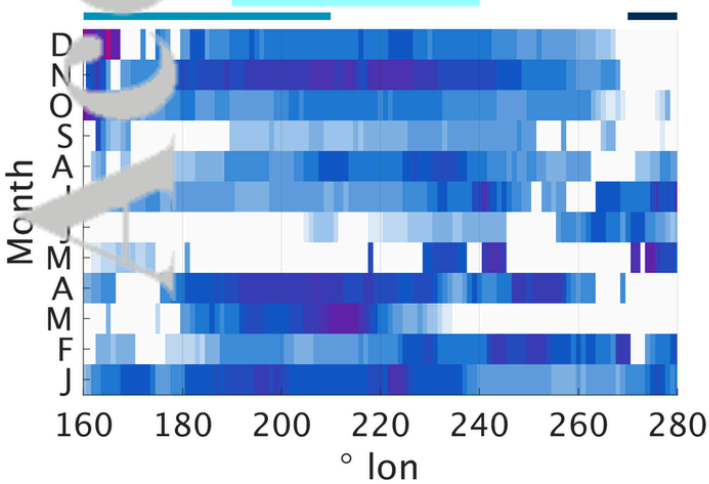
c) Pacific: USTR



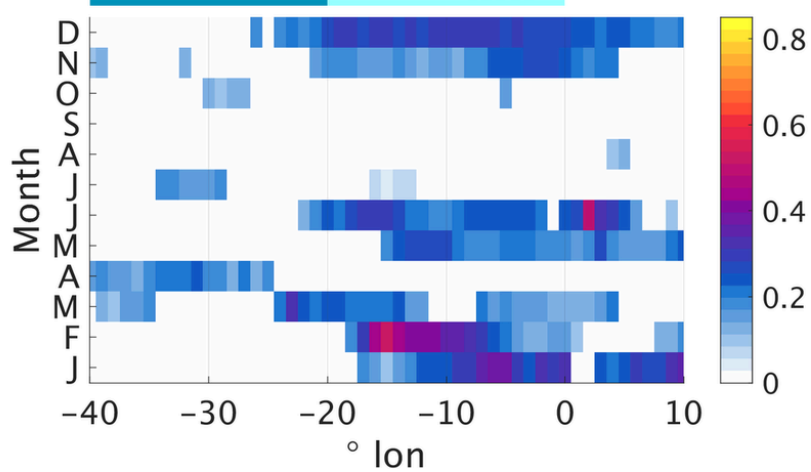
g) Atlantic: USTR



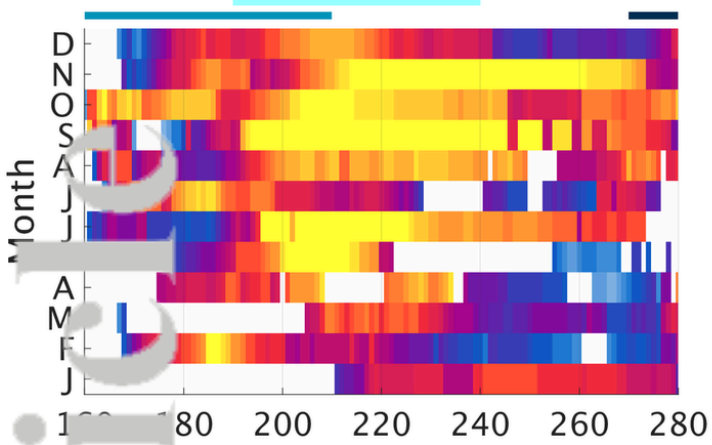
d) Pacific: all



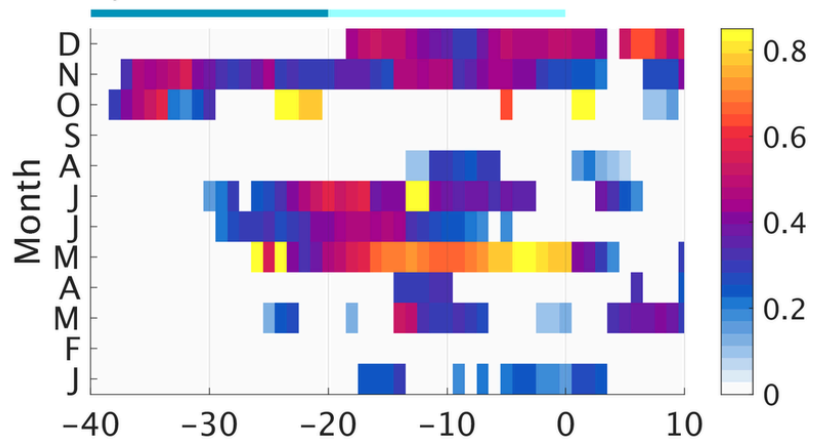
h) Atlantic: all



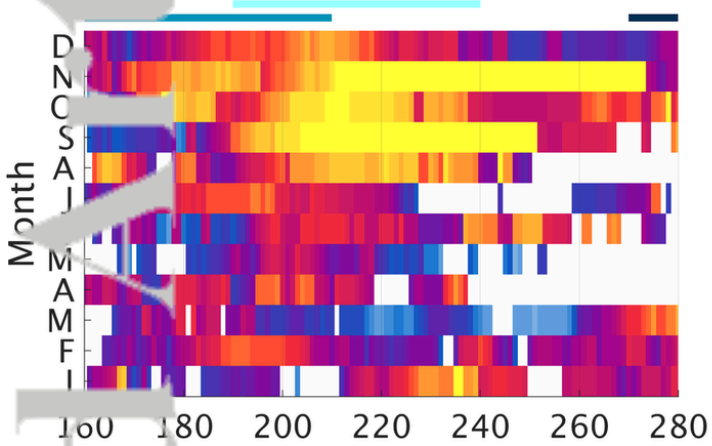
a) Pacific: SST



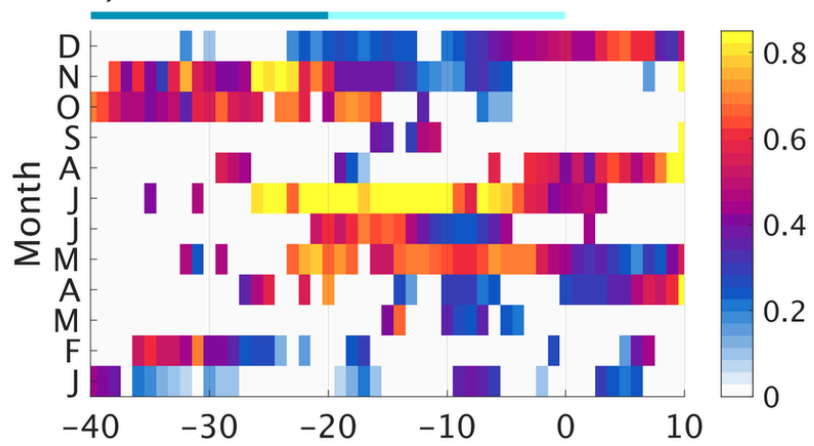
e) Atlantic: SST



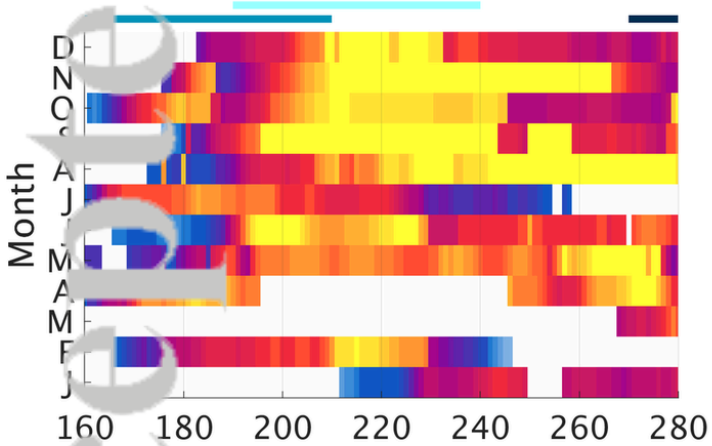
b) Pacific: SSH



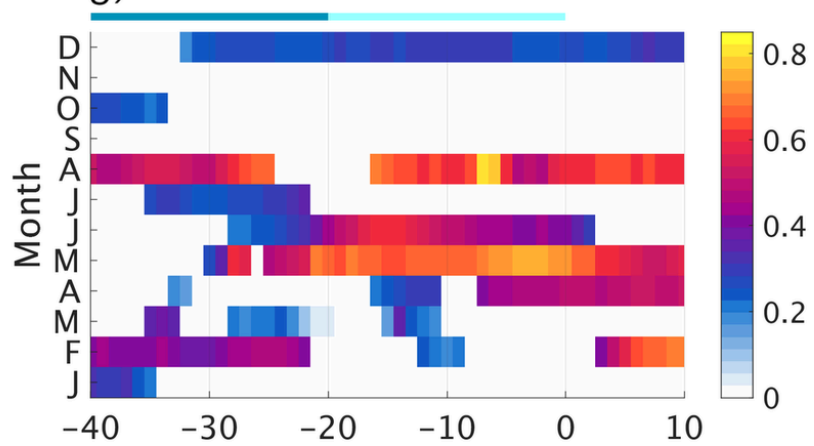
f) Atlantic: SSH



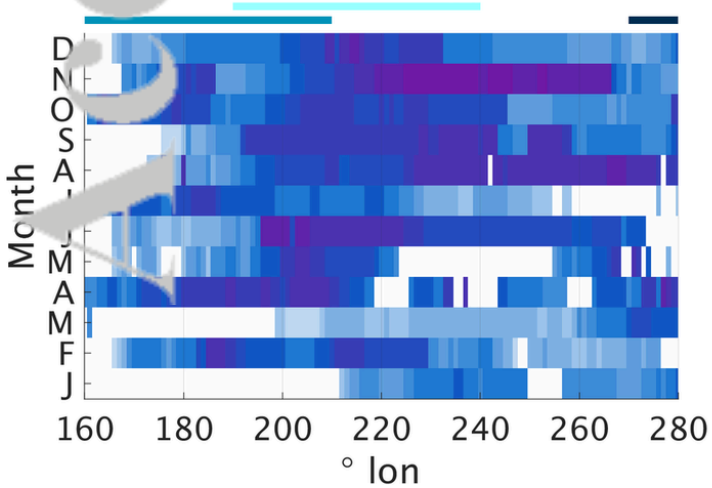
c) Pacific: USTR



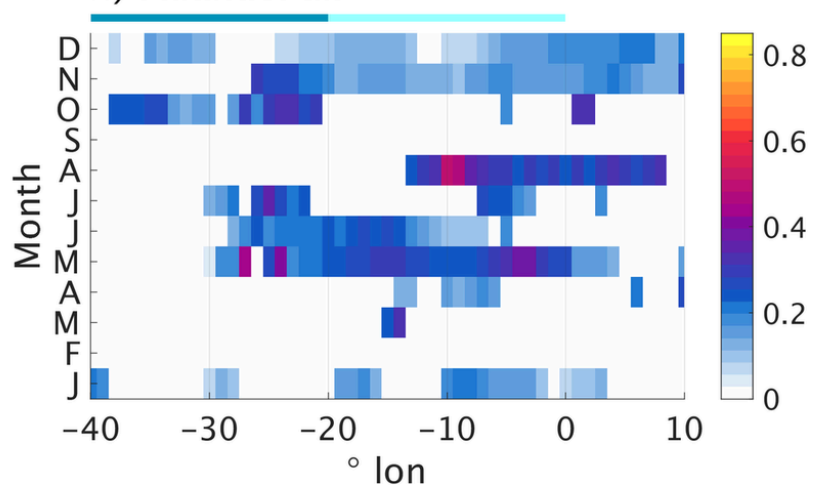
g) Atlantic: USTR



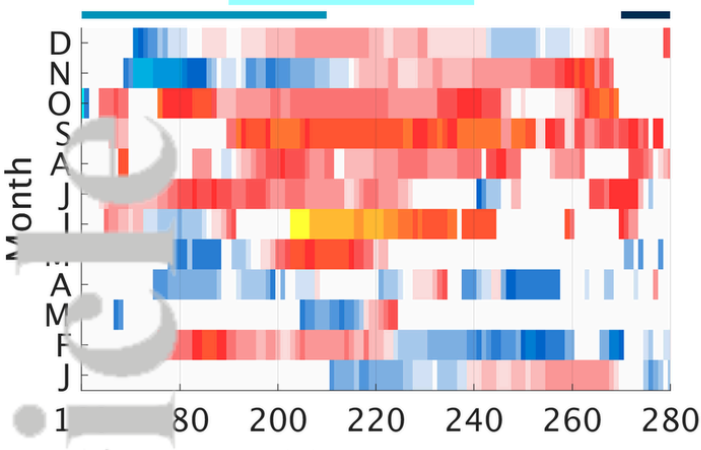
d) Pacific: all



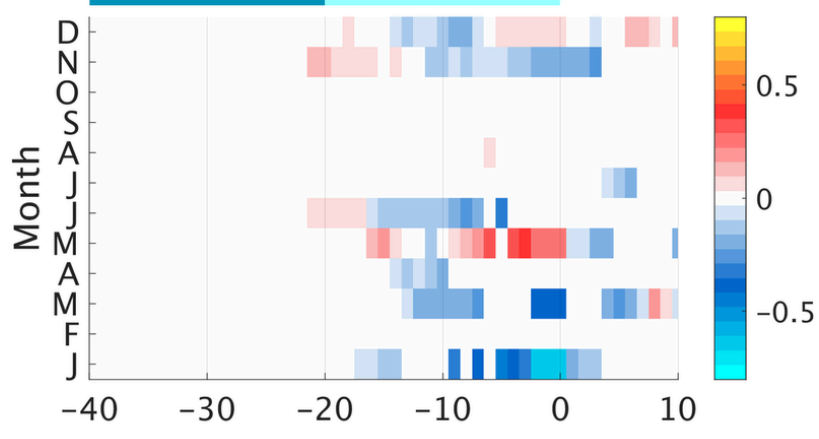
h) Atlantic: all



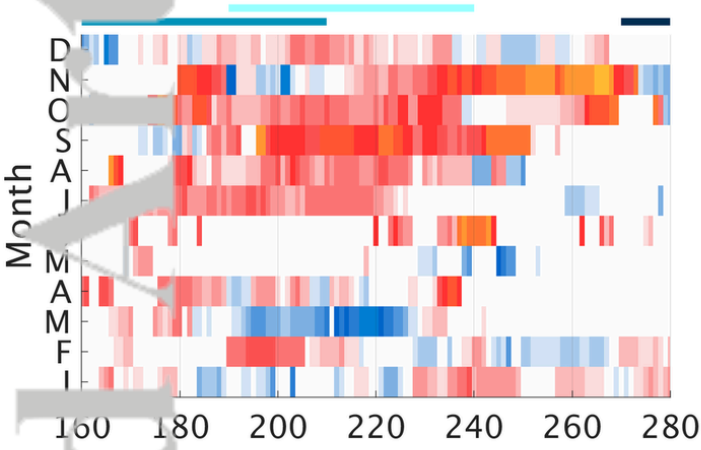
a) Pacific: SST



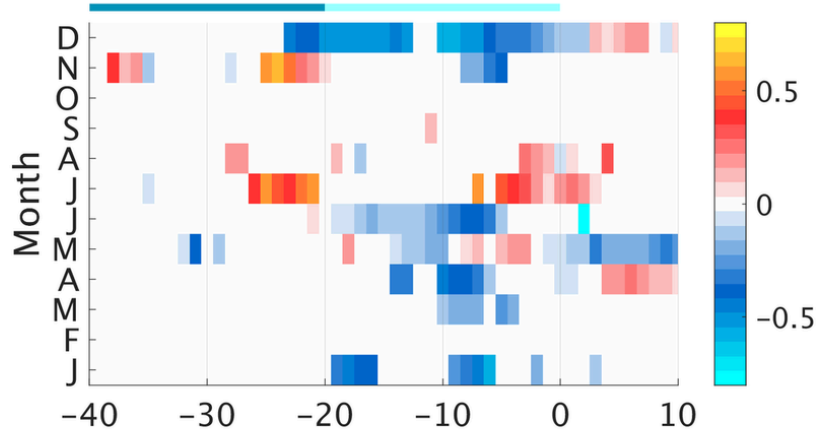
e) Atlantic: SST



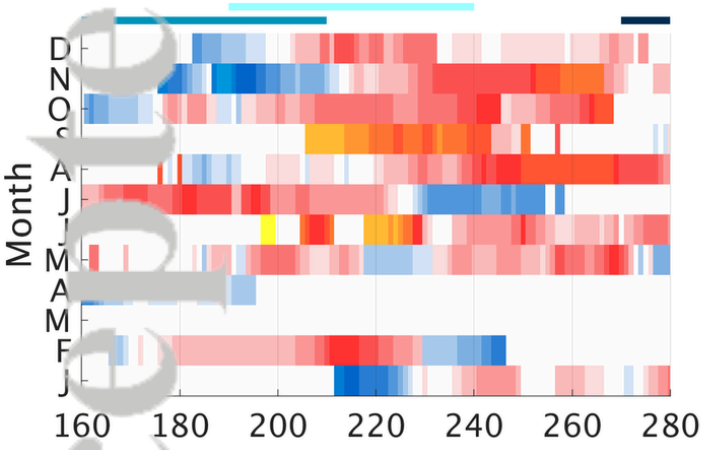
b) Pacific: SSH



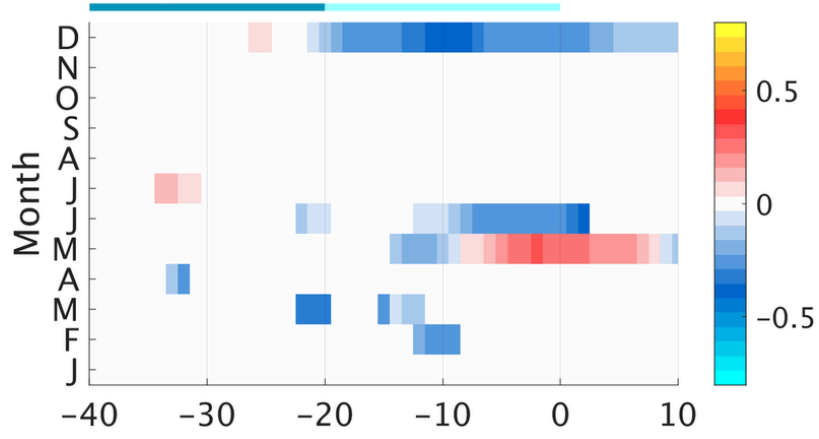
f) Atlantic: SSH



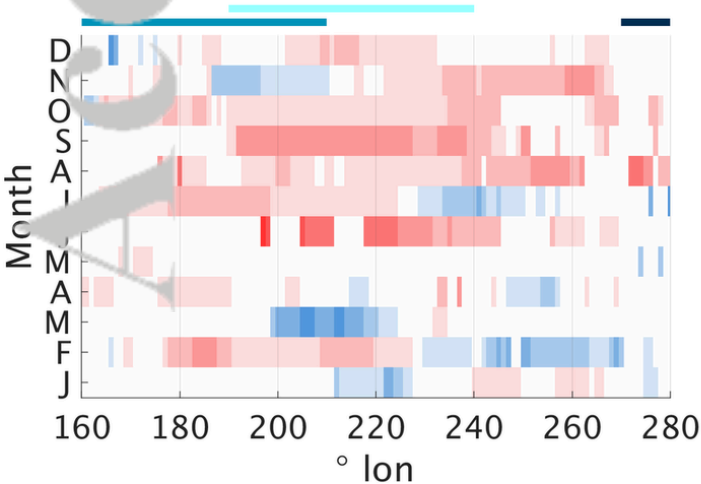
c) Pacific: USTR



g) Atlantic: USTR



d) Pacific: all



h) Pacific: all

